Ministry of Higher Education and Scientific Research
University of Baghdad
Institute of Laser for Postgraduate Studies

Multiwavelength Q-switched Doped Fiber Laser Based on Nanoparticle Saturable Absorbers

A Thesis Submitted to the Institute of Laser for Postgraduate Studies, University of Baghdad in Partial Fulfillment of the Requirements for the Degree of Doctor of Philosophy in Laser / Electronic and Communication Engineering

By

Ali Abdullah Salman

B.Sc. Laser and Optoelectronics -2008
M.Sc. Laser and Optoelectronics -2012

Supervisor

Prof. Dr. Abdul Hadi M. Al-Janabi

2019 AD **1441 AH**

ACKNOWLEDGMENT

Firstly, I would like to present thanks and appreciation to my mentor and supervisor, **Prof. Dr. Abdul Hadi Al-Janabi**, for being an excellent advisor. Even when he was the dean of the Institute of Laser for Postgraduate Studies, he still gives some of his precious time to me. Without his guidance, creative thinking, experimental research experience and patience in technical writing, this work would not have been possible. I will be in his debt forever.

I am deeply grateful to **Asst. Prof. Dr. Hussein A. Jawad**, Dean of the Institute of Laser for Postgraduate Studies, for his support.

Special thanks go to, Asst. Dean of the Institute of Laser for Postgraduate Studies **Dr. Mahmod S. Mahmod**.

My sincere thanks to **Asst. Prof. Dr. Mohammed K. Dhaher,** head of the Engineering and Industrial Applications Department for generously providing the oscilloscope.

I want to express my sincere thanks to the faculty members and staff of Institute of Laser for Postgraduate Studies, University of Baghdad, especially to**, Asst. Prof. Dr. Zaineb Fadhal**, **Asst. Prof. Dr. Shelan Khasro**, **Asst. Prof. Dr. Ziyad Ayad Taha** and **Dr. Jawad A. Hasan** from whose lectures I benefited greatly.

Most importantly, I would like to thank my parents, giving me enormous support, encouragement over the past years.

I am deeply indebted to all my friends and colleagues at the ILPS during my Ph.D. for their great support and kind advice.

Ali

DEDICATION

I would like to dedicate my thesis to:

MY FATHER

MY MOTHER

MY BROTHERS

Whose advice, patience, love, encouragement and prayers day and night make me able to get such success and honor

ABSTRACT

Multiwavelength generation from fiber laser represents a challenge due to the inherent homogenous broadening of the rare earth fiber lasers. Therefore, it is difficult to achieve stable multiwavelength at room temperature. A lot of focus has been given recently for using new methods to achieve this goal. In the present thesis, two types of nonlinear nanomaterials namely aluminum (Al) and tungsten trioxide (WO_3) have been used as saturable absorber (SA) for pulse generation as well as a nonlinear medium for multiwavelength generation. Aluminum nanoparticles were hosted by PVA (polyvinyl alcohol) to form a polymer based thin film. On the other hand, tungsten oxide thin films were prepared using two different approaches, as a solid thin film embedded in PVA and also as a liquid based solution mixed with Sodium dodecyl sulfate (SDS).

The Q-switching performance of aluminum nanoparticles as a saturable absorber was investigated in erbium doped fiber ring laser (EDFL) at 1567.6 nm. The modulation depth of the prepared aluminum thin film was 7% and it has the lowest verified saturation intensity of 0.0015 MW cm^{-2}. The repetition rate tuned from 34.13 to 48.8 kHz, while the resultant pulse width varies from 3.4 to 2.17 μs accordingly with the pump power. In order to enhance multiwavelength stability, Sagnac comb filter has been designed and employed into the EDFL to form a figure-of-eight cavity. The aluminum nanoparticles have contributed to the generation of multiwavelength in EDFL. 13 wavelength peaks were achieved with ~ 0.48 nm spacing between adjacent channels. Also, concurrent Q-switched pulses were observed having a shortest pulse width of 2.36 μs and maximum repetition rate of 33.45 kHz.

The second proposed nanomaterial was WO_3 based thin film which embedded onto fiber facet to generate multiwavelength in EDFL. The film

has a modulation depth of 20% and 15 lasing lines were obtained with aid of Sagnac filter. Q-switched pulses were also achieved with a minimal pulse duration of 4.24 μs.

On the other hand, WO_3/SDS solution was prepared and two consecutive coatings were applied by immersing the fiber tip in the liquid solution. After embedding the prepared SA into ytterbium-doped fiber laser (YDFL), self-starting Q-switched was realized at a threshold of 179 mW having a minimum pulse width of 2.92 μs and maximum pulse peak power of 3.17 mW with variable repetition rates from 14.8 to 71.3 kHz. Simultaneously, dual- and triple-wavelength emissions were obtained around 1.3 μm wavelength. The proposed fiber lasers can be exploited in many applications such as dense wavelength division multiplexing (DWDM) and light detection and ranging (LIDAR) systems.

LIST OF CONTENTS

LIST OF SYMBOLS

SYMBOLS	DESCRIPTION	UNITS
A_{eff}	Fiber effective area	m^2
c	Speed of light	m/s
$E(t)$	Electric field	V/m
h	Planck constant	m^2.kg /s
I	Laser intensity	W/m^2
I_s	Saturation intensity	W/m^2
k	Wavenumber	cm^{-1}
Δk	Phase matching	-
L	Total orbital angular momentum	$kg.m^2/s$
L_r	Resonator length	m
L_b	Beat length	m
N	Number of loops	integer
Δn	Fiber birefringence	-
P	Optical power	W
Q	Quality factor	-
R	Bend radius	m
r	Fiber radius	m
S	Total spin	-
t	Relaxation time	s
Δt	Time delay	s
α	Fiber loss	dB
ΔT	Modulation depth	%

SYMBOLS	DESCRIPTION	UNITS
α_{ns}	Non-saturable absorption loss	%m
β_w	Propagation constant	rad/m
$\Delta\beta_1$	Group-velocity mismatch	m/s
γ	Nonlinear coefficient	rad/W.m
δ	Phase difference	-
ϵ_0	Free space permittivity	F/m
η	FWM efficiency	-
λ	Wavelength	m
$\Delta\lambda$	Wavelength spacing	nm
υ	Frequency	Hz
υ_g	Group velocity	m/s
σ_{abs}	Absorption cross section at pump	m^{-2}
σ_{em}	Emission cross section at pump	m^{-2}
τ_r	Round trip time	s
τ_p	Pulse width	s
Ω_s	Sideband frequency difference	Hz
ω	Angular frequency	rad/s
$\Delta\phi$	Bend-induced phase difference	-
χ^1	First order susceptibility	-
$\mathcal{R}e(\chi^3)$	Real part of 3rd order susceptibility	esu
$Im(\chi^3)$	Imaginary part of 3rd order susceptibility	esu

LIST OF ABBREVIATIONS

ABBREVIATION	DESCRIPTION
ASE	Amplified spontaneous emission
CW	Continuous wave
dB	Decibel
dBm	Decibel per milliwatt
EDF	Erbium-doped fiber
EDFL	Erbium-doped fiber laser
Er^{+3}	Erbium ion
EDX	Energy dispersive x-ray
FBG	Fiber Bragg grating
FDM	Frequency division multiplexing
FFT	Fast Fourier-transform
FSR	Free spectral rang
FTIR	Fourier-transform infrared spectroscopy
FWHM	Full width at half maximum
FWM	Four wave mixing
GVD	Group velocity dispersion
ISO	Isolator
KHz	Kilohertz
LD	Laser diode
MD	Modulation depth
MFD	Mode field diameter

ABBREVIATION	DESCRIPTION
MFL	Multiwavelength fiber laser
MMF	Multimode fiber
MZI	Mach-Zehnder interferometer
MHz	Megahertz
ms	Millisecond
mW	Milliwatt
μW	microwatt
NA	Numerical aperture
NIR	Near infrared
nJ	Nanojoul
NL	Non-linear
NLE	Nonlinear equation
NPs	Nanoparticles
ns	Nanosecond
OC	Output coupler
OSA	Optical spectrum analyzer
OSC	Oscilloscope
OSNR	Optical signal to noise ratio
PC	Polarization controller
PD	Photo darkening
PCF	Photonic crystal fiber
PMD	Polarization-mode dispersion

ABBREVIATION	DESCRIPTION
PMF	Polarization maintaining fiber
PVA	Polyvinyl alcohol
RF	Radio frequency
RI	Refractive index
SA	Saturable absorber
SDS	Sodium dodecyl sulfate
SEM	Scanning electron microscopy
SMF	Single mode fiber
SNR	Signal to noise ratio
TEC	Thermoelectric cooling
TIR	Total internal reflection
TMD	Transition metal dichalcogenide
TMO	Transition metal oxide
WDM	Wavelength division multiplexing
XRD	X-ray diffraction
VCSEL	Vertical-cavity surface-emitting laser
Yb^{+3}	Ytterbium ion
YDF	Ytterbium-doped fiber
YDFL	Ytterbium-doped Fiber Laser

LIST OF TABLES

LIST OF FIGURES

Chapter One

Introduction

CHAPTER ONE

Introduction

1.1 Background

Multiwavelength fiber lasers (MFLs) have gained considerable research efforts due to their appealing features and potential utilizations in many fields, such as optical communication, sensing, testing and spectroscopy [1–3]. However, achieving a stable multiwavelength operation at room temperature is challenging due to the fact that rare-earth doped fibers suffer from inherent homogenous line broadening. Various scientific approaches have been used to relieve the competition between modes of the laser and to sustain a steady lasing operation such as such as four-wave mixing (FWM), nonlinear polarization rotation and stimulated Brillouin scattering [4,5]. In the ring cavity, a comb filter could be included to perform multiwavelength lasing. Various filtering methods have been described, such as the Fabry–Perot, fiber Bragg and Mach–Zehnder [6–8]. In addition, Sagnac loop filter has distinct advantages due to its diverse properties, for example, simple setup, low loss, polarization-free and good noise rejection ratio [9]. Furthermore, a stable multiwavelength production based on the FWM method using highly nonlinear nano-material can be realized by employing a few layers into the laser cavity to serve as a multi-oscillation stabilizer and a saturable absorber (SA). Such responses are commonly correlated with the real and imaginary parts of the 3rd-order nonlinearity in such substances. Various types of saturable absorbers (SAs) have been demonstrated to acquire passive Q-switching, such as carbon-based materials [10,11], transition metal oxides [12] and transition metal dichalcogenides [13]. Lately, metal nanoparticles (NPs) have attracted lots of attention due to their huge optical nonlinearity, fast switching, good optical limiting features and high absorption; especially in the wavelength

region of surface plasmon resonance [14,15]. Numerous researchers have demonstrated the exploitation of metal nanoparticles as SAs [16]. Among the diverse types of metal NPs, aluminum nanoparticles (AlNPs) have revealed pronounced potential for photonic applications. Furthermore, former researches have indicated that transition metal oxides (TMO) own a noteworthy high 3rd-order nonlinearity, swift response time, and saturate at low intensity [17,18]. Among these tungsten oxide (WO_3), has gained less focus and stayed unexploited material for the generation of pulsed and multi-wavelength lasers and emerges as a potential candidate for nonlinear photonic applications.

1.2 Fiber Laser

The rapid development of the physics and technology of fiber lasers, as well as vast expansion of their application areas, greatly stimulate the quest for and the study of more advanced operational modes of such lasers, including generation of multiwavelength, ultra-short and high-energy pulses. Since the invention of the laser researchers has continuously strived to generate shorter laser pulses. Simultaneously achieving a short duration and multiwavelength is, certainly, more challenging than improving one of these parameters independently. However, it is this combination that becomes increasingly important in a wide range of scientific, technological, medical, and other applications.

1.3 Optical Elements of Fiber Laser

A variety of passive fiber optic devices are used in optical fiber communication systems to perform specific tasks. Passive devices work without using an external power supply, while active devices need external power to work. Passive devices split, redirect, or combine light waves. The most common passive fiber optic devices that are widely used are couplers,

wavelength division multiplexers, filters, polarization controller and isolators are explained in detail in the next sections.

1.3.1 Coupler

The possibility to branch between several fibers often requires that a signal be split into two (or more) fibers, or two (or more) signals are to be combined into one fiber [19]. Fused coupler is a device that can achieve this function. The coupler is usually made by twisting two pairs of fibers together and then pulling them while heating the twisted area. This method creates a simple, rugged, compact method of splitting or combining optical signals. As a result, the two claddings fuse and the thickness of cladding at the twisted area reduces and the two cores lie close to each other, allowing modes to couple from one fiber to the other.

When light propagates in one fiber, the evanescent fields in the cladding generate guided waves in the other fiber. The energy oscillates back and forth between the two fibers as a function of the coupling distance and the radius of the fibers. Therefore, by controlling these parameters the coupling ratio can be controlled. In general, the power entering from one side splits between the two outputs on the other side [20]. Fused couplers are bidirectional and offer low back reflection and insertion losses. The most cases 2x2 or 1x2 ports couplers with different splitting are used for the output of laser radiations of the fiber laser as shown in Fig. (1-1).

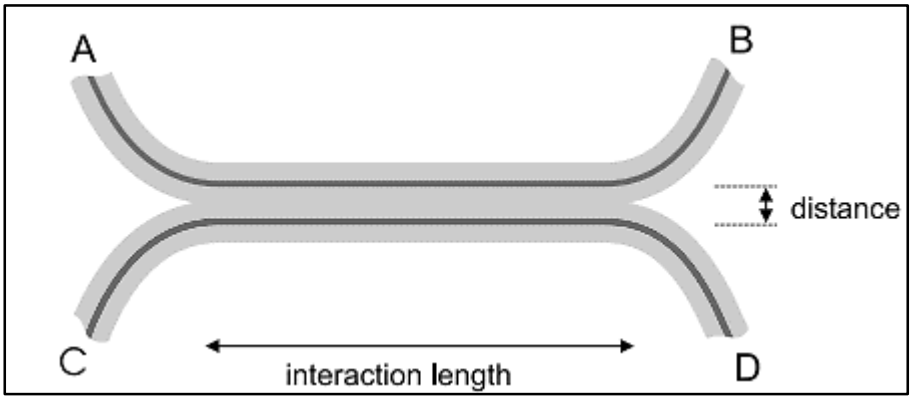

Figure (1.1): Fused coupler [19].

1.3.2 Isolator

As light travels along fiber splices, connectors and other optical components there are many opportunities for back reflection. These reflections usually happen when light passes through an interface perpendicular to the direction of light propagation. Return lights are known as back reflections and they have a destabilizing effect on oscillation of the laser source [21]. An angled interface, such as in an APC connector, significantly reduces such reflections. However, an isolator is used to reduce the amount of light reaching back to the laser. An optical isolator is a two-port passive component that allows light (in a given wavelength range) to pass through with low attenuation in one direction, while isolating (providing a high attenuation for) light propagating in the reverse direction [20].

Isolators normally work on the principle of rotation of the light polarization by a Faraday rotator. As Fig. (1-2) shows, the isolator consists of two polarizer plates that are at 45° angle with respect to each other with a Faraday rotator placed in between them and a permanent magnet for applying a designated magnetic field, so that permit only forward light to pass, while shutting out backward light. Forward light passing the optical isolator undergoes the following [21]:

- When passing through the polarizer, the incident light is transformed into linearly polarized light.
- When passing through the Faraday rotator, the polarization plane of the linearly polarized light is rotated 45°.
- This light passes through the analyzer without loss, since the light polarization plane is now in the same direction as the light transmission axis of the analyzer, which is tilted 45° from the polarizer in the direction of Faraday rotation.

On the contrary, backward light undergoes a slightly different process:

- When passing through the analyzer, the backward light is transformed into linearly polarized light with a 45° tilt in the transmission axis.

- When passing through the Faraday rotator, the polarization plane of the backward light is rotated 45° in the same direction as the initial tilt.
- This light is completely shut out by the polarizer because its polarization plane is now tilted 90° from the light transmission axis of the polarizer.

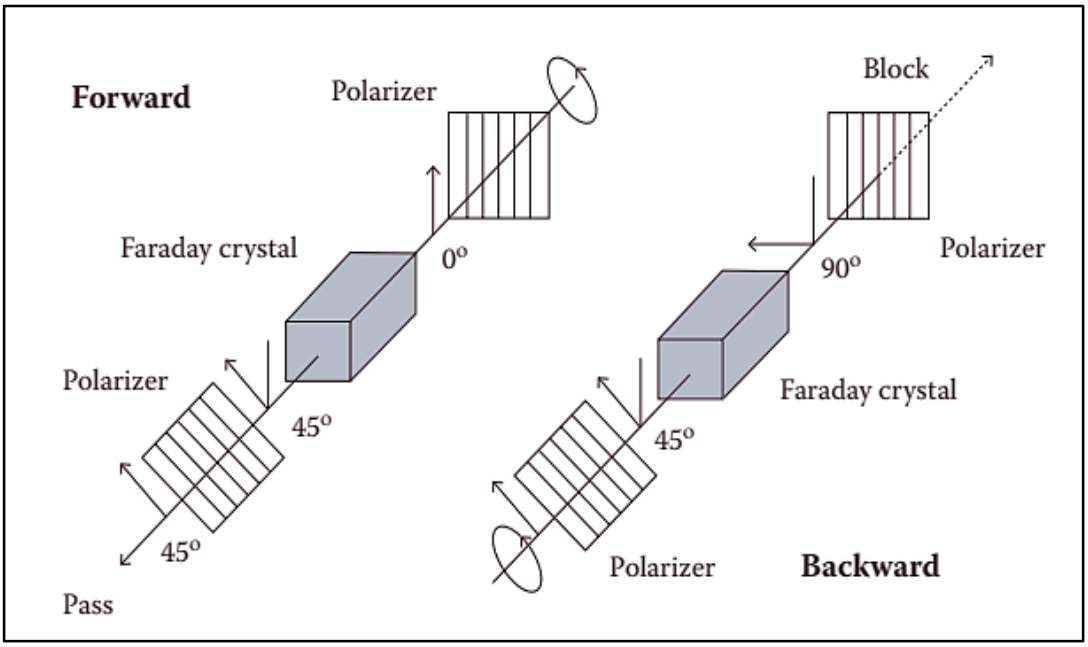

Figure (1.2): Isolator operation [22].

1.3.3 Polarization Controller

A fiber polarization controller is a device that allows one to control the state of polarization of light within a fiber. The polarization controller exploits the birefringence that is induced by bending a fiber [23]. Circular core fibers whose axes are straight are not birefringent- that is, the two orthogonally polarized LP_{01} modes have the same effective indices. Bending such a fiber introduces stresses in the fiber and makes the fiber linearly birefringent with the fast and slow axes in the plane and perpendicular to the plane of the loop, respectively [24]. The most common plates are half-wave

plates (λ/2 plates) with retardation of one-half wavelength which allow to rotate the plane of polarization of a linearly polarized light beam by any angle, and quarter-wave plates (λ/4 plates) which can transform linear polarization into circular polarization. The bending-induced birefringence of a single-mode silica fiber is given by:

$$\Delta n = b\,(r/R) \tag{1-1}$$

where r the fiber radius, and R the bend radius and b is an empirical constant that depends on the fiber material and the elasto-optic properties of the fiber, for silica fibers b ~ 0.133. Equation (1-1), implies that the smaller the loop radius, the larger is the birefringence. This birefringence provides a phase difference between the orthogonal polarization components parallel and perpendicular to the plane of the loop [19]. Thus, if the fiber is coiled around N loops of radius R, then the bend-induced phase difference between the two polarizations is given by [24]:

$$\Delta\phi = \left(2\pi/\lambda\right) \Delta n\, 2\pi\, RN \tag{1-2}$$

Figure (1-3) shows an in-line fiber polarization controller that utilizes bend-induced birefringence. It consists of three fiber birefringence components; the first and the last are quarter-wave retarders and the central one is a half-wave retarder. This combination is capable of transforming any input polarization state to any other output polarization state [24].

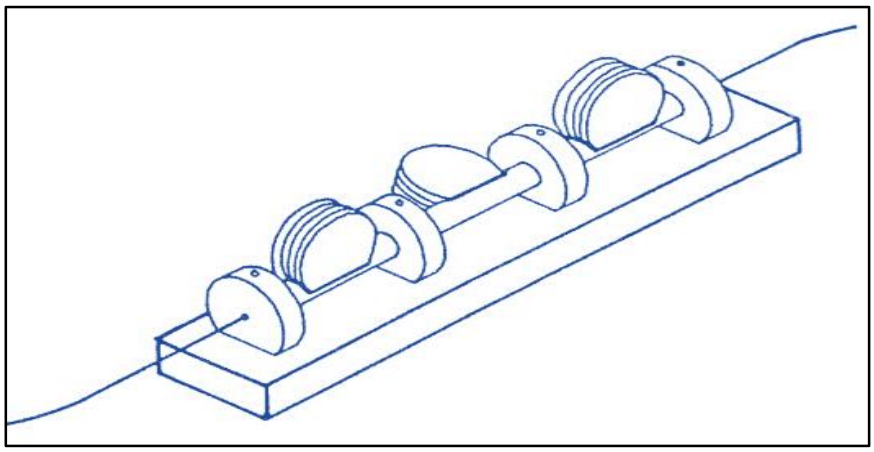

Figure (1.3): Fiber polarization controller [24].

1.3.4 Wavelength Division Multiplexer (WDM)

Frequently, it is desired to split or combine various signals in fibers according to their wavelength [19]. WDM devices are a specialized coupler type which enable light from two or more optical sources of different optical wavelength to be launched in parallel into a single optical fiber. In spectral terms, the optical WDM is analogous to electrical FDM. In this context, WDM couplers either combine the different wavelength optical signal onto the fiber (multiplex) or separate the different wavelength optical signals output from the fiber (demultiplex) [25]. These couplers are in general, wavelength sensitive since the propagation constants of the modes and the coupling coefficient are functions of wavelength [24].

The important optical parameters associated with the WDM coupler are the attenuation of the light over a particular wavelength band, the interband isolation and the wavelength band or channel separation. Ideally, the device should have a low-loss transmission window for each wavelength band, giving a low insertion loss. In addition, the device should exhibit high interband isolation, thus minimizing crosstalk [25].

1.3.5 Optical Filter

Optical filters are used in a wide variety of applications within optics and optical fiber devices. Optical filters are essentially frequency domain devices that selectively attenuate or pass certain wavelengths. The common factor in all-optical filters is their dependence on some wavelength-sensitive phenomena. In general, optical filters are based either on interference or diffraction effects [20]. There is an extensive range of optical filter types. The following filters are the most common [21]:

- Fabry-Perot filter
- Mach–Zehnder filter
- Fiber Bragg gratings
- Acousto-optic filter/ Thermo-Optic filter

1.3.6 Fiber-Coupled Diode Laser

Laser diodes for pumping fiber lasers may be split into two different families, fiber-coupled pumps based on individual single-emitter laser diodes and those based on fiber-coupled diode bars. One advantage of single-emitter pumps over diode bars is the lifetime associated with these pumps. Pump sources based on single-emitters are consist of a single laser diode chip or multiple single-emitters coupled into one delivery fiber [22].

The use of fiber-coupled laser diodes in laser pumping applications allows the achievement of easy (alignment-free) diode laser maintenance. Usually, diode lasers are fiber-coupled into single-mode or multimode optical fibers, depending on the mode structure of the original diode laser. Small, edge-emitting laser diodes, as well as most vertical-cavity surface-emitting laser (VCSELs), emit in a single spatial mode, allowing efficient coupling to a single-mode fiber with a lens (imaging the diode facet to the fiber core) or sometimes with butt coupling (direct coupling) [26]. Fiber coupling efficiencies depend strongly on the power level of the diode laser, the diode laser structure, and the approach of fiber coupling (lens-based or fiber profiling) [27].

Wavelength-stable diodes can be achieved using Bragg grating and with temperature control using water or thermoelectric cooling TEC [22]. In addition, there is a trade-off between the long-term lifetime of the diode and operating power and temperature. Along with obvious and important advantages, a fiber-coupling approach has several disadvantages, including the higher cost compared with free-space diode lasers and susceptibility to optical damage due to back reflections. Also, power diode laser systems with high average power may create overheating conditions at the fiber entrance, which in turn may result in stress and damage of the fiber end face. Special care has to be taken with the fiber termination enclosure facing the diode laser beam [27].

1.4 Types of Fiber Laser Resonators

The physics of optical resonators used in fiber lasers is similar to the physics of traditional laser resonators (i.e. gain and feedback mechanism). The main differences are in intracavity components and geometry of the active medium. Intracavity optical components of fiber laser resonators have certain features, mostly related to the tolerance for optical damages and fiber coupling. The active medium of fiber lasers is an optical waveguide usually with a significantly longer length than in traditional lasers and a very small diameter of the optical wave propagating medium. Long length and small fiber diameters are the reasons for optical nonlinearities [27].

Fiber lasers can be divided into two classes according to configurations of the resonator as ring and linear. The simplest linear fiber lasers have a resonator with reflecting elements at the two ends of an active fiber [23]. Figure (1-4) shows a laser with two fiber Bragg gratings which can acts as a high-reflectivity mirror for the laser wavelength while being transparent to pump radiation. Another approach makes use of fiber–loop mirrors that can be designed to reflect the laser light but transmit pump radiation [28].

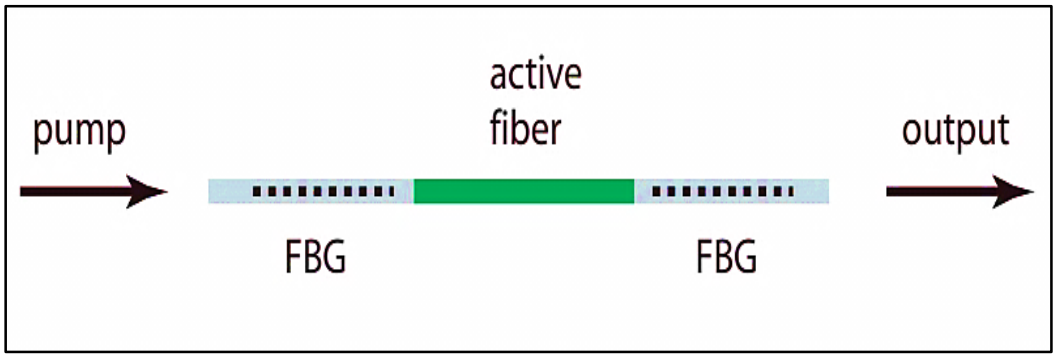

Figure (1.4): Linear fiber laser [23].

On the other hand, optical fiber ring resonators are popular in communication systems. These resonators consist of fiber as a waveguide, in a closed-loop coupled to one or more input/output directional couplers for in and out-coupling [21]. As shown in Fig. (1-5), pump light from a fiber-

coupled laser diode is injected into the fiber ring with a fiber WDM coupler and an isolator which allows the unidirectional propagation of the light wave inside the laser cavity. Therefore, ring resonators demonstrates no spatial hole burning effect. Additional components could be incorporated into the ring, for example, a polarization controller or a tunable bandpass filter for wavelength tuning [23].

When the light of the appropriate wavelength is coupled into the loop via the WDM, the light builds up in intensity over multiple round-trips [21]. The ring laser output power can be estimated using the following general expression [27]:

$$P_{out} = \eta_{ring} (P_{pump} - P_{th}) \qquad (1\text{-}3)$$

Ring fiber lasers are known to be susceptible to power fluctuations. However, the laser output power stability can be improved through an appropriate choice of laser parameters like the EDF lengths, the coupling ratio on the output and the total cavity length [28].

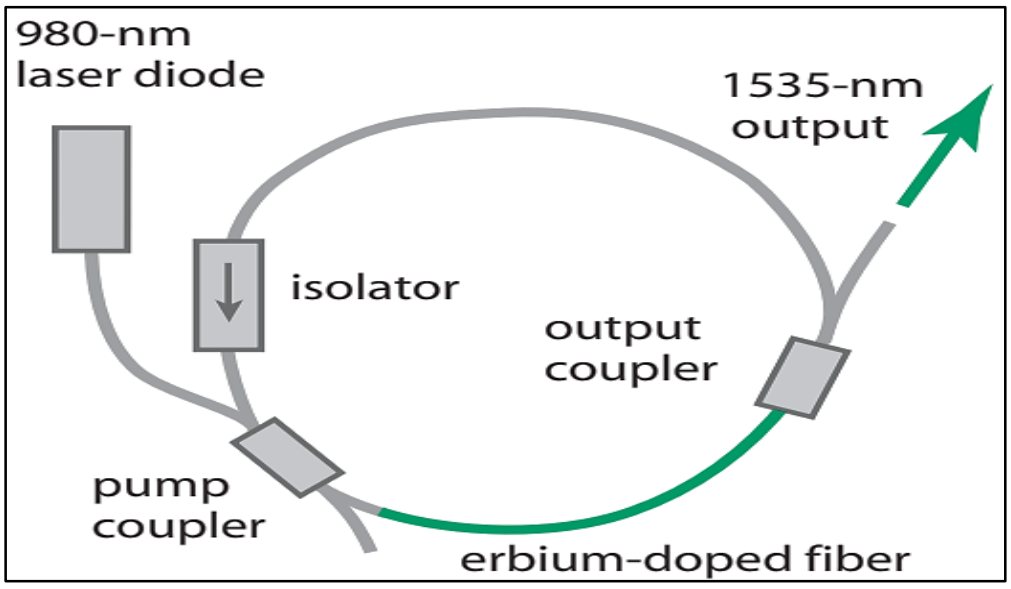

Figure (1.5): Ring fiber laser [23].

1.5 Fiber Nonlinearity

Nonlinear effects take place in the dielectric medium as an outcome of the alteration of the optical properties of a material system by applying sufficient intense laser light. The optical nonlinearity depends on interaction between the polarization of a material P(t) and the intensity of the used optical field E(t). First of all, linear polarization can be described as [29]:

$$P_{lin}(t) = \epsilon_0 \chi^1 E(t) \quad (1\text{-}3)$$

where χ^1 is the linear susceptibility and ϵ_0 is the free space permittivity. While the nonlinear polarization can be given by the following power series:

$$P_{nl}(t) = \epsilon_0 [\chi^2 E(t)^2 + \chi^3 E(t)^3 \dots \dots .] \quad (1\text{-}4)$$

where χ^2 and χ^3 are identified as the 2nd and 3rd nonlinear susceptibilities, respectively. 2nd nonlinearity can happen only in non-isotropic crystals without inversion symmetry. Since many materials such as liquid, gas and amorphous glass display inversion symmetry, these media do not provide 2nd nonlinearity. Otherwise, 3rd nonlinearity exists for both non-isotropic and isotropic materials. In fibers, the refractive index of the silica glass changes with intensity [30].

$$n(I) = n_0 + n_2 I \quad (1\text{-}5)$$

$$n_2 = \frac{3}{8\,n} \mathcal{R}e(\chi^3) \quad (1\text{-}6)$$

$$I = P/A_{eff} \quad (1\text{-}7)$$

where,

n_0: the linear refractive index

n_2: nonlinear refractive index

I: intensity

P: optical power

A_{eff}: mode area

Mode area represents the region of the cross-section that light propagates in the fiber; which involves the core and a part of the clad and its calculated by:

$$A_{eff} = \pi\,(MFD/2)^2 \qquad (1\text{-}8)$$

where MFD is the mode field diameter. The real part of n_2 is related to four-wave mixing, while the imaginary part is related to the nonlinear absorption (saturable absorption):

$$\alpha_2 = \frac{3\omega_0}{4cn}\, Im(\chi^3) \qquad (1\text{-}9)$$

where ω_0 is the angular frequency. Large intensities can be found in single-mode fibers as the cross-section is small. The dependency of the refractive index on the intensity is accountable for the Kerr effect. The Kerr non-linearity reveals itself in different impact like self-phase modulation (SPM) and four-wave mixing (FWM). FWM can appear with two frequency components propagate mutually in a nonlinear medium like the optical fiber where two added frequency components forms. In order to conserve energy:

$$\omega_1 + \omega_2 = \omega_3 + \omega_4 \qquad (1\text{-}10)$$

There is a special case where one input beam is applied which known as degenerate FWM ($\omega_1 = \omega_2$). This is a common case in fiber optics. Degenerate FWM arises when two photons from the pump wave are depleted and extra photons are produced (signal, idler). A powerful pump wave (ω_1) generates two sidebands symmetrically positioned at frequencies ω_3 and ω_4 [30].

$$\Omega_s = \omega_1 - \omega_3 = \omega_4 + \omega_1 \qquad (1\text{-}11)$$

However, utilization of nanomaterial-based thin film to induce FWM can be advantageous in term of dispersion. The dispersion of light passing through a few micron-layers is ineffective and can be neglected. The efficiency of FWM (η) is related to the power P, 3rd nonlinear coefficient γ and fiber length L as follows [31]:

$$\eta \propto (P\,\gamma\,L) \qquad (1\text{-}12)$$

Where the nonlinear coefficient is given by:

$$\gamma = \frac{(n_2\omega)}{(c\,A_{eff})} \qquad (1\text{-}13)$$

1.6 Q-Switching Operation

Q-switching is a method to produce short pulses (giant pulse) with a time scale of (μs to ns). This can be achieved via modulating the Q factor inside the cavity. The quality factor is defined as a ratio of accumulated energy in the cavity to energy wasted in every round trip and it is a dimensionless quantity. A large Q value reveals a lower loss and vice versa. The Q-factor can be expressed as [32,33]:

$$Q = 2\pi\upsilon \left[{}^{E_{stored}}/_{E_{lost}} \right] \qquad (1\text{-}14)$$

where υ is central frequency of laser. Varying the Q value of the resonator can be realized by introducing a switching mechanism inside the cavity. This consequently results in a series of pulses called Q-switched pulses equivalent to the upper level life time [34]. The switching operation can be either passive or active. Active loss modulation can be controlled acoustically, electrically or even optically. The passive approach is preferred because it is simple and cost-effective which eliminate the need for complex component and external trigger. Passive Q-switching is appropriate for high repetition rates, although it lead to reduced pulse energy.

1.6.1 Pulse Generation in Passive Q-switching

1. When the active medium is pumped, the output laser is prevented by retaining the resonator loss high (Q-factor low) and population inversion is developed.
2. The loss introduced by the passive Q-switcher is very high that prevent laser operation to begin (without feedback mechanism).
3. Typically, the power grows exponentially until the gain is saturated as shown in Fig. (1-6). The saturable absorber is then rapidly switched from low to high Q-value and so that the feedback operation is resumed.

4. Finally, the output pulse draws out a large portion of the stored energy. For significant pulse energy, the gain medium needs to have a long lifetime of the upper-level. The typical gain media for Q-switched lasers are rare-earth crystals and glasses [32].

So that the 3dB pulse width (τ_p) can be estimated by:

$$\tau_p \approx 4.6\ t_r/(g-l) \qquad (1\text{-}15)$$

$$\tau_r = L_r/c \qquad (1\text{-}16)$$

where,

l: resonator loss

t_r: round trip time

g: gain

L_r: resonator length.

It clearly seen from the previous relation that short pulse generation is achievable with short cavity length and high gain medium.

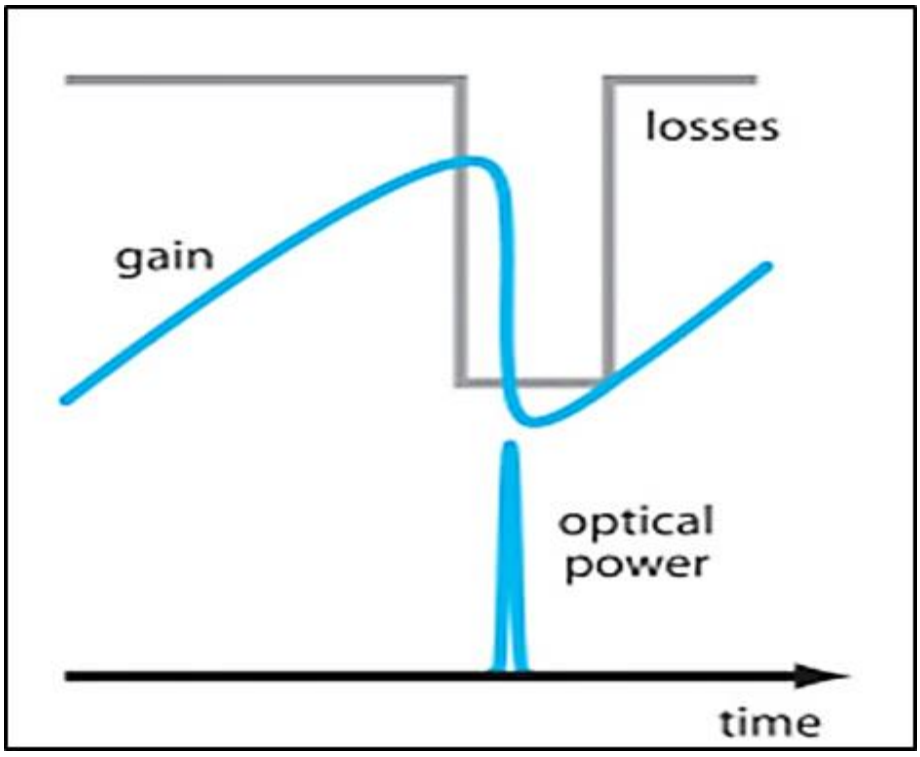

Figure (1.6): Mechanism of Q-switching [32].

1.6.2 Saturable Absorber (SA)

The SA is a nonlinear optical substance that modulates the loss inside the cavity. At certain bleaching threshold, the transmission of the material increases nonlinearly with intensity [35,36]. So that, light with low intensities is blocked while higher intensities pass and consequently establish pulse formation in the laser cavity. In other words, the peak of optical pulse travels in fiber has high intensity and saturates (bleach) the absorber material more than its wings with low intensity. This occur when multiple longitudinal modes are in phase and interfere constructively. Therefore, the SA operates like an optical switch. These nonlinear devices are broadly used in the generation of Q-switched and mode locked fiber lasers.

Typically, SA performance is analyzed by figure of merits such as modulation depth, operating wavelength, saturation threshold, response time and finally, the maximum intensity a substance can handle before damage takes place [37,38]. The operation principle of SA can be viewed by the assumption of a simplified two-electronic levels which contains ground level and upper level as shown Fig. (1-7) [35]. At low intensity, the atoms in the ground state will be excited to a higher state. However, most of the atoms are reside in the ground level. At strong intensity, large number of atoms excite to upper level very quickly and the ground state is depleted. Finally, the absorption saturates and discontinue. So the material becomes transparent. After specific lifetime the particles return to lower level and this manner will be repeated and so on. The governing Equation is given by [39]:

$$T(I) = 1 - \Delta T \exp\left(\frac{-I}{I_s}\right) - \alpha_{ns} \qquad (1\text{-}17)$$

where T(I) is the transmission, ΔT is the modulation depth, I is the input intensity, I_{sat} is the saturation intensity, and α_{ns} is the non-saturable loss.

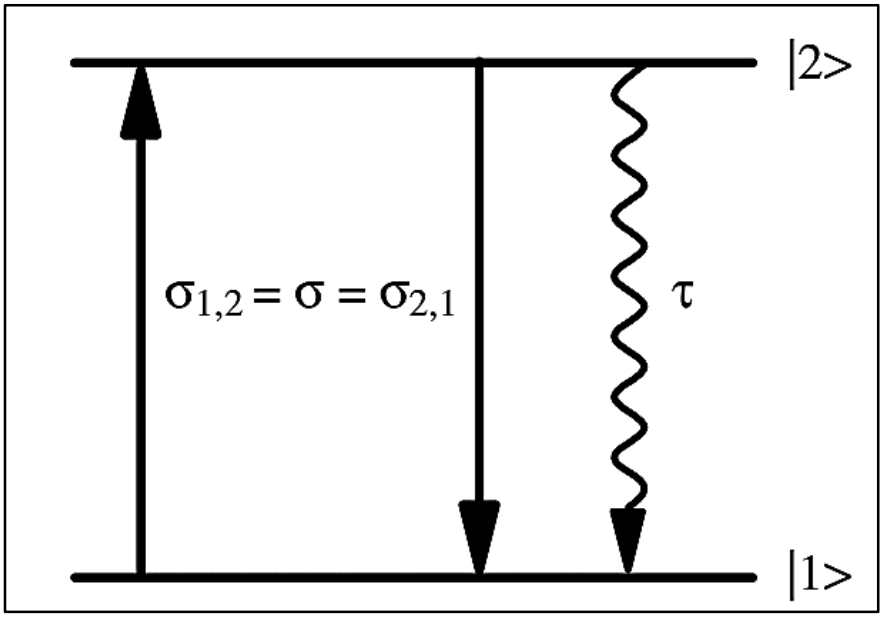

Figure (1.7): Two-level saturable absorber [35].

The saturation intensity can be calculated by:

$$I_s = h\nu/\tau\sigma \qquad (1\text{-}18)$$

where,

$h\nu$: photon energy

σ: cross section of absorption

τ: relaxation time.

Figure (1-8) shows an example of a nonlinear transmission curve for a saturable absorber where the modulation depth is defined as the difference in the transmission between the non-saturable loss and the background absorption loss (α_0). The modulation depth is typically estimated using a twin detector method. The scheme is based on the principle differential detection. A home-made ultrashort fiber laser source operating at 1560 nm is used as the pump light. Then, 50:50 fiber coupler is used to split the laser power between a sensing arm and a reference arm, and a separate photodiode is used to measure each. The two powers then are subtracted as shown in Fig. (1-9). The sense beam passes through the sample to be measured, while the reference beam is unaffected (i.e. to monitor the power). By continuously adjusting the attenuator, the transmitted power is recorded as a function of

incident optical power on the SA film. With no change in sample transmission, the two powers are nulled; any change in the transmission produces a differential output. Finally, the dataset from a twin-detector measurement can be well fitted with a two-level SA model [40,41]. Typically, large modulation depth is desired for effective pulse formation and for large pulse energy. The non-saturable loss should be kept at minimum values and its originates from scattering and absorption of the SA material itself. This greatly affected by the type SA material, crystal structure, preparation method, and the thickness of the fabricated thin film [42].

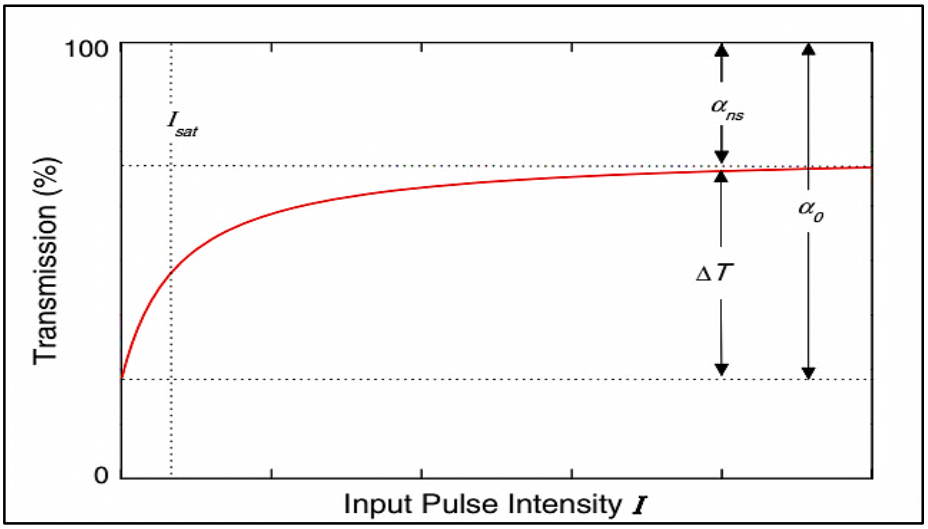

Figure (1.8): Bleaching curve of two level system [39].

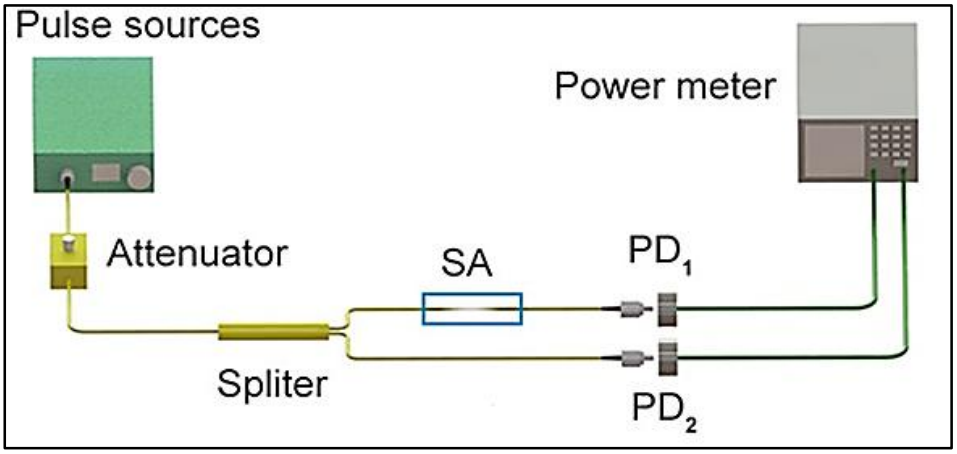

Figure (1.9): Twin detector setup [40].

1.7 Rare-Earth Spectroscopy

Rare-earth-doped glasses are actually extensively employed as an active medium for fiber lasers. Rare-earth ions are doped into the fiber core and they pumped by optical schemes using diode lasers. The most significant rare-earth fiber lasers are ytterbium, erbium, and thulium [43]. Depending on the active medium, fiber lasers can generate radiation at different wavelengths.

Many glasses have been produced as host materials for Er and Yb such as phosphate, chalcogenide or fluoride glasses. The glass is unlike crystals has a disordered and isotropic nature which shows broad absorption and emission spectra. Silica fibers are formed essentially from silicon dioxide (SiO_2). Silica has arbitrary arrangement of Si atoms each surrounded by four oxygen atoms. It is preferred over other glasses because it can be produced with good quality and long length fibers. Silicate fibers are also mechanically sturdy, non-hygroscopic, chemically hard and provide the minimum loss for optical communication at 1.5 μm wavelength. Some modifiers are blended at small amounts to simplify the incorporation of large-sized rare-earth ions in the host structure.

Generally, the energy level is specified by spectroscopic notations as follow [27]:

$$^{2S+1}L_J \qquad (1\text{-}19)$$

where (2S + 1) is the multiplicity and L is the term. The quantum number S is a total spin and is always an integer. J is the total angular momentum, which is either an integer or a half-integer. L is the total orbital angular momentum, which is assigned a letter (S, P, D, F, G, H, I, K, L, M, N, etc.) that corresponds to an integer (0, 1, 2, 3, 4, 5, 6, 7, 8, 9, 10, etc.). Russell–Saunders coupling (LS coupling) is most often used for the states of lanthanides and actinides. In this scheme, L and S are vectorially added to form the total angular momentum J, and the states are labeled $^{2S+1}L_J$ [44].

Broadening the sharp line structure is attributed to homogeneous and inhomogeneous processes. The relative contribution of each mechanism has important device implications, and there has been considerable interest in understanding these mechanisms. For a homogeneously broadened transition, a given wavelength will interact with all ions with equal probability. Thus, any pump wavelength will produce the same gain spectrum and any signal wavelength can saturate the entire band. If inhomogeneous broadening dominates, individual sections of the gain spectrum act independently and can be individually addressed by photons of different wavelengths.

For the Er^{3+} 1500-nm bands (quasi-homogeneous behavior) mixed homogeneous and inhomogeneous effects are existed, but with predominantly homogeneous saturation characteristics [44]. The interaction between the rare earth ion and the intrinsic electric field associated with the host results in a broadening of the absorption and emission line shapes associated with the rare earth ion. Optical frequency transitions in solids can be broadened by lifetime, dipolar or thermal broadening, or by random inhomogeneities [45].

1.7.1 Er-doped Fiber (EDF)

Trivalent erbium Er^{3+} doped in silica glass is one of the rare earth elements used as an active medium to generate laser emission at 1.55 μm. It is widely used for optical data transmission due to reduced attenuation in this wavelength window. The energy level of Er^{3+} which is a three-level gain system is shown in Fig. (1-10) [27]. The laser transition is from $^4I_{13/2}$ to $^4I_{15/2}$, which supply gain for the 1550 nm. The erbium can be pumped at either 980 or 1480 nm. Core pumping scheme with 980 nm laser diode from ground level to the $^4I_{11/2}$ using is preferable due to the higher quantum efficiency which makes the 1480 nm diodes less productive than 980 nm diodes in terms of efficiency.

Figure (1-11) shows the emission spectra which have luminescence with broad spanning. The erbium has a non-radiative decay to a state $^4I_{13/2}$. This level has a longer lifetime of about 10 ms. The laser quantum efficiency relies on the time spent the upper level. Moreover, erbium has visible florescence at 550 nm (green). However, due to low optical to optical efficiency, about 70% of pump power is transformed into heat. This can be challenging and impede high power application of erbium-doped lasers which require a great care with cooling issues. Some 1500 nm emission cross-section spectra for different glass types is shown in Fig. (1-12). The emission cross-sections describe the probability of a specific transition to take place [44]. The amounts of absorbed or emitted power at a particular frequency can be determined as:

$$P_{abs} = \sigma_{abs} I \quad (1\text{-}20)$$

$$P_{em} = \sigma_{em} I \quad (1\text{-}21)$$

where, σ_{abs} : absorption cross-section and σ_{em} : emission cross-sections

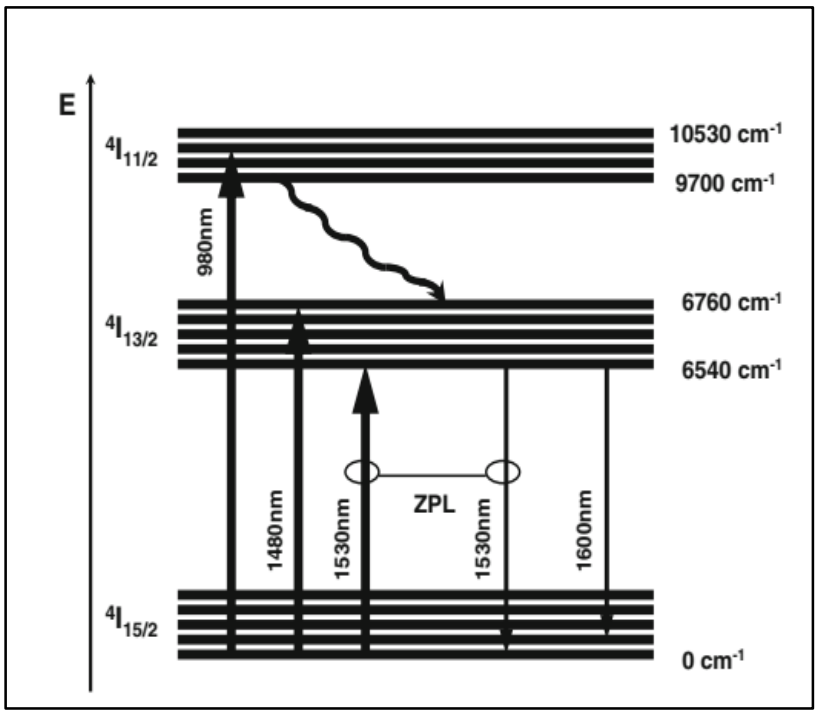

Figure (1.10): Energy levels of erbium [27].

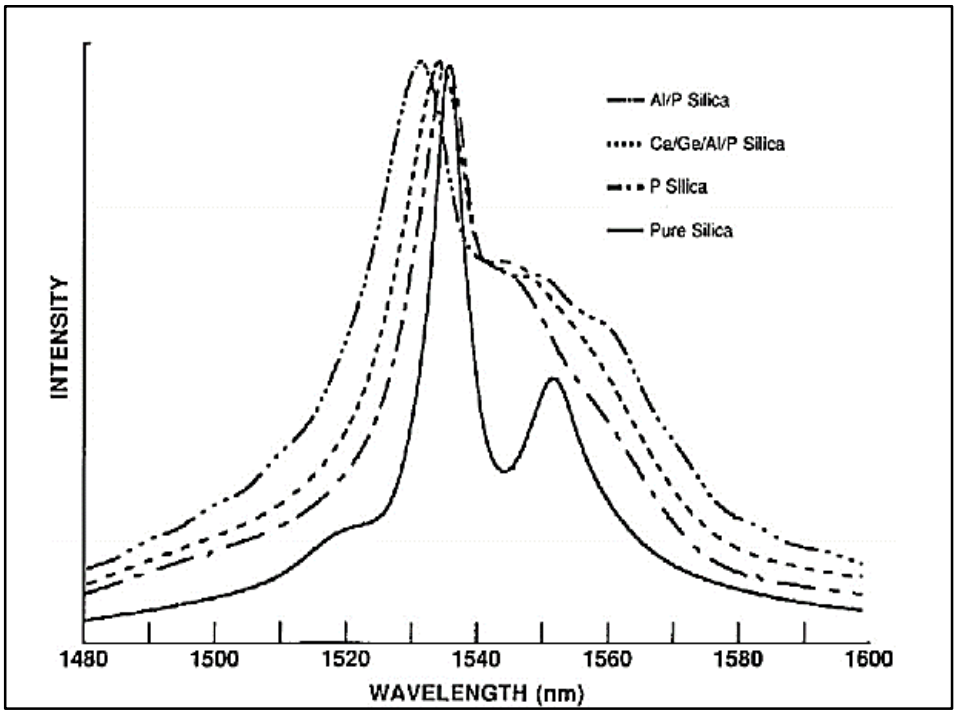

Figure (1.11): Emission of erbium doped silica fibers [44].

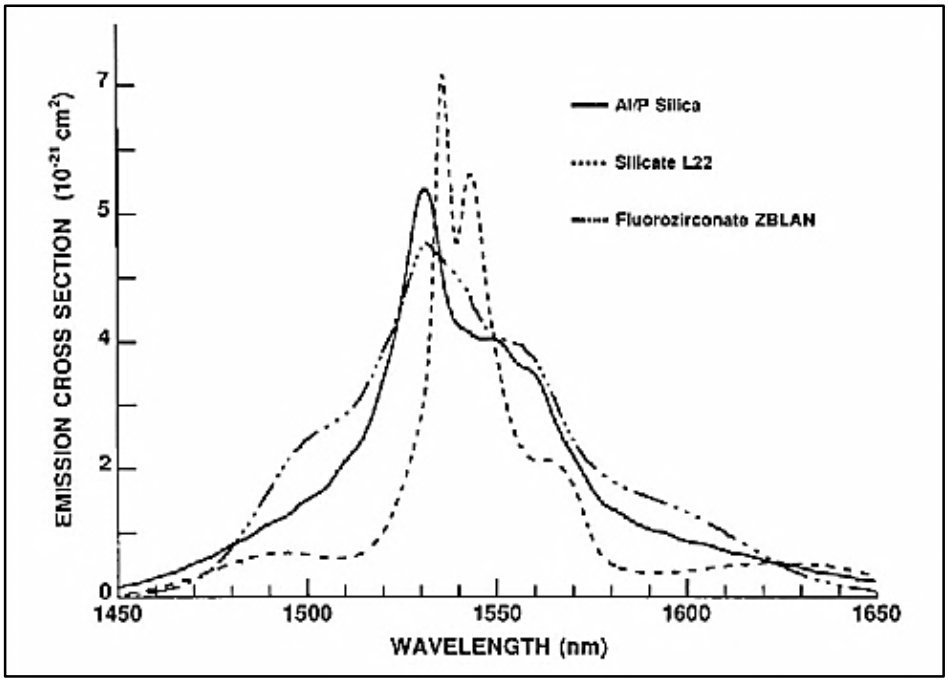

Figure (1.12): Emission cross section of erbium for various glasses [44].

1.7.2 Yb-doped Fiber (YDF)

The ytterbium Yb^{+3} has a simplified electronic band which contains only two manifolds (levels), therefore, there is no excited states absorption and no up-conversion. Ytterbium is attractive due to several features such as reduced quantum defects, a lengthy lifetime of the upper-level (~ 1 ms), wide emission bandwidth and the possibility of high power scaling. In addition, Yb^{3+}-doped laser glasses have broad and sufficiently intense emission bands in the spectral range between 950 and 1200 nm. Due to broad emission lines, Yb^{3+}-doped laser glasses (in particular, fiber lasers) demonstrate tunable laser action in a wide spectral range. Figure (1-13) shows the energy levels of ytterbium which contains the ground $^2F_{7/2}$ and the excited $^2F_{5/2}$ band. A major shortcoming of ytterbium is the quasi-three-level system that causes re-absorption of the generated light. Fig. (1-14) display the absorption and emission cross-sections. Yb^{3+}-doped laser-active glasses have strong and wide absorption bands near 915 and 976 nm and are suitable for diode pumping by the robust InGaAs laser diodes.

All challenges existing in the field of Yb^{3+}-doped fiber lasers and amplifiers can be divided into two categories: (1) challenges associated with obtaining efficient lasing in the 980 nm spectral range where the pumping scheme is quasi-three level or extension of the laser operation range to more than 1100 nm, where the gain is much lower than in the maximum of the gain band. (2) challenges related to the operation of Yb^{3+}-doped fibers at high power pump levels are associated with so-called photodarkening of Yb^{3+}-doped silica fibers [27]. Photodarkening (PD) causes degradation in power and reduces the operational lifetime for rare-earth doped silica fiber especially ytterbium-doped fibers. PD originates from absorption at various structural defects which leads to the formation of color center. These color centers can absorb light from ultraviolet to near-infrared wavelengths which and consequently generate heat and damage the fiber. This process is a temperature-dependent and time- dependent. Fibers with a low (OH)

concentration are found to withstand photo darkening and by using fluorine as a different dopant [46].

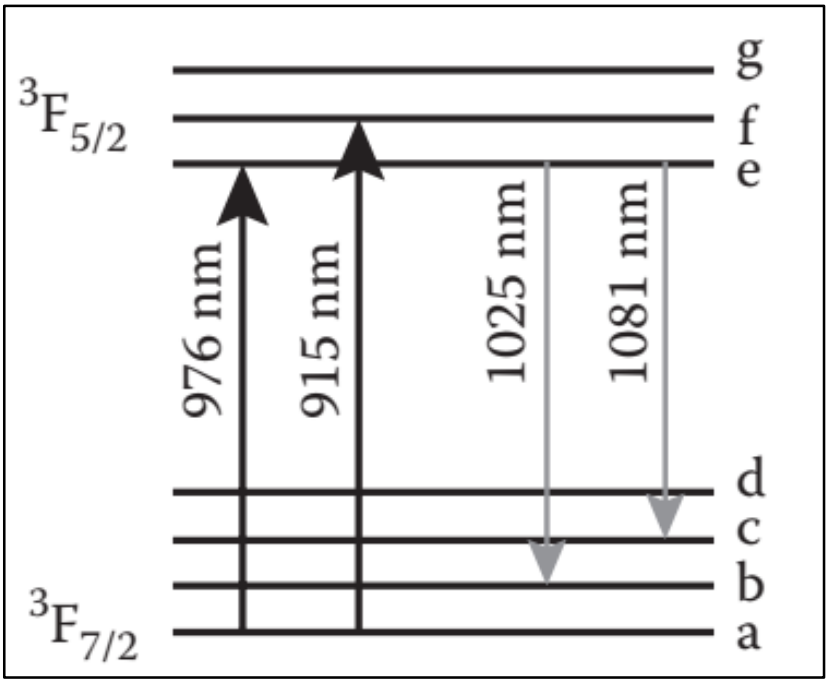

Figure (1.13): Energy levels of ytterbium [22].

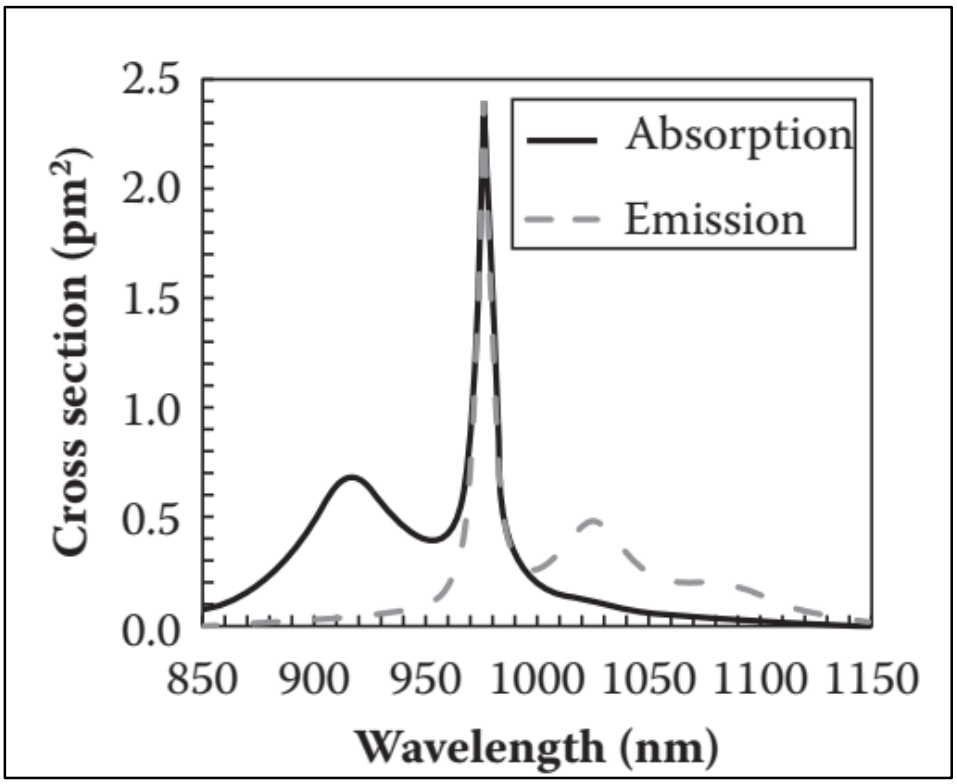

Figure (1.14): Ytterbium emission and absorption cross-section [22].

1.8 Polarization Maintaining Fiber and Birefringence

PMF is a single-mode fiber where the plane of polarization of the propagating light remains unchanged without coupling of power between the modes. A standard single-mode fiber has circular core where the fundamental propagating mode consists of two modes with perpendicular linear polarization in x and y orientation. Due to fiber inhomogeneity during fabrication of SMF, there always exist difference in the propagation constants where:

$$\Delta k = k_x - k_y \tag{1-22}$$

These modes are propagating in different velocity and causes periodic mode coupling. Polarization components are phase-shifted and the polarization pattern varies with distance. This periodic alteration in the polarization condition is determined by the beat length (L_b) which represents the distance where the original polarization is reached after 2π phase shift [47]:

$$L_b = 2\pi/\Delta k = \lambda/\Delta n \tag{1-23}$$

where (Δn) is the fiber birefringence and is expressed as:

$$\Delta n = n_x - n_y \tag{1-24}$$

Regular SMF with symmetrical core cannot hold identical polarization states along the path of propagation (random polarization) and it will be always subject to environmental fluctuations. Several designs have been demonstrated by altering the core geometry or by introducing stress rods into the clad. There are many types of PMF: elliptical core, Panda, and Bow-tie. Among them, Panda is the most commonly used geometry as shown in Fig. (1-15). It was first produced by Fujikura Ltd from Japan. It preserves the polarization by introducing large birefringence which is realized by stress rods on both of the core sides therefore coupling between modes is reduced. Thus, small birefringence induced by bending, pressure or temperature is not effective to the polarization state.

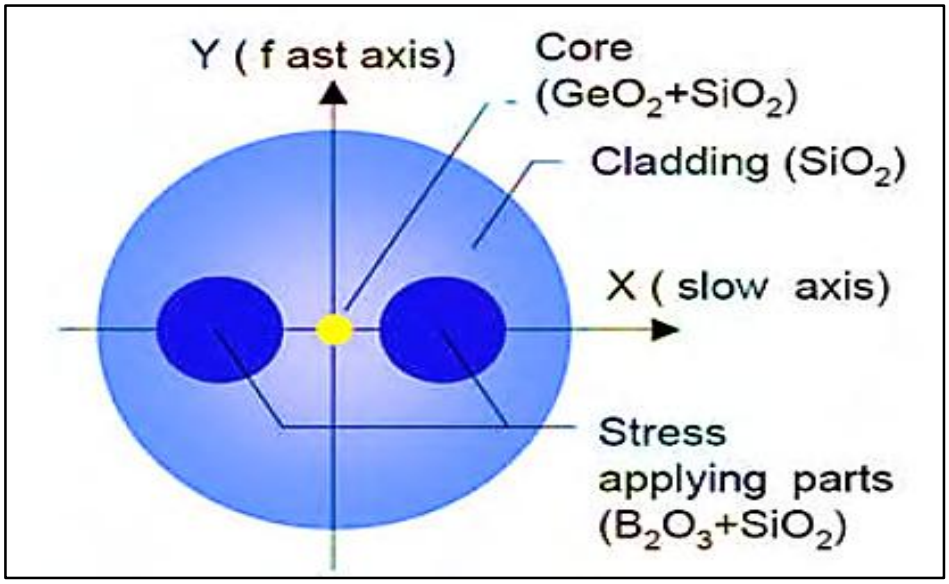

Figure (1.15): Panda PMF structure [48].

The orientation along the line where rods and the core are situated is called the slow axis while the orthogonal line is called the fast axis. When a linearly polarized light incident on the slow or the fast axis, polarization is kept unaltered during propagation. In contrary, when the polarization orientation makes an angle with those vertical and horizontal axes, polarization rotates constantly over the fiber in a periodic fashion as shown in Fig. (1-16).

If an optical pulse is injected into the fiber, it experiences broadening due to dissimilar group velocity of the orthogonal polarization components of the pulse. This is called polarization-mode dispersion (PMD). Therefore, time delay is introduced between the two polarization components which is described by [30]:

$$\Delta t = \left|\frac{L}{v_{gx}} - \frac{L}{v_{gy}}\right| = L|\beta_{1x} - \beta_{2x}| = L\Delta\beta_1 \qquad (1\text{-}25)$$

where,

L: length of fiber

v_{gx}: group velocity in X path

v_{gy}: group velocity in Y path

$\Delta\beta_1$: group-velocity mismatch

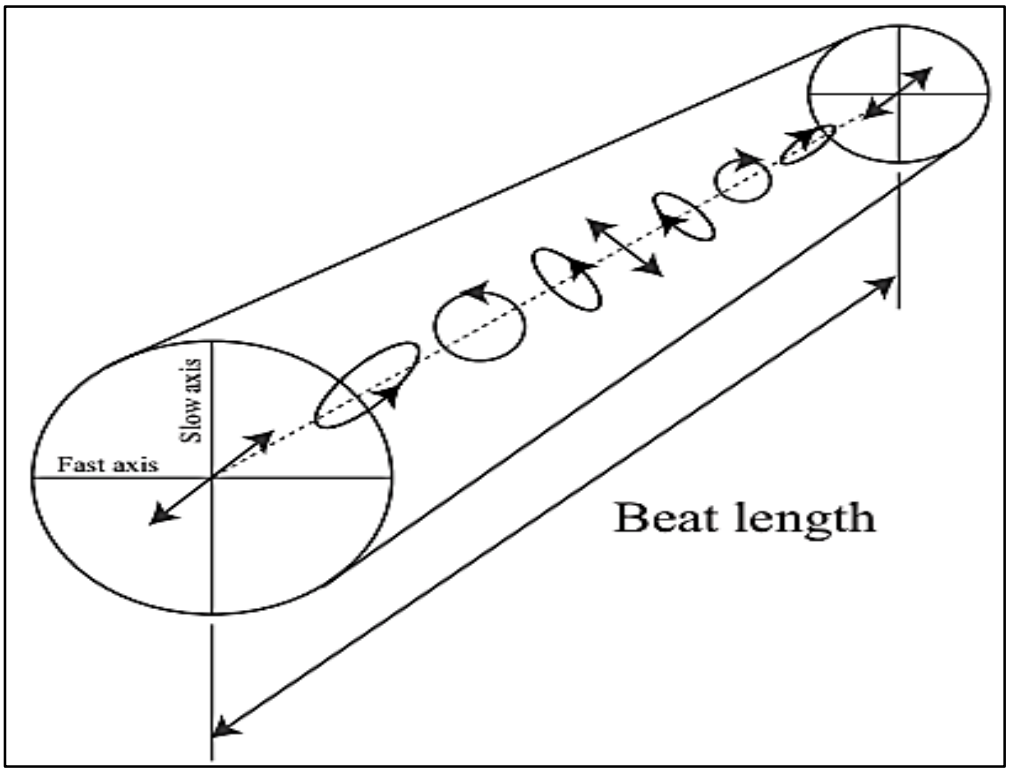

Figure (1.16): Polarization states inside PMF [49].

1.8.1 Sagnac Loop Filter

Sagnac loop filter simply consists of a section of polarization maintain fiber (PMF) and 3 dB fiber coupler to form a loop. It resembles a ring cavity but performs differently because it has no feedback (single round trip) [50]. The operation principle of the loop filter is based on dividing the input light into two beams traveling with opposite arms. The two beams merge and create an interference pattern at the output of the (50:50) coupler as shown in Fig. (1-17). Sagnac interferometer is incorporated inside the cavity form a figure of 8 configuration and acts as a comb filter. The transmitted intensity of birefringent filter relies on the wavelength as shown in the formula [51]:

$$\frac{I_t}{I_i} = (1-\gamma)^2\, exp[-2\alpha\,(l-L)]\, sin^2\left(\frac{\delta}{2}\right) \qquad (1\text{-}26)$$

where,

γ: insertion loss of 3dB coupler

α: fiber loss

l: SMF length in Sagnac loop

L: PMF length in Sagnac loop

δ: phase difference between traveling components which is given as follows:

$$\delta = (2\pi\Delta n\, \mathrm{L})/\lambda \qquad (1\text{-}27)$$

The wavelength spacing between two successive peaks is related to the beat length and PMF length in the loop filter as below [52]:

$$\Delta\lambda = \lambda\, L_b/L \qquad (1\text{-}28)$$

Through the modification of the polarization controller (PC) the number of laser wavelengths can be varied. The transmission intensity of the filter is shown in Fig. (1-18). Sagnac loop filter has numerous benefits such as simple design, low cost and high signal to noise ratio thus its used in fiber-based gyroscope and current sensors. This filter is mainly used to generate and stabilize multiwavelength fiber laser.

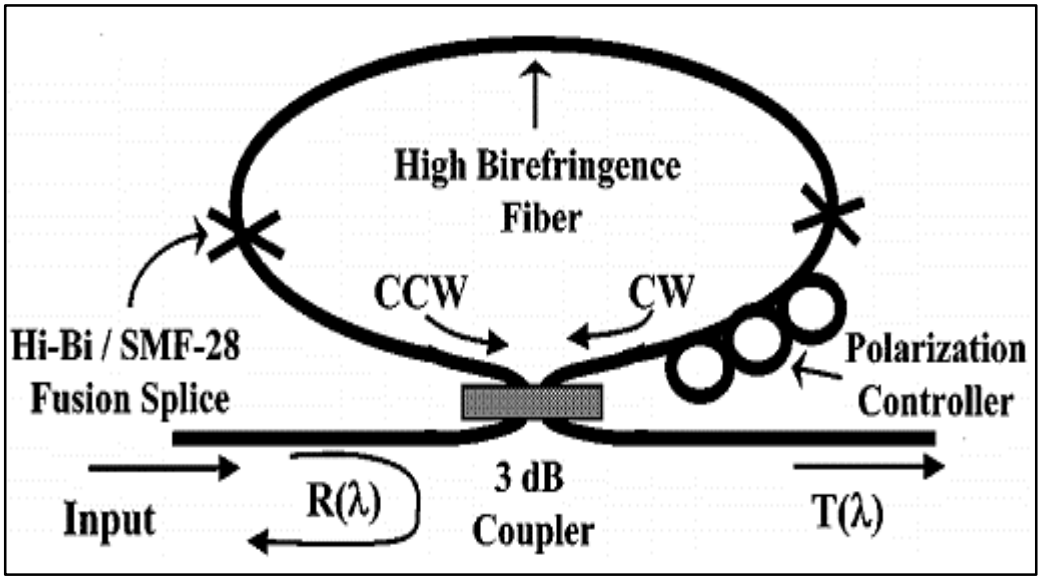

Figure (1.17): Setup of Sagnac loop filter [53].

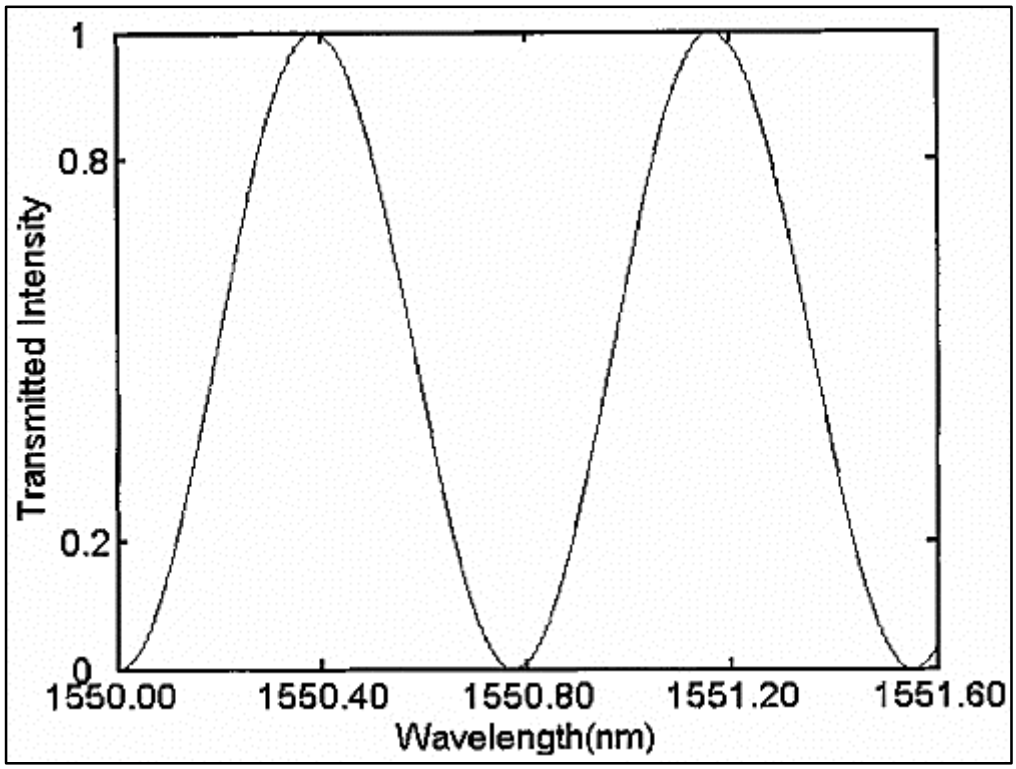

Figure (1.18): Transmission spectrum of Sagnac loop filter [51].

1.9 Thin Film Materials

Passive Q-switching can be realized using different materials with saturable absorption capability such as carbon derived materials (graphene, carbon nanotube), black phosphorus (BP), transition metal oxides (TMO), Transition metal dichalcogenide (TMD) and topological insulator (TI). Moreover, various film-forming polymer were applied in the fabrication of SA thin film for example Polyvinyl Alcohol (PVA), Poly(methyl methacrylate) (PMMA) and Polyethylene glycol (PEO). These are transparent polymer with refractive index comparable to that of silica glass of the fiber. As well as several surfactants were used as a dispersing agents put into a solution to enhance the separation of nanoparticles and to inhibit clumping. For example, sodium dodecyl sulfate (SDS). The next sections explain in details the materials used in this research and their properties.

1.9.1 Pure Metal (Aluminum)

Metal nanoparticles are bringing more attention for their powerful third-order susceptibility, surface plasmon resonance and rapid response dynamics. Many researchers have described the usage of metal NPs as an SA like silver, gold and copper [54–56]. Nevertheless, little attention was paid to aluminum nanoparticles in the scope of ultrafast optics. Recently, a Z-scan procedure was used to examine the optical nonlinearity of AlNPs planted in PVA film. This NL response was associated with the saturation absorption [57]. Basically, SA is linked with the imaginary part of the 3rd order nonlinearity, while FWM is related to the real part. Consequently, the SA with huge nonlinearity can produce multiwavelength Q-switched laser. In addition, nonlinear features like two-photon absorption, nonlinear scattering, and optical limiting effects of AlNPs in different solutions have been published in a previous study [58]. In comparison to other plasmonic metals, aluminum has a wider plasmon resonance range, lower manufacturing cost and a lower melting point of nearly 660 °C, which aid the fabrication process of AlNPs. Besides, AlNPs display physical and chemical traits that profoundly depend on the size of nanoparticles [59,60]. Fig. (1-19) shows the linear absorbance of aluminum for different film thickness. For these features, AlNPs has various applications like surface-enhanced Raman scattering, surface-enhanced fluorescence, photocatalysis, wide-band polarizer and photovoltaics [61–65].

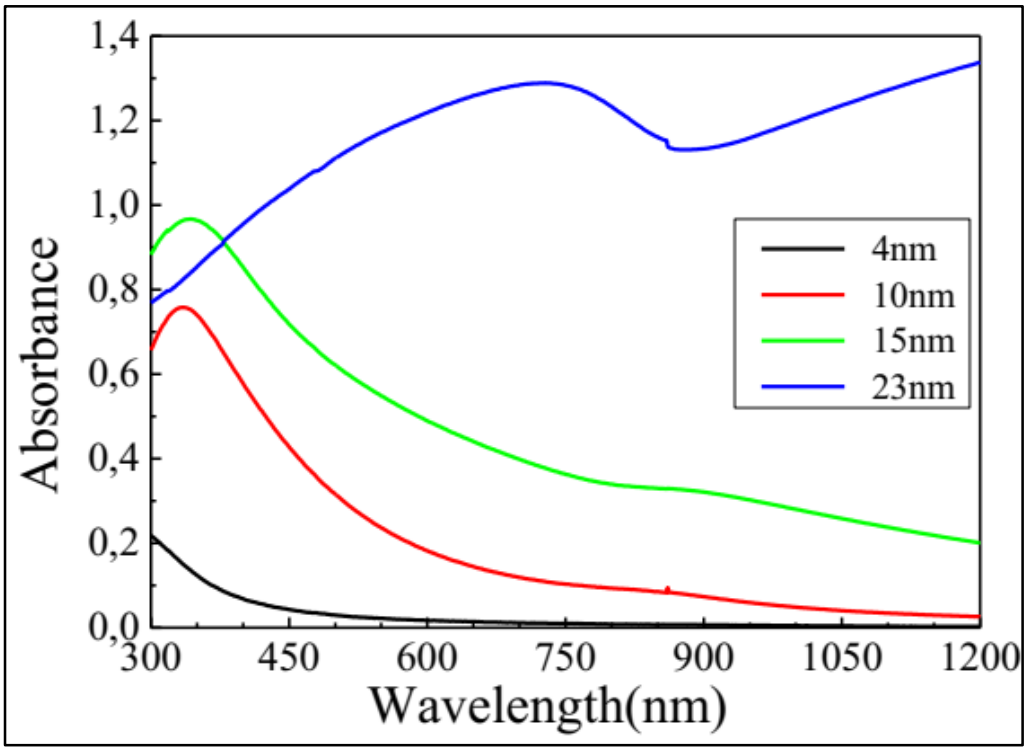

Figure (1.19): Absorbance of Al-NPs at different thicknesses [66].

1.9.2 Metal Oxide (Tungsten oxide)

New studies have discovered that transition metal oxides (TMO) hold a high 3rd nonlinearity, swift recovery time, and low saturation intensity, which makes them an encouraging SA. Among TMO materials, WO_3 has gained less concentration and remained undiscovered substance for pulsed and multiple wavelength generation. WO_3 emerges as a new SA competitor for nonlinear applications. Lately, tungsten oxide has been a subject of serious studies mainly because of its electrochromic, photo-catalytic, high T_c superconductivity and gas-sensing characteristics [67–69]. WO_3 is considered as an oxide semiconductor with an energy gap of 2.7 eV [70]. The linear absorption of WO_3 is depicted in Fig. (1-20). The conduction band has d-orbital with delocalized electrons which gives rise to charge-transfer characteristics for this oxide material. Semiconductors exhibit a simplistic two energy configuration consists of a conduction and valence bands.

Photons with energy greater than the energy of bandgap can stimulate charges from valance to conduction level. Another essential aspect of semiconducting SA is relaxation time. Faster relaxation time leads to shorter pulse duration. The relaxation time is greatly affected by electron mobility and the conductivity of the semiconductor materials. In recent study, Z-scan analysis at near infrared region confirmed high optical nonlinearity of WO_3 nanostructures [71]. It has been found that the nonlinear characteristics strongly depend on the shape of WO_3 nanostructures [72]. Moreover, pump induced birefringence Δn (t) for tungsten-based glasses has shown a response time >100 fs at 800 nm [73]. Very recently, Muller et al. has shown optical limiting properties in sphere WO_3 NPs with nonlinear 3rd susceptibility around 10^{-8} esu [74]. In addition, it has good thermal attributes, which is helpful for the SA material to dissipate the stored heat.

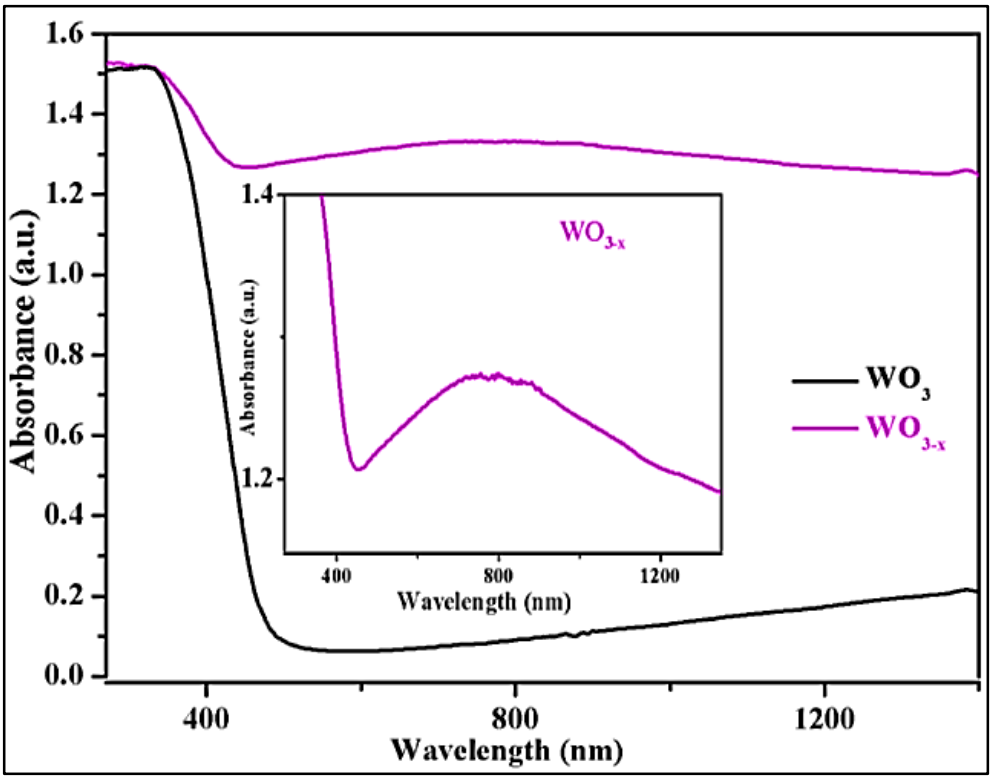

Figure (1.20): Absorbance of WO_3-NPs using UV-Vis diffuse reflectance technique [75].

1.9.3 Polyvinyl Alcohol

Polyvinyl alcohol is a translucent and water-soluble polymer broadly used in many applications such as adhesives, coatings, and plastics because of its ability to form films. PVA chemical formula anddensity is $(C_2H_4O)_x$ and 1.19 g/cm³, respectively. Also, it is considered to be biocompatible, thermally stable and hydrophilic which available in white powder form with varying grades and solubility properties [76]. PVA can efficiently preserve the nanoparticles from agglomeration. It has limited absorption in the visible domain. The bandgap of the PVA decreases with increasing the concentration of metal nanoparticles in the film. Moreover, the RI of PVA increases with boosting the concentration of implanted nanoparticles [77].

1.9.4 Sodium Dodecyl Sulfate

Sodium dodecyl sulfate (SDS) is most studied and extensively used as an anionic (negatively charged) surfactant. It is an organic material obtained in the shape of powder which easily dissolve in water [78]. The chemical formula consists of a twelve carbon series joined to a sulfate assembly ($CH_3(CH_2)_{11}SO_4Na$). SDS has density of ~ 1.01 g/cm³ which is very comparable to that of water. SDS is largely used in detergents for cleaning purposes which demand the removal of the greasy stains. An influential obstacle in the formation of thin films is the clusters of small particles due to van der Waals forces [79]. One possible treatment is to use certain dispersions to reduce the attractive electrostatic forces and to de-aggregate nanoparticles. Also, stable homogeneous colloids can be achieved with the aid of sonication process by applying ultrasonic frequencies to agitate particles and avoid clumping. SA based aqueous solution fabricated by using this method is proven to be simple and effortless.

1.10 Literature Survey

Multiwavelength operations as nonlinear phenomena have been demonstrated by various techniques. Previous studies regarding multiwavelength emission in 1μm, 1.5μm and 2μm wavelength bands will be reviewed and summarized in the following survey in chronological order.

In 2011, Luo et al. [31] proposed multiwavelength EDFL based on FWM using graphene. 11 wavelengths were achieved at room temperature with a SNR of 57 dB when the pump power reached 178 mW. Sagnac loop filter was incorporated into EDFL and wavelength spacing of 0.54 nm was obtained. EDFL was operating at CW state without Q-switching or mode locking pulses.

In September 2011, Luo et al. [52] also confirmed FWM driven by graphene in EDFL and YDFL by monitoring the spectral broadening. At 1550 nm waveband, a stable 23 peaks were generated with Q-switching pulse having a spacing of 0.2 nm. The maximum pulse energy, maximum repetition rate, and minimum pulse width were 72.5 nJ, 63kHz and 2.5μs respectively. While in 1um band, 5 peaks were observed with simultaneous Q-switching pulses having a duration of 3 μs and repetition rate of 56.2 kHz.

Multiwavelength operation in EDF based on FWM in SMF and HNL was reported by **Wang et al. in 2013** [80]. A multiwavelength comb was obtained by FWM that improve the suppression of homogeneous broadening in Er ions. At maximum pumping power of 300 mW, 5 lasing peaks were observed using the single mode fiber. In comparison, the SMF was replaced by 110m high nonlinear fiber and at 300 mW 7 lines were generated. The power fluctuation in HNL was 0.18 dB while for SMF was 3.18 dB indicating that FWM induced by HNL has better stability.

At tunable dual wavelength centered at 1521.1 and 1525.1 nm in EDFL using cascaded Sagnac loop was experimentally demonstrated by **Lin Ma et al. in 2014** [81]. Two segments of PMF were used and wavelength tuning of 40 nm was achieved by altering the refractive index of the filter using glycerol solution. The system achieved 50 dB signal to noise ratio.

In 2015, Huang et al. [82] multiwavelength generation in thulium-doped fiber laser was demonstrated. FWM in the ring cavity was caused by introducing 50 m of HNL to suppress mode competition in TDFL. 36 lines were obtained having 0.86 nm spacing. Long term stability test has shown that power fluctuation was about 1.6 dB.

Rashid et al. in 2016 [83] used black phosphorus (BP) was used in a YDFL to demonstrated a dual-wavelength and Q-switching operation. The setup included a D-shaped fiber as a spectral-selective filter. The dual outputs were at 1038.68 and 1042.05 nm. Moreover, the repetition rate enhanced from 52.52 to 58.73 kHz with the increase of the pump power. The lowest pulse width and greatest pulse energy of 1.16 μs and of 2.09 nJ were achieved respectively.

The multiwavelength generation from EDFL was described by **Ahmed et al. in 2016** [84]. 50 m of PCF fiber included into the cavity to obtain unstable multiwavelength. When inserting graphene, a stable 7 oscillation was achieved with fixed spacing of 0.47 nm. Also, the proposed EDFL was tunable over a range from 1550-1560 nm. It has good stability with ≤ 3 dB fluctuation.

In 2018, Liu et al. [85] proposed and realized switchable dual wavelength Q-switched EDFL utilizing black phosphorus coated on microfiber. The SA

has a modulation depth of 16% and saturation intensity of 6.8MW/cm^2. The two wavelengths were traced at 1542.4 and 1543.2 nm.

In 2018, Shi Li et al. [86] described a multiwavelength mode-locked EDFL based on WS_2 with microfiber knot. After inserting SA, which has a modulation depth of 5.6% a pulse width of 16.3 ps was achieved. Seven lasing lines by adjusting the polarization controller at pump power of 250 mW. The results obtained were attributed to the twin effect of WS_2 as a saturable absorber and excellent nonlinear component.

In 2018, Shi Li et al. [87] also achieved a multiwavelength CW thulium doped fiber laser by embedding a microfiber coil coated with black phosphorus so that 12 peaks with 0.54 nm spacing achieved at pump power of 427 mW located at 1882.5 nm. Signal to noise ratio of 40 dB and intensity fluctuation about 1.5 dB. The lasing spectrum was mainly due to combining a comb filter effect with FWM induced by black phosphorus.

In 2018, Salim et al. [88] described dual-wavelength process in the 1060 nm region by applying a highly nonlinear fiber as the wavelength selective filter. Due to its high nonlinear and birefringence features, the HNL fiber serves as a stabilizer for twin-wavelength fiber laser generation.

Al-Masoodi et al. in 2018 [89] demonstrate a passively Q-switched multi-wavelength YDFL applying carbon nanotubes incorporated in PEO host as SA. A spacing was 1.9 nm when pump level is between 62. 4 mW and 78.0 mW. The repetition rate is varied from 10.41 to 29.04 kHz. The largest pulse energy was 38 nJ and the least pulse duration of 8.87 μs was observed.

Sarah et al. in 2018 [90] reported the emission of a three wavelengths in passively Q-switched YDFL by means of SA based on zinc oxide NPs. The triple wavelength operation was located at 1054.7, 1058 and 1065.9 nm

respectively. In Q-switching regime, the laser produced a largest repetition rate of 87.9 kHz and minimum pulse width of 2.7 μs.

Qiongyu Hu et al. in 2019 [91] prepared tin diselenide and was included into PVA to form a SA to generate dual-wavelength mode locking in YDF. The laser showed an average power of 2.55 mW and a slope efficiency of 1.3%. By controlling the polarization orientation, four types of variable wavelength spacing of 0.4, 1.0, 1.5 and 1.9 nm were observed.

Shi Li et al. in 2019 [92] demonstrated a double-wavelength soliton mode-locked EDFL utilizing two-dimensional (2D) materials (SnS_2) implanted into PVA film to act as SA. The laser generates 2 peaks placed at 1536.7 and 1562.6 nm, with a pulse duration of 5.3 ps. The dual peaks were simply obtained at low threshold power of 75 mW.

1.11 Aim of the Work

The goal of this research is to realize multiwavelength generation in both erbium-doped and ytterbium-doped fiber lasers based on ring cavity configuration utilizing high nonlinear nanoparticles embedded in thin films. Moreover, Sagnac loop as a comb filter will be designed and incorporated inside the ring cavity to enhance the stability and obtain fixed wavelength spacing. The research objectives will be validated through the fabrication, characterization and testing the nonlinear performance of two new materials namely Al NPs and WO_3 NPs at 1μm and 1.5μm wavelength bands.

1.12 Thesis Outline

This thesis consists of four chapters including this chapter which serves as an introduction while the rest of the thesis is arranged as follow:

Chapter 2: explores the preparation and application of Al-NPs as a new type of NL nanomaterial. Moreover, the design calculations and transmission spectrum of the bandpass filter were presented as well. The figure-8 cavity configuration was adopted by including a Sagnac comb filter. Multiwavelength operation accompanied by Q-switching was also described in this chapter.

Chapter 3: demonstrates the fabrication procedures of the proposed WO_3 in two different methods as well as the characterization techniques. Throughout this chapter, multiwavelength operation as well as passive Q-switching in WO_3 were reported and discussed and conduct performance comparison between FWM in standard SMF and by using highly NL nanoparticles in terms of the number of wavelengths, stability, and signal to noise ratio (SNR) which can be useful in the field of optical communication.

Chapter 4: highlight the main conclusions based on the obtained results. This is followed by suggestions and recommendation to improve and extend this work in the future.

Chapter Two

Multiwavelength and Q-switching Generation in EDFL Using Aluminum Nanoparticles

CHAPTER TWO

Multiwavelength and Q-switching Generation in EDFL Using Aluminum Nanoparticles

2.1 Introduction

On the road to design a stable multiwavelength fiber laser, a type of high nonlinear nano-metal of pure aluminum are utilized to fabricate thin films to act simultaneously as a pulse modulator and nonlinear medium to assist multiwavelength generation for EDFL. In this chapter, drop-casting process followed by dehydration was adopted to prepare the thin film. PVA was chosen as a base polymer doped with metal NPs to form a NL film. The nonlinear materials were characterized by various techniques such as SEM, EDX, FTIR, XRD, linear and nonlinear absorption as well. Moreover, multiwavelength stabilization has been achieved by using interference loop filter based on Sagnac effect. It consists of a slice of panda fiber and a polarization controller. Design parameters including panda fiber length, beat length, birefringence and consequently, wavelength spacing have been calculated in this chapter. The proposed filters were characterized in terms of transmission spectra using a broadband source as shown in the following sections. The structure of chapter two is presented in Fig. (2-1).

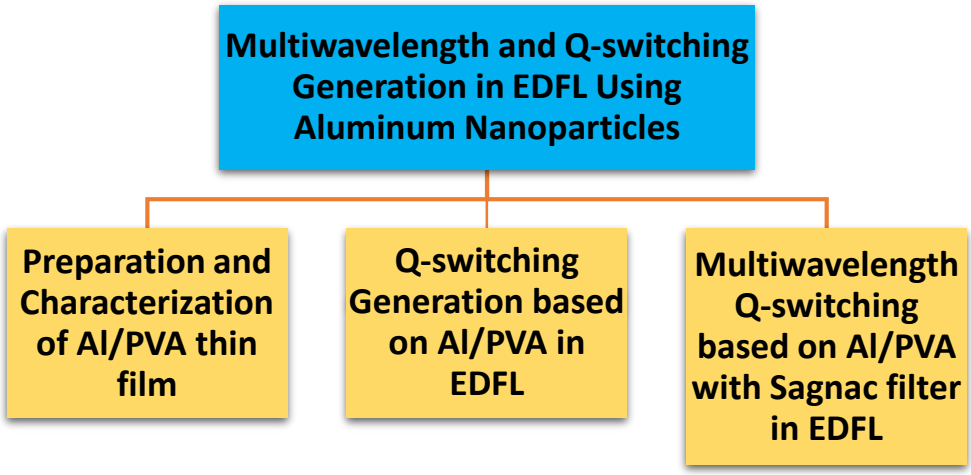

Figure (2.1): Structure of chapter two.

2.2 Q-switching Generation based on Al/PVA in EDFL

This section contains the film preparation, experimental setup, results, and discussion of the suggested Q-switched EDFL based on AlNPs thin film.

2.2.1 Aluminum/PVA Film Preparation

The Al-polymer thin film was made by drop-casting and solvent drying method. Firstly, PVA solution was formed by combining 1 g of PVA powder into 100 ml of deionized water and the blend was stirred utilizing a magnetic stirrer for 45 min at about 120 °C till it fully melted and converted into a transparent and uniform solution. then, 5 mg of high quality (99.9%) Al nanoparticles, having particles size of 40 nm, was blended with 5 ml of PVA solution and agitated gently for 2 h. Eventually, the prepared solution was dropped into a petri dish and kept to dehydrate at room temperature for a duration of 4 days.

After that, the SA thin film was ready to be used onto the fiber tip. However, such process cannot ensure a standardized film thickness or homogeneity. In general, this method presents several benefits like simplicity, low cost and the absence of sophisticated deposition equipment.

2.2.2 Aluminum/PVA Film Characterization

The fabricated thin film was characterized by various methods. In the first place, the morphology of Al-SA was examined via scanning electron microscopy (SEM) as shown in Fig. (2-2). The image exhibits that the SA thin film is clear from fractures, bubbles, and voids that may induce non-saturable loss. The image also shows the existence of micro-scale aggregates of Al-NPs. The SA insertion loss was affirmed to be about 10 dB.

The side-profile of the film was identified under a microscope and the measured thickness was about 25 μm. The linear absorption range of the synthesized film was examined via an ASE source (Thorlabs SLD1550s-A1), as presented in Fig. (2-3).

Aluminum nano-sphere was analyzed by the means of EDX spectroscopy, as depicted in Fig. (2-4). The EDX test gives a sharp peak of aluminum. Also, trace quantities are seen for oxygen and carbon, which can be linked to the occupation of carbonaceous impurities and partial oxidation of aluminum surface.

Moreover, (XRD) analysis was conducted to define the aluminum crystal arrangement as shown in Fig. (2-5). Strong peaks show high crystallinity of the material. The obtained peaks coincide with previous studies according to the lattice planes of (111), (200), (220) and (311), respectively [93,94].

As shown in Fig. (2-6), the FTIR manifested influential IR absorption around 430 cm^{-1} and 808 cm^{-1}, which means the existence of functional groups of (O–Al–O), which are the spectral fingerprint of Al with water or alcohol. Peaks, emerged about 2850 , 2310 and 3500 cm^{-1}, were associated with the effect of water vapor and carbon dioxide [95].

The nonlinear absorption of the proposed SA was identified by means of a twin detector setup. As represented in Fig. (2-7), the fitting of the obtained data was according to a two-level saturable system using Equation (1-17). The prepared SA sample has a modulation depth of 7%, a non-saturable loss of 10%, and a very low saturable intensity of 0.0015 MW cm^{-2}.

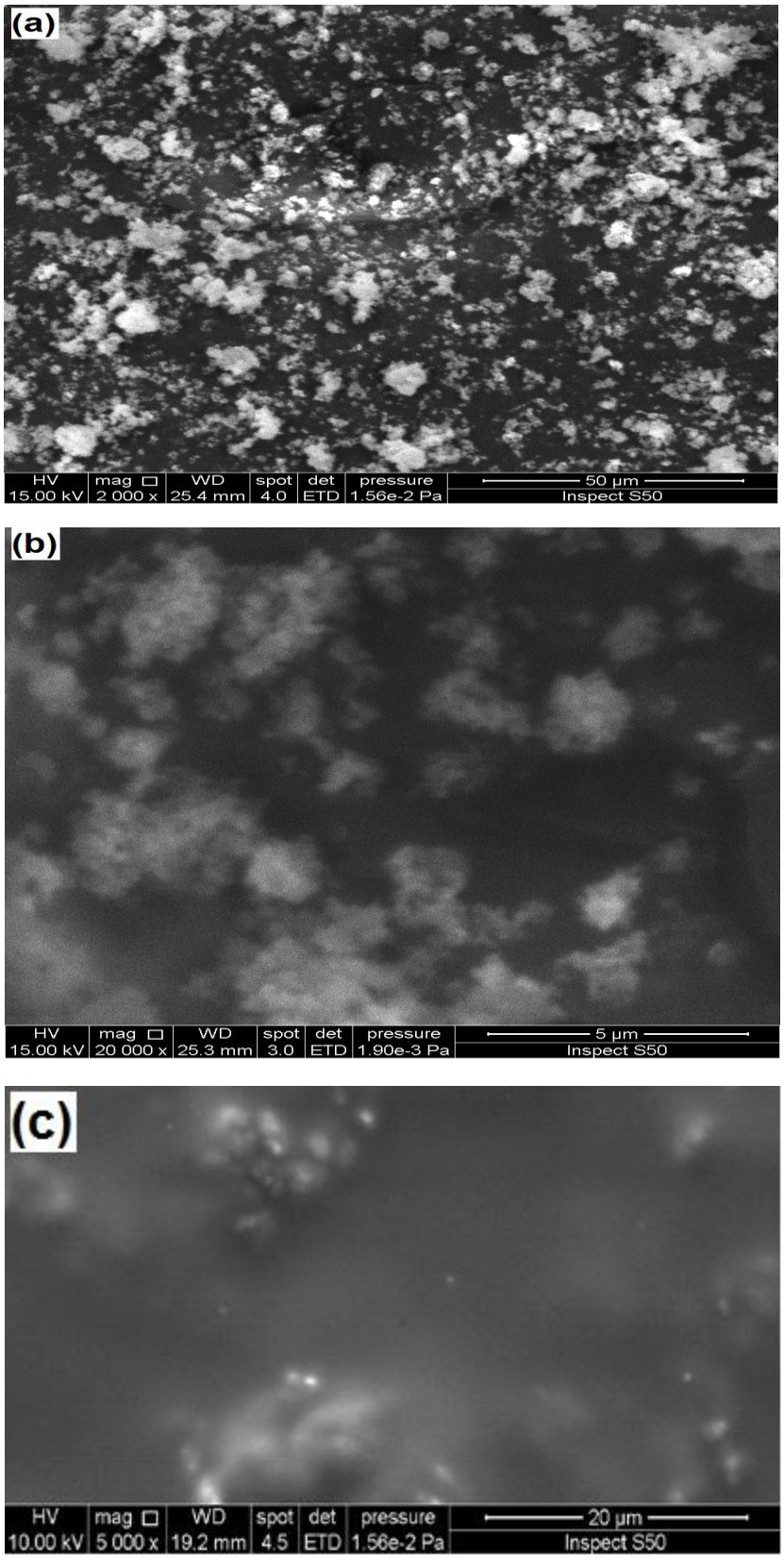

Figure (2.2): (a-b) SEM images of aluminum NPs (c) SEM of the Al/PVA film.

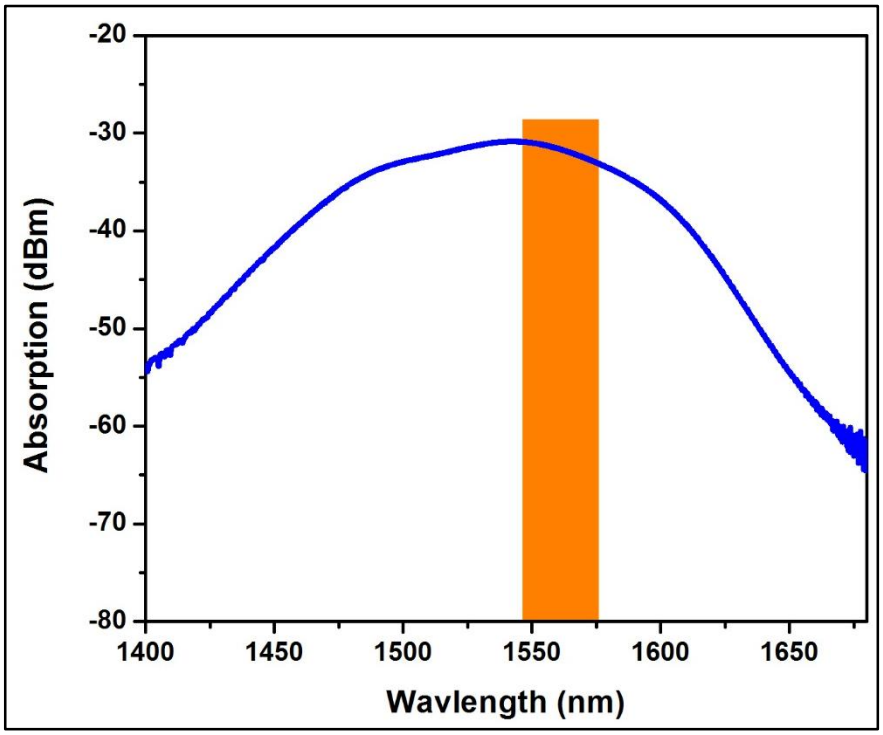

Figure (2.3): Linear absorption of aluminum-PVA film.

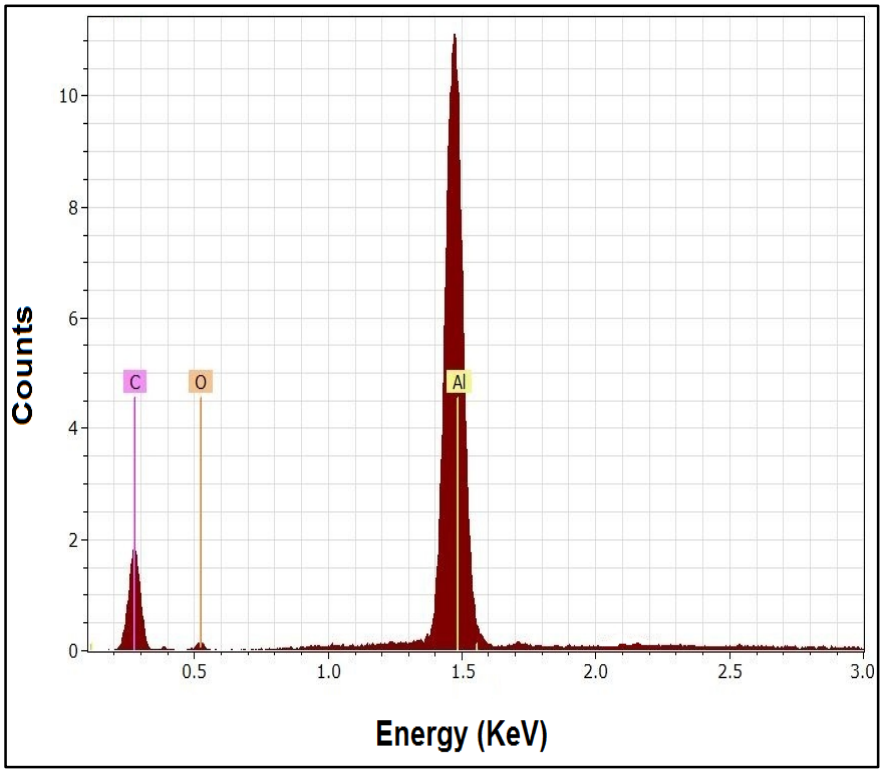

Figure (2.4): EDX analysis of aluminum NPs.

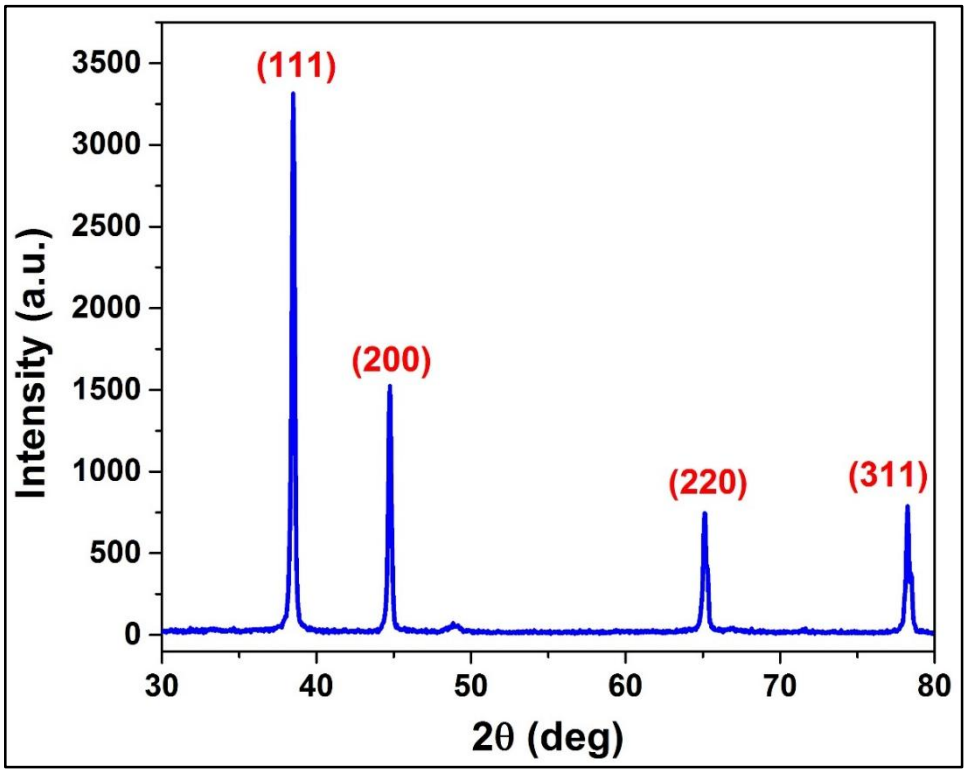

Figure (2.5): XRD pattern of aluminum NPs.

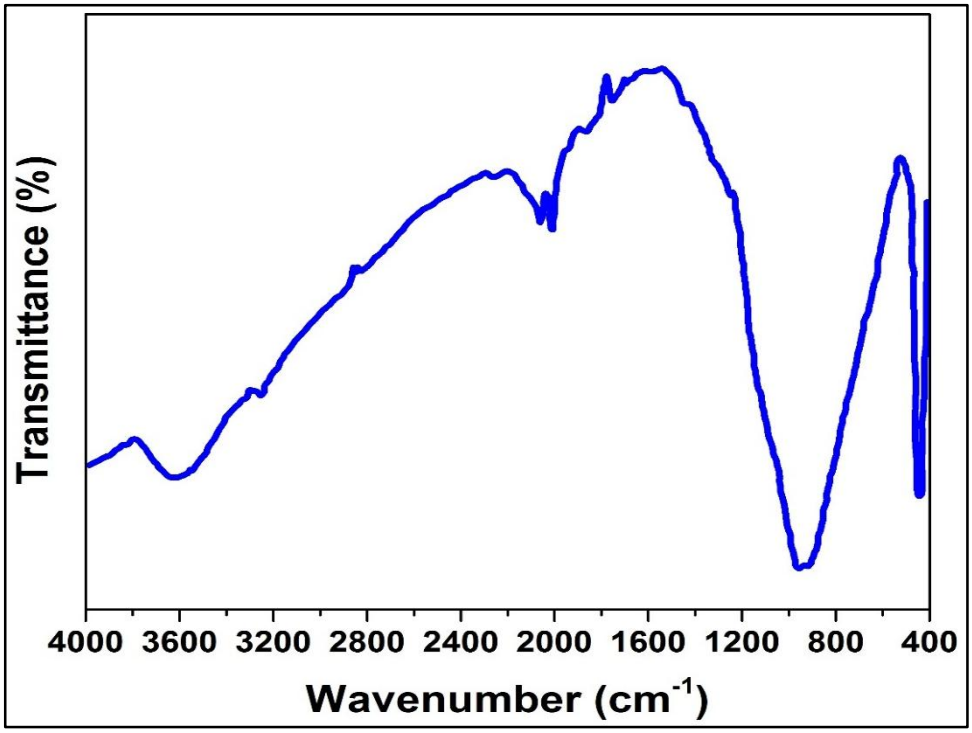

Figure (2.6): FTIR absorption of aluminum NPs.

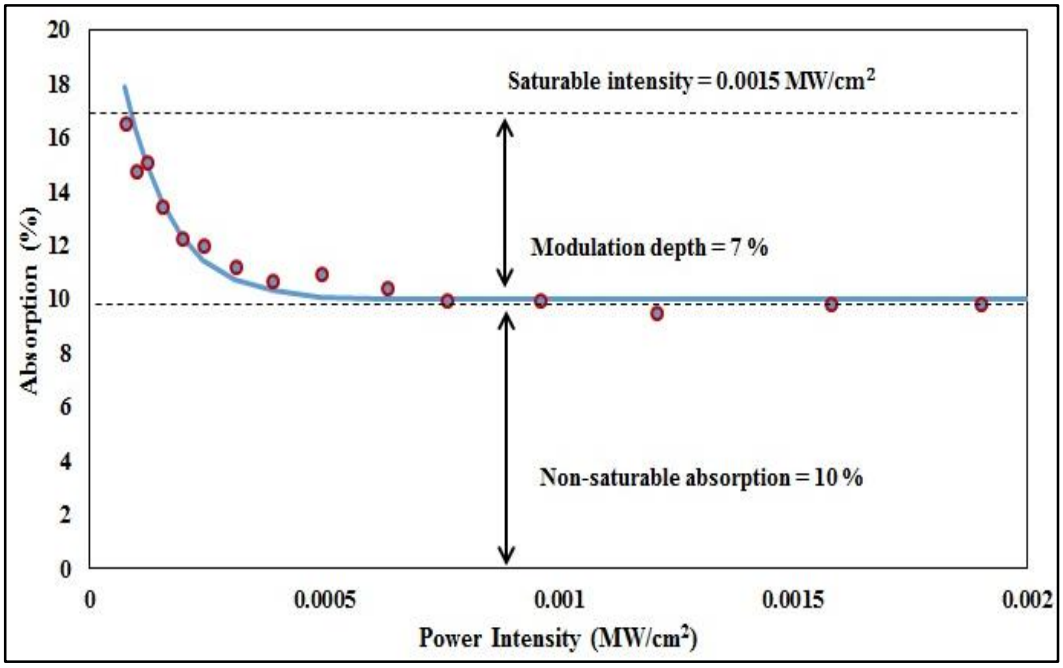

Figure (2.7): Nonlinear absorption of Aluminum-PVA film.

2.2.3 Experimental Details

The configuration of a Q-switched EDFL by utilizing aluminum-derived SA is demonstrated in Fig. (2-8). The system is formed of a 2 m Er-doped fiber (Liekki ER80- 4/125) as a gain medium, with 3000 ppm doping concentration, 0.2 numerical aperture and absorption coefficient of 27 dB m^{-1} at 975 nm. A polarization-independent isolator is included to ensure a single-propagation direction of light and limit back-reflection in a counter-clockwise path inside the cavity. The pump is provided by a 976 nm laser diode with an allowable power of 300 mW via a 980/1550 wavelength division multiplexer. The laser diode (BL976-SAG300) was controlled by a current and temperature module (Thorlabs ITC-4020). A 10 dB output coupler (OC1) was employed to leave 90% feedback into the ring cavity and drain 10% of the power inside the ring for observing the output signals. Another 3 dB coupler (OC2) was used to split the output power to provide two simultaneous measurements. The fabricated aluminum SA was implanted into the cavity between the fiber ferrules. The total length of the

cavity was 8 m and all parts were spliced using the fusion splicer (Fujikura FSM-60S). The Q-switching characteristics were monitored by an optical spectrum analyzer (Yokogawa AQ6370C), a 500 MHz digital phosphor oscilloscope (Tektronix DPO3052) connected with a 5 GHz ultrafast InGaAs photodetector (Thorlabs) and optical power meter (Gentec-EO Maestro).

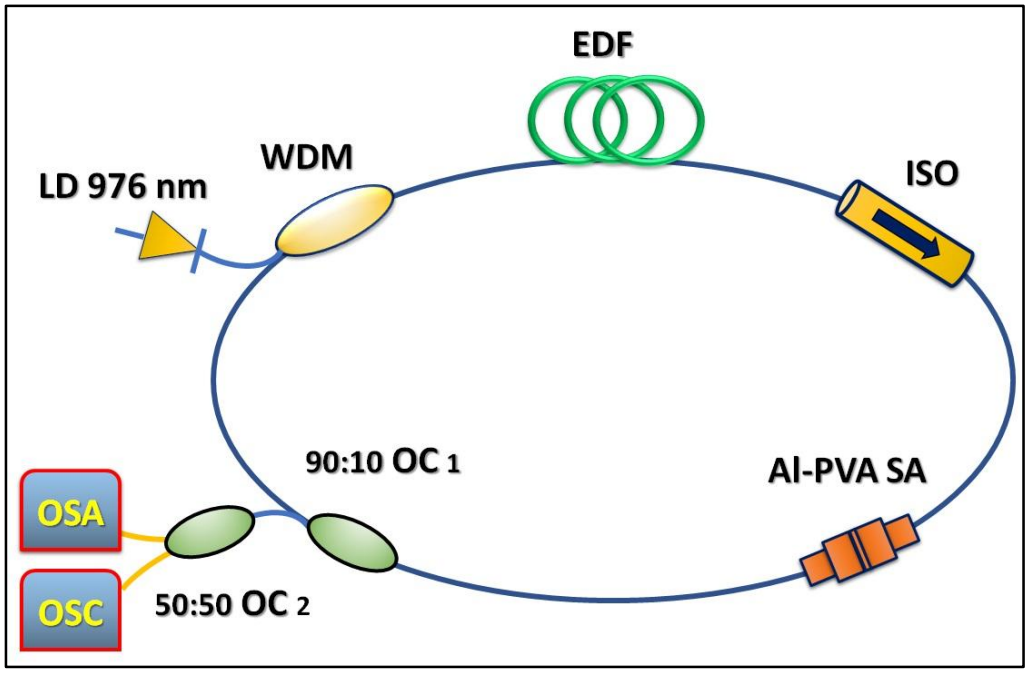

Figure (2.8): Setup of EDFL cavity.

2.2.4 Results and Discussion

The realization of the CW EDFL was examined first. The continuous-wave process was observed at a threshold pump level of 35 mW. When embedding the SA into the cavity, a Q-switched operation was achieved when the pump power approaches 156 mW. Fig. (2-9) depicts the spectrum of EDFL at a pump power of 300 mW and the central wavelength was located at 1567.6 nm and the FWHM was determined to be 1.9 nm. Fig. (2-10) represents the scope trace of Q-switched pulses at the threshold power 156 mW and the highest pump power 300 mW. The graph reveals a stable pulses train with consistent shape and amplitude. The individual pulse

envelope at 300 mW is given in Fig. (2-11). The pulse width and the repetition rate dependence on pump power are described in Fig. (2-12).

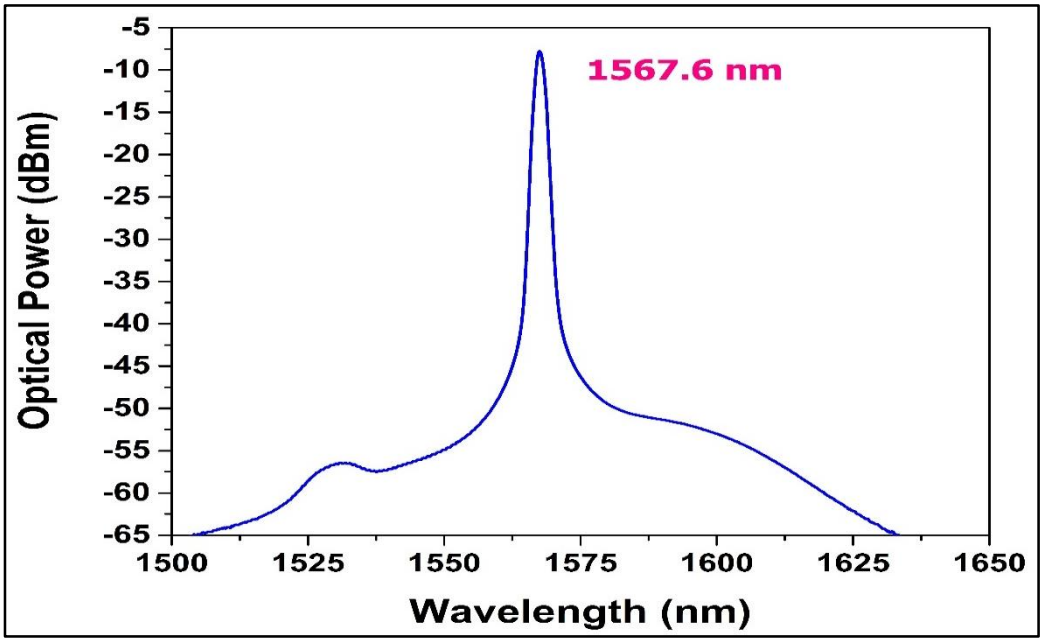

Figure (2.9): The output spectrum at 300 mW for the Q-switched laser.

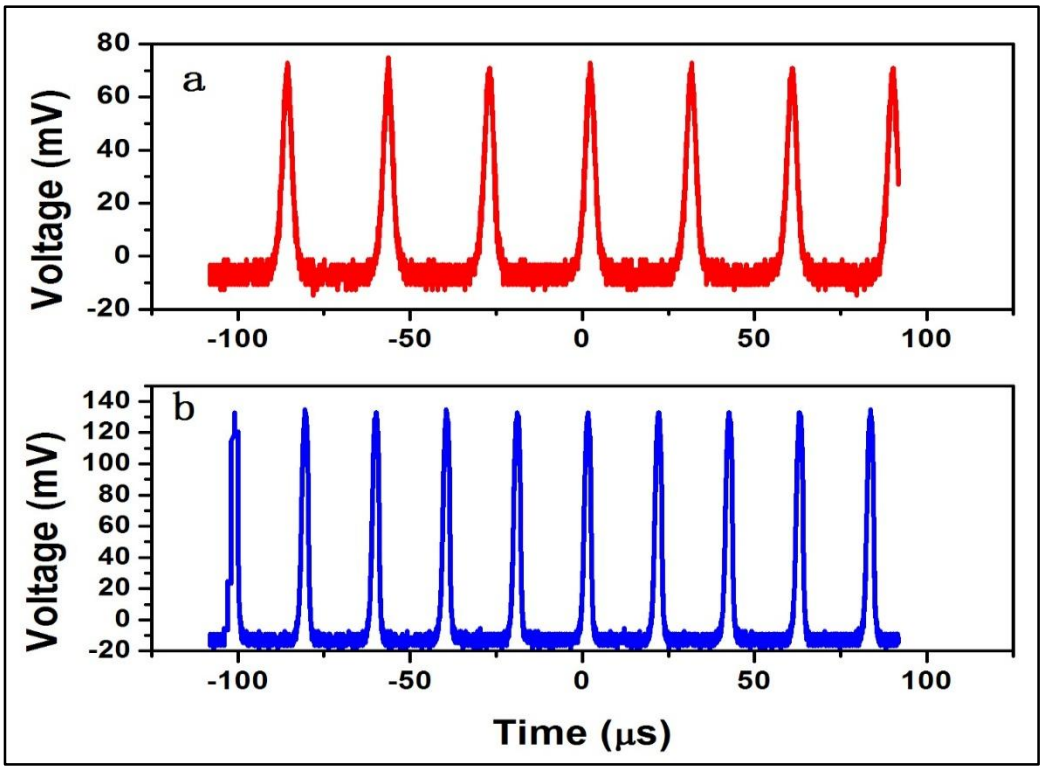

Figure (2.10): Pulses train at two pump powers (a) 156 mW (b) 300 mW.

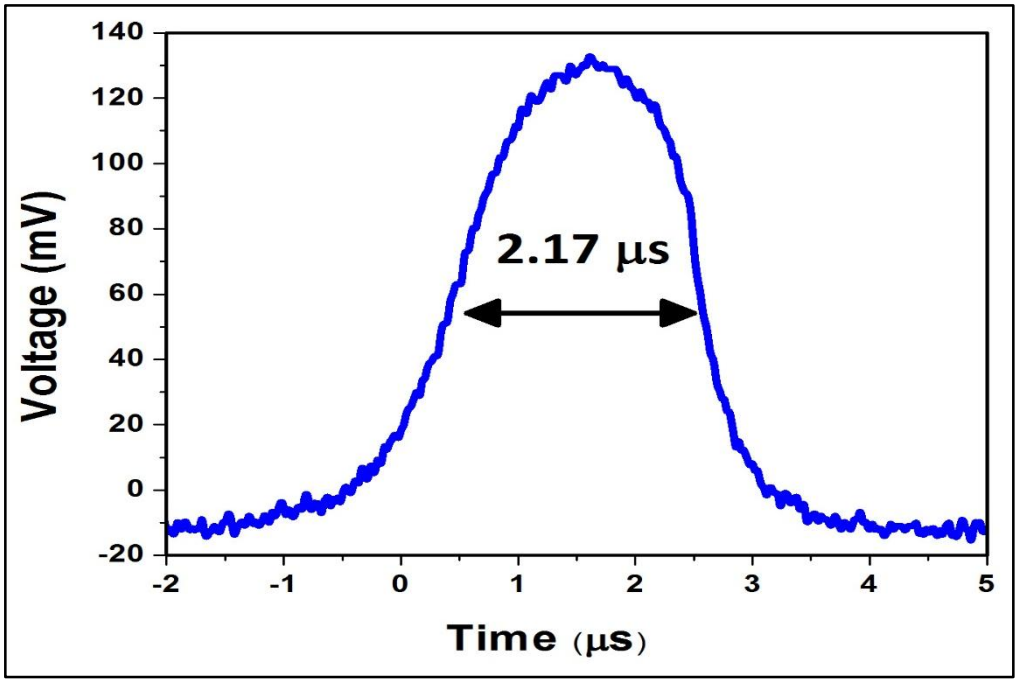

Figure (2.11): The single-pulse form at 300 mW.

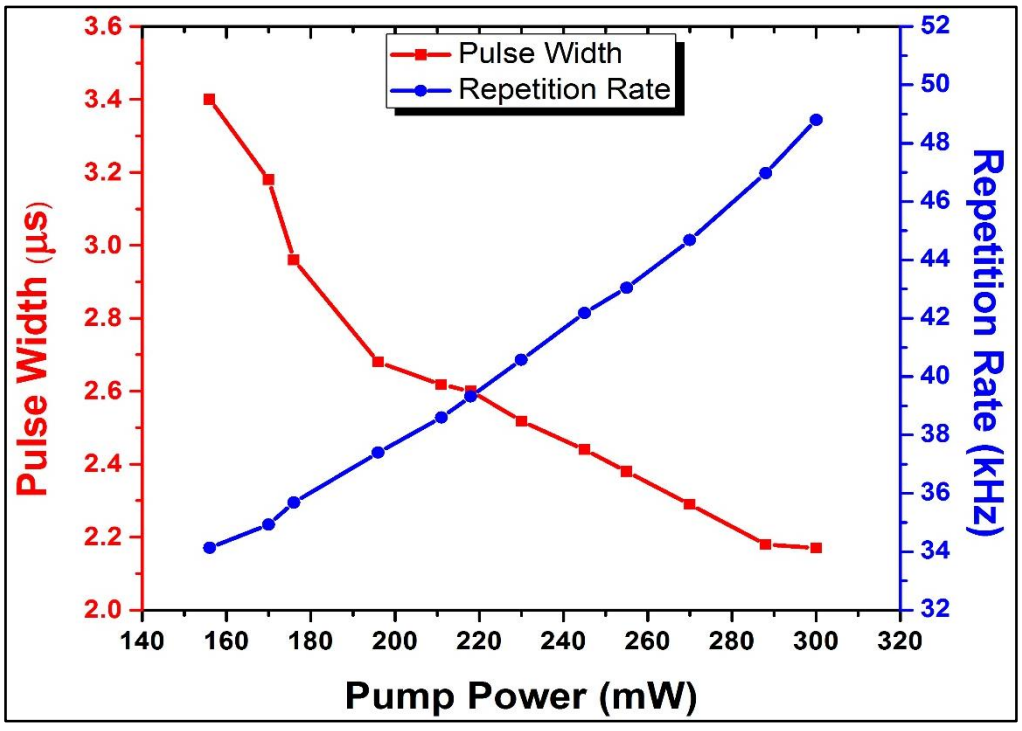

Figure (2.12): Pulse width and repetition rate vs pump power.

When regulating the pump level from 156 to 300 mW, the pulse width was diminished from 3.4 to 2.17 µs, whilst the repetition rate was grown from 34.13 to 48.4kHz because of population inversion in the medium arrives at the threshold swiftly at powerful pumping [31]. Fig. (2-13) exhibits a linear relationship of the pulse energy and the average power on the pump power. The energy is lightly increased from 8.7 to11.29 nJ and the power from 0.29 to 0.55 mW when the pump power is raised. The laser efficiency can be magnified by diminishing the insertion loss caused by the SA and reducing the cavity length and improve the splicing.

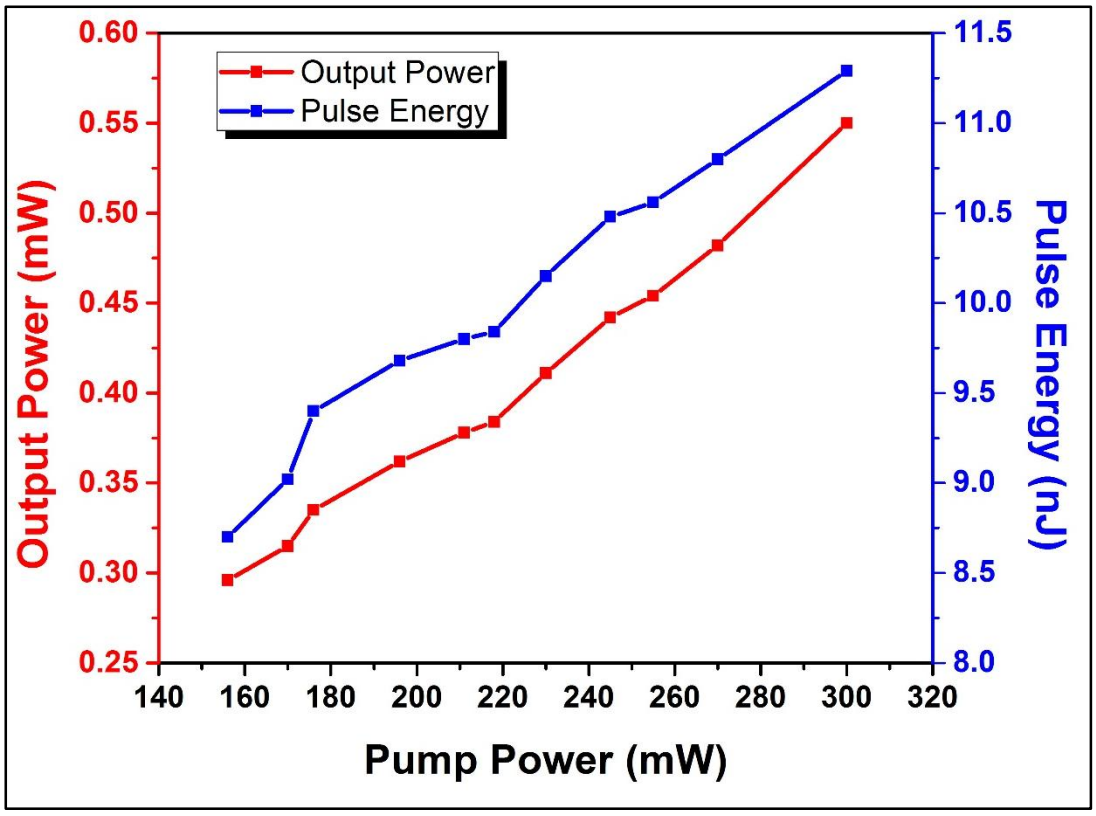

Figure (2.13): Average power and pulse energy vs the pump power.

Fig. (2-14) displays the RF pattern by using a fast Fourier transform algorithm stored in the digital scope to visualize the frequency content of the signal at pump power 300 mW. The fundamental frequency was taken at 48.8kHz with a signal-to-noise ratio approximately 45 dB, which means

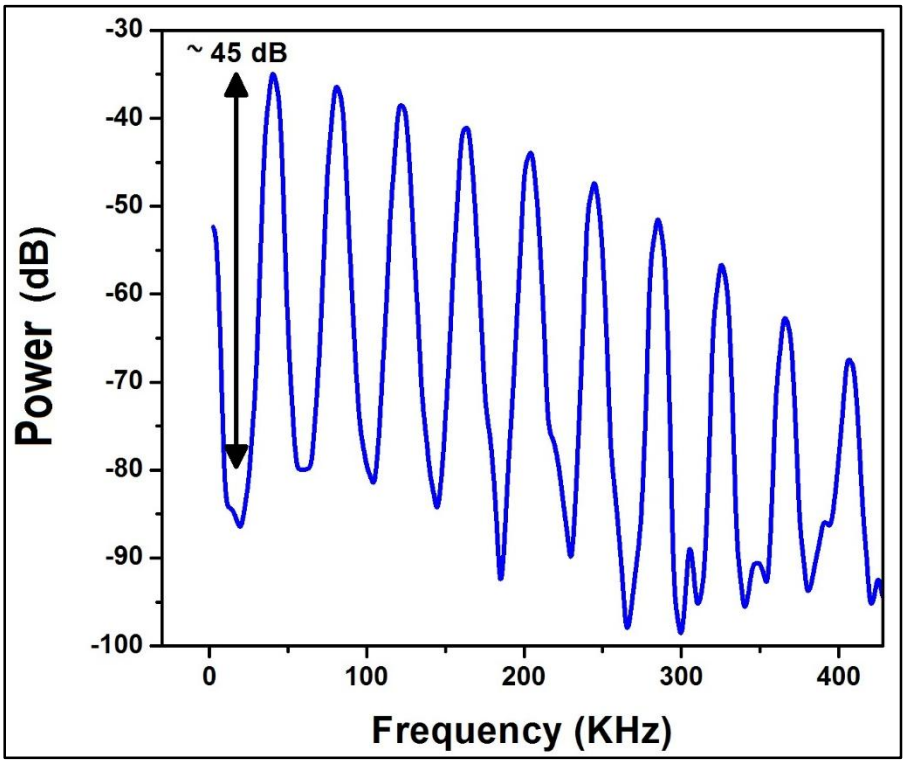

Figure (2.14): RF pattern of Q-switching based on AlNPs-SA.

a decent and stable Q-switched performance of the proposed laser configuration. The acquired results are related to a third-order nonlinearity of the aluminum. One of the most crucial aspects for the increase of optical nonlinearity of Al/PVA films is the dielectric confinement effect. AlNPs have a nonlinear refractive index of $n_2 \sim (3 \times 10^{-8})$ $cm^2\ W^{-1}$ and nonlinear susceptibility of Im $\chi^{(3)} \sim (4 \times 10^{-14})$ esu [57]. The saturable intensity of our proposed SA is low, which indicates the prospect of a mode-locking using this SA. Furthermore, the experiment was successfully repeated in the following weeks and, throughout the operation, the SA has no optical damage. This point out that our suggested SA is durable and dependable. Table (2-1) show a survey of the lately published outcomes of Q-switching regarding diverse types of SA materials. As shown in the table, the Al-based SA maintains an excellent saturable absorption performance. It has the least saturation intensity that has been ever published.

Besides, aluminum SA has a larger modulation depth than Al_2O_3, InSe, $MoSe_2$, and ITO. The pulse duration comparison reveals that the proposed SA has a comparably short pulse width between other SAs. the findings obviously demonstrate that the AlNP-SA is a good competitor for pulse formation.

Table (2-1): Comparison between diverse types of SA in Q-switched EDFL.

SA	Operating Wavelength (nm)	Max. Repetition Rate (kHz)	Min. Pulse width (µs)	Modulation Depth%	Saturable Intensity (MW/cm^2)	Ref.
CuNP	1561	101.2	4.28	36	20	[55]
InSe	1532.2	13	8.3	3.4	60.1	[96]
Al_2O_3	1560.6	81	2.8	3.5	0.03	[18]
Sb	1559	98.04	5.36	23	15	[97]
ITO	1530.3	81.28	1.15	0.83	9.87	[98]
$MoSe_2$	1566	35.4	9.2	4.7	3.4	[99]
SnO_2 + filter	1521–1565	65.6	2.92	27.42	0.0018	[100]
AlNPs	1568.8	48.8	2.17	7	0.0015	This work

2.3 Multiwavelength Q-switching Generation based on Al/PVA with Sagnac Filter in EDFL

This section includes filter design, experimental setup, results, and discussion of the proposed multiwavelength Q-switched EDFL based on AlNPs thin film.

2.3.1 Sagnac Filter Design and Characterization

The Sagnac filter, that serves as a comb filter, is assembled from a combination of a 12 m PMF (panda type) purchased from Thorlabs (PM1550-XP) with a beat length of around 5mm at 1.5 μm and (2 × 2) coupler with a coupling ratio of 50:50. A cross section image of PM fiber was taken using optical microscope as shown in Fig. (2-15). The specification details of PM fiber are presented in Table (2-2). The tuning element in the filter was the polarization controller to alter cavity birefringence by adjusting the polarization of the perpendicular states via wave plates (paddles). FPC560 is an unloaded controller which can be loaded with any fiber type. It contains 3-paddles which act as a λ /4 wave plate, a λ /2 wave plate, and a λ /4 wave plate connected in sequence as shown in Fig (2-16). By modifying the angels of paddles, the output polarization can be in any arbitrary orientation. According to the manufacturer data sheet, 3 turns for λ/4 retardation and 6 turns for λ/2 retardation per paddle were used respectively utilizing a 900 μm SMF jacketed fiber. The specification of PC and coupler are given in Table (2-3) and Table (2-4), respectively. After assembling the filter, the transmission range of the Sagnac filter has been obtained by employing the experimental arrangement as presented in Fig. (2-17).

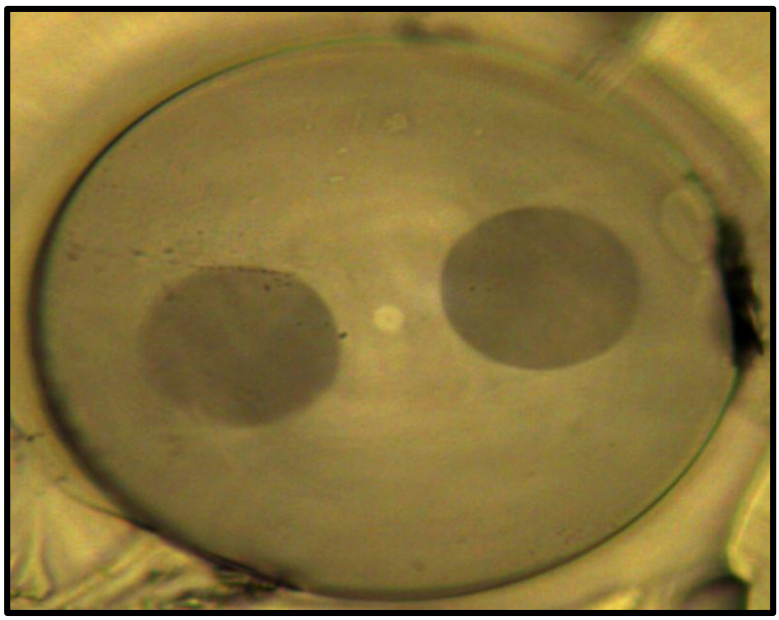

Figure (2.15): Polarization maintaining fiber (panda type).

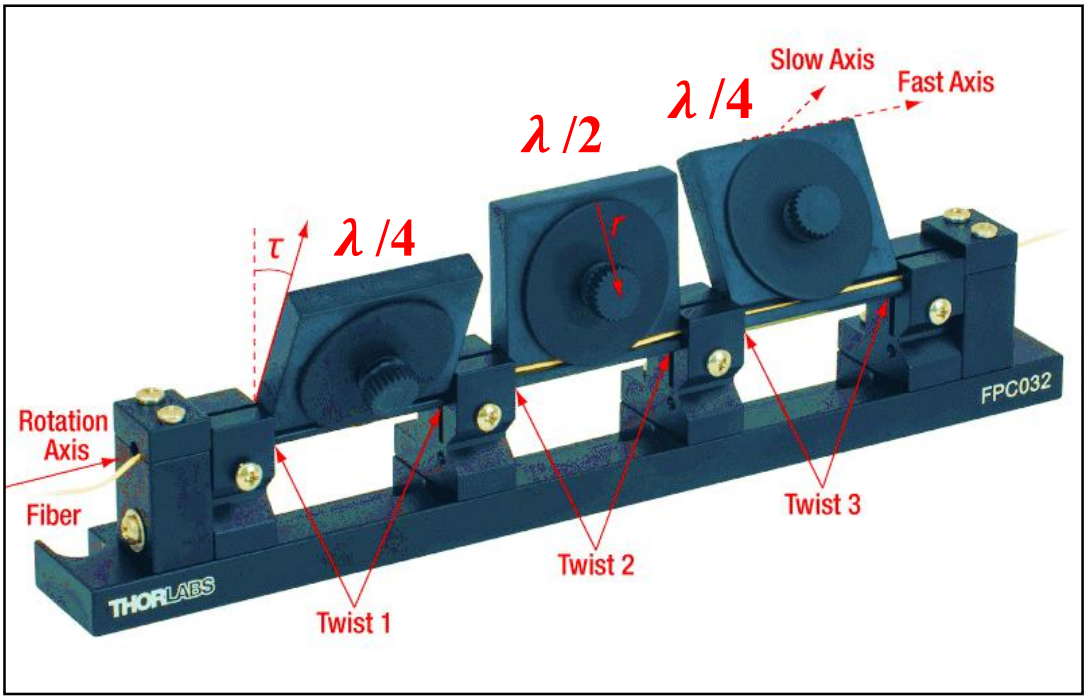

Figure (2.16): Polarization controller [101].

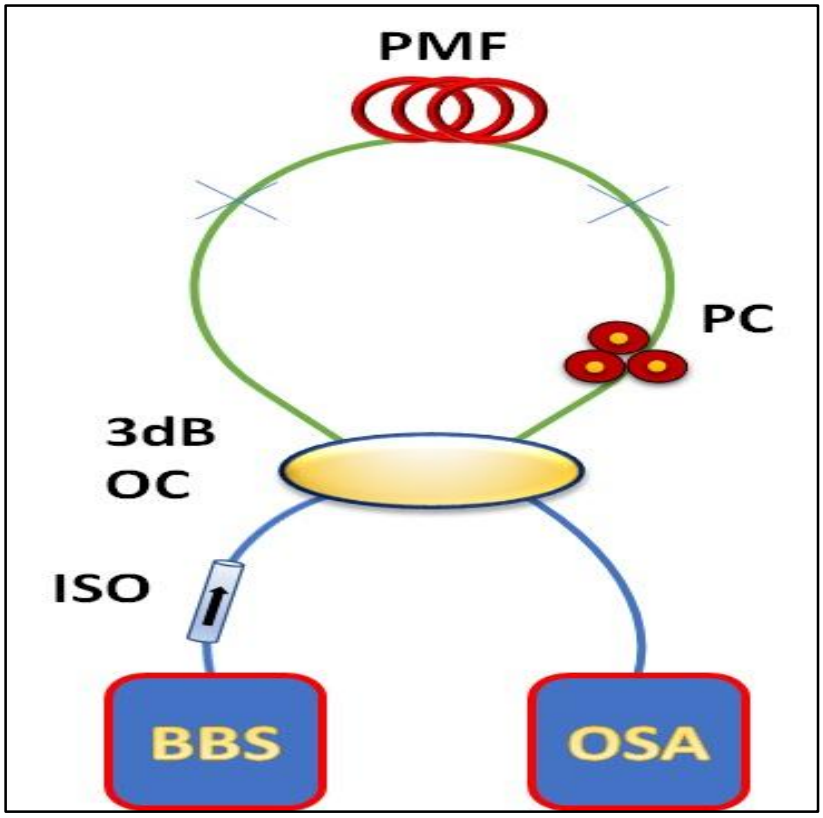

Figure (2.17): Setup for Sagnac filter characterization.

A broadband source from Thorlabs (SLD1550s-A1) was coupled to the input arm of the coupler. An isolator was employed to protect the source from reflected optical power. The transmitted power was collected at the output arm which was connected directly to the optical spectrum analyzer as depicted in Fig. (2-18) which clearly shows the wavelength spacing of 0.48 nm. Fiber birefringence was determined from the relation (1-23) in the previous chapter and it was equal to (3.1×10^{-4}). The beat length was obtained from Thorlabs datasheet shown in Table (2-2). The wavelength spacing also called the free spectral range was calculated using Equation (1-28) from chapter one and was found to be (0.48 nm).

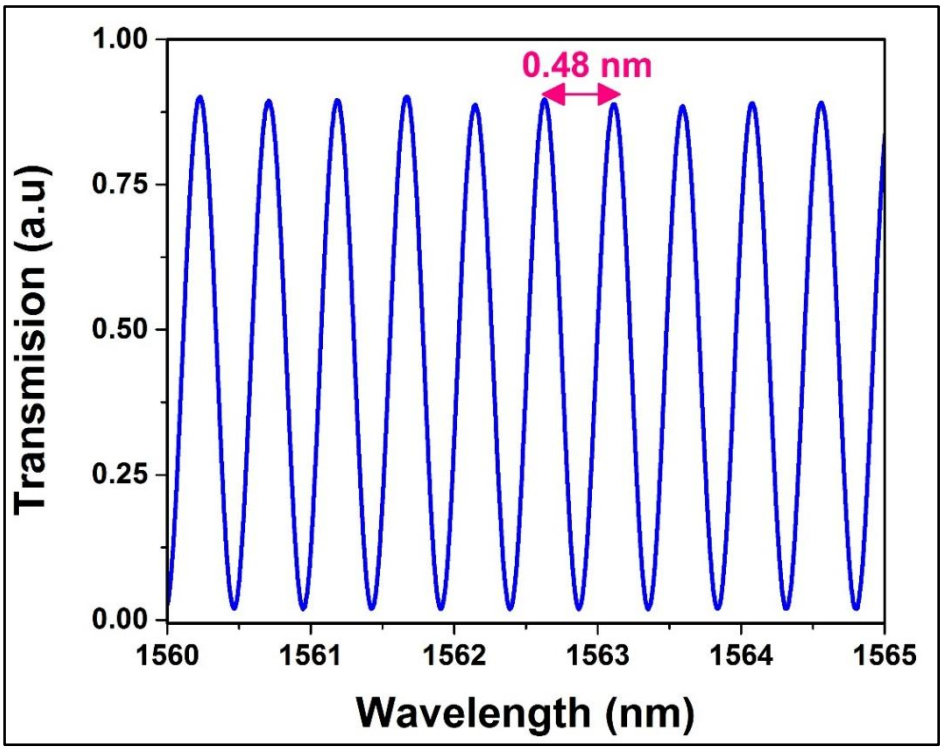

Figure (2.18): Comb filter transmission spectrum.

Table (2-2): Polarization-maintaining fibers (PM1550-XP).

Parameter	Value
Core Diameter	8.5 μm
Cladding Diameter	125 ± 2 μm
Coating Diameter	245 ± 15 μm
Numerical Aperture	0.125
Attenuation	< 1.0 dB/km @ 1550 nm
Operating Wavelength	1440 - 1625 nm
Mode Field Diameter	10.1 ± 0.4 μm @ 1550 nm
Beat Length	≤ 5.0 mm @ 1550 nm

Table (2-3): Specification of the 3-Paddle Polarization Controller (FPC560).

Parameter	Value
Operating Wavelength Range	1260 - 1625 nm
Fiber type	Bare fiber or a jacket up to Ø900 µm
Loop Configuration	3:6:3
Loop Diameter	56 mm
Bend Loss	≤ 0.1 dB
Number of Paddles	3
Paddle Rotation	±117.5°

Table (2-4): Wideband coupler **(**TW1550R5F2).

Parameter	Value
Coupling Ratio	50:50
Center Wavelength	1550 nm
Minimum Bandwidth	±100 nm
Insertion Loss	≤ 3.6 dB
Max. Power Level	1 W (With Connectors or Bare Fiber) 5 W (Spliced)

2.3.2 Results and Discussion

The experimental setup is the same for the previous section except with the inclusion of Sagnac loop filter as shown in Fig. (2-19). At the start, the CW process was seen at 72 mW of threshold pump power centralized around 1563.18 nm. The Q-switching threshold was obtained at 196 mW. Following the incorporation of the comb filter into the ring cavity, and by boosting the pump level from 75 to 300 mW, multi-oscillating wavelengths were obtained with a suitable PC adjustment. The multiwavelength laser has a SNR of about 30 dB and a free spectral range (FSR) of around 0.48 nm, as shown in Fig. (2-20) and Fig. (2-21).

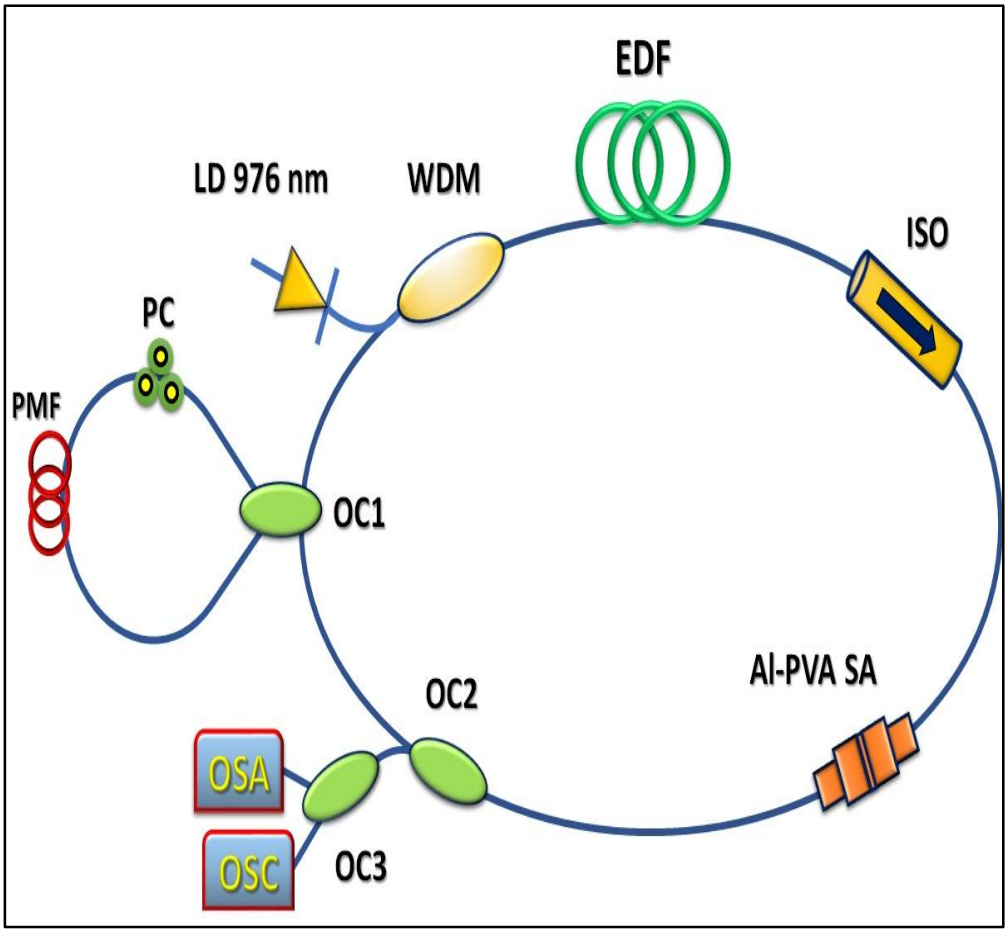

Figure (2.19): Figure-of-8 of multiwavelength EDFL.

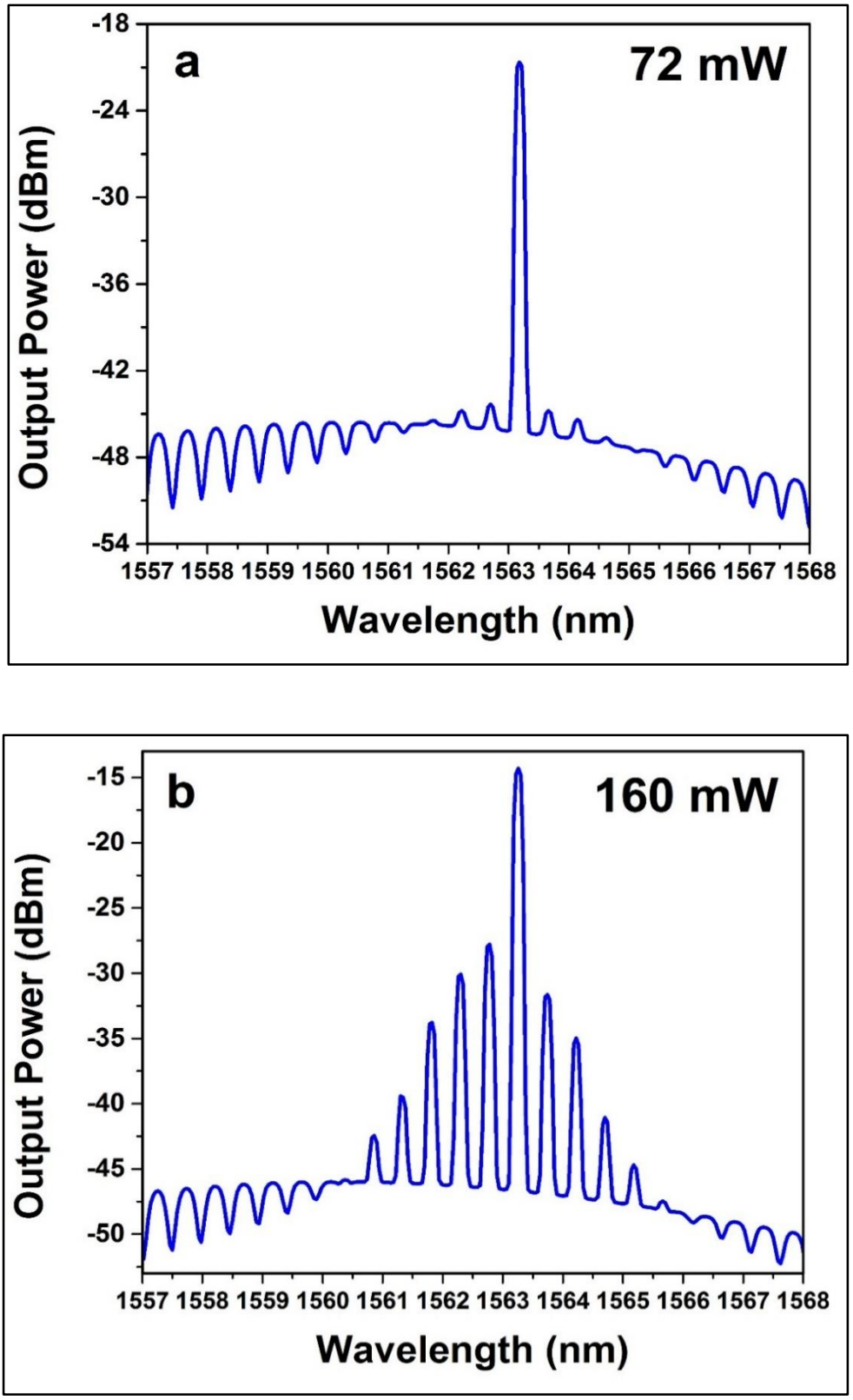

Figure (2.20): Multiwavelength spectra based on Al-PVA at various pump power: (a) 72 mW, (b) 160 mW.

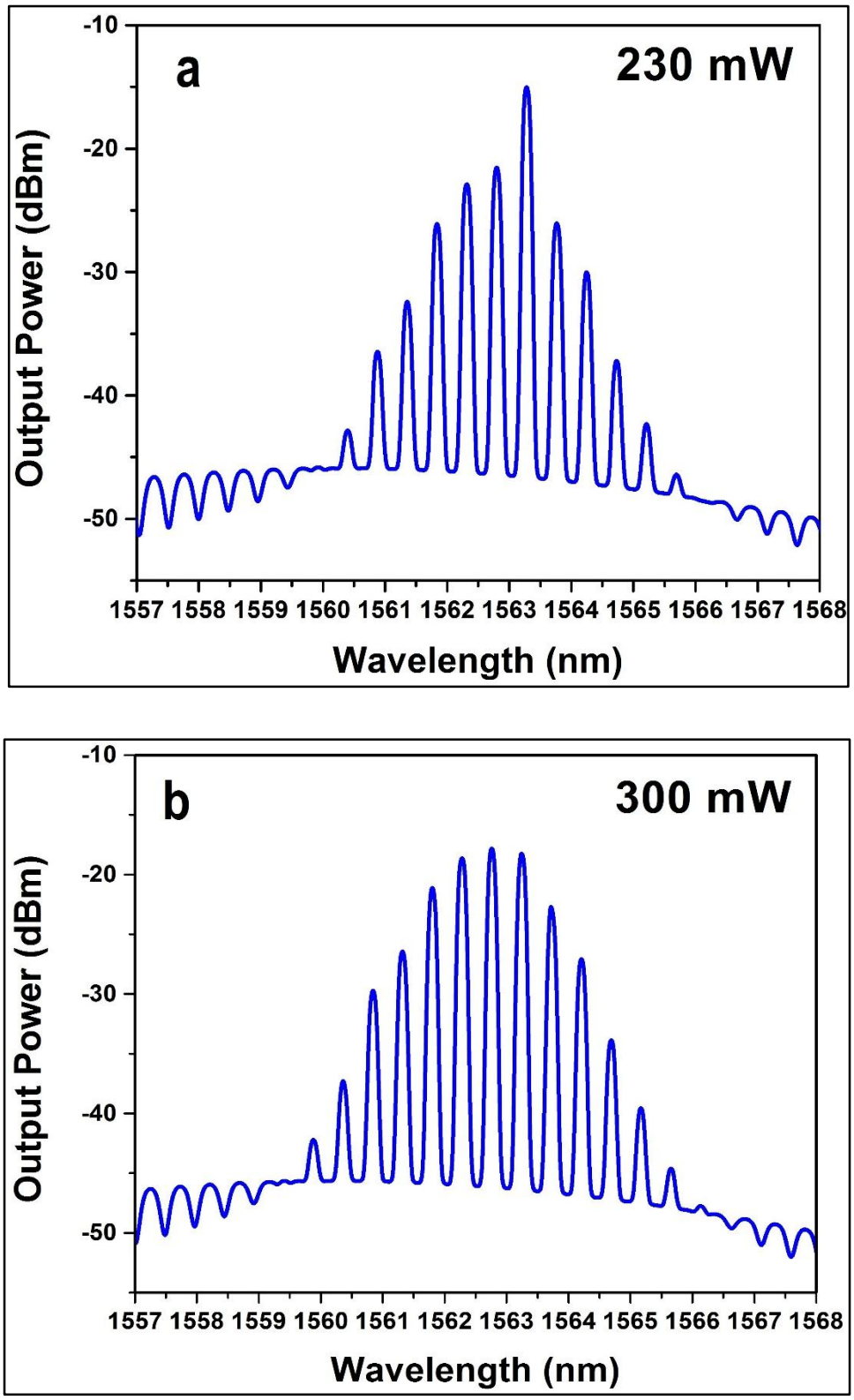

Figure (2.21): Multiwavelength spectra based on Al-PVA at various pump power: (a) 230 mW, (b) 300 mW.

In order to confirm the stability of multiwavelength lasing, the laser output was recorded at 5 min periods for 25 min when the pump power at maximum, as described in Fig. (2-22). The results reveal remarkable long-term stability of the proposed SA. The multiline oscillation has shown a wavelength deviation of 0.35 nm and a power fluctuation of 5.7 dB. Also, peaks 5 and 6 settled at 1562.24 nm and 1562.72 nm, respectively, show the utmost power stability as plotted in Fig. (2-23) and Fig. (2-24) respectively.

The non-linear refractive index (n_2) for aluminum was estimated to be ~ (3×10^{-8}) cm^2 W^{-1} [32], which created influential participation to improve the FWM and consequently the limitation of mode competition and hopping to stabilize the multiwavelength laser. It is worth noting that the nonlinear properties of a SA material rely on several parameters for example, concentrations of nanoparticles in the polymer matrix, preparation process and thickness of the SA film.

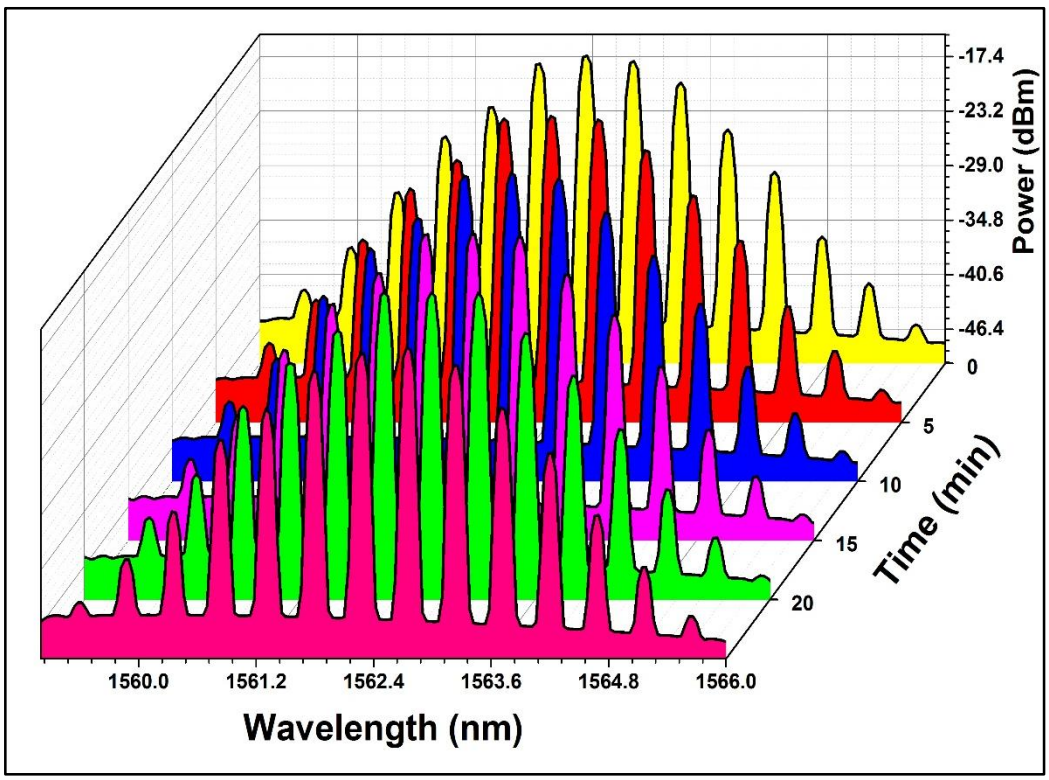

Figure (2.22): Multiwavelength stability spectrum.

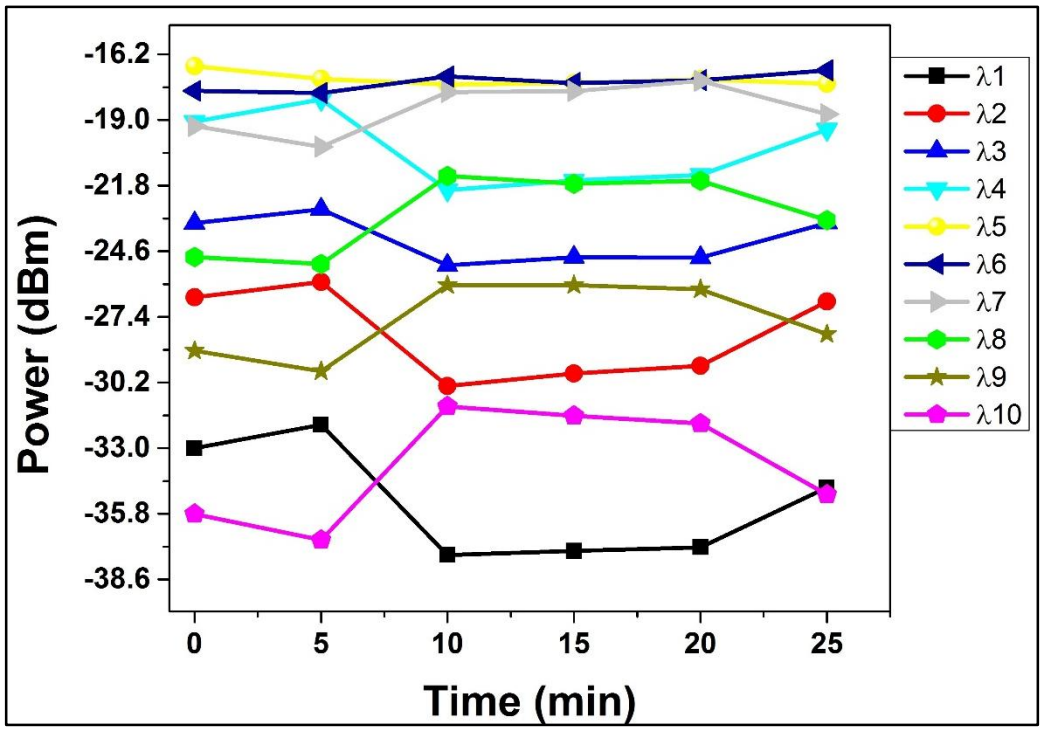

Figure (2.23): Power fluctuation with time.

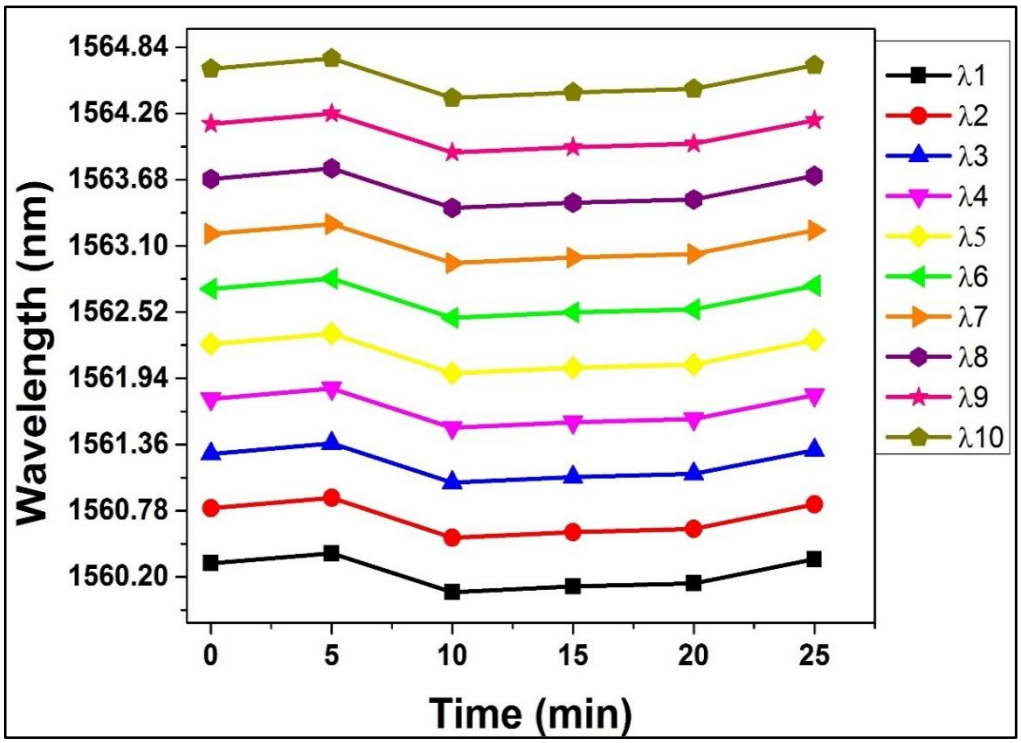

Figure (2.24): Wavelength drift with time.

Once the pump power reached 300 mW, the pulse has a minimum width of 2.36 µs and a maximum rate of pulse 33.45 kHz, as presented in Fig. (2-25). The train of pulses and the single pulse shape at the highest pump power is given in Fig. (2-26) and Fig. (2-27) respectively. As given in Fig. (2-28), the pulse energy and the average output power have generally linear dependence on the pumping and they were raised up to 7.67 nJ and 0.25 mW, respectively.

The opportunity for additional enhancements, like more oscillating lines and more average power, can be reached by optimizing the performance of the SA, reducing cavity length and improve filter designs [102]. Figure (2-29) exhibits the RF spectrum showed by the digital oscilloscope at a pump power of 300 mW. The fundamental frequency was at 33.45 kHz with SNR around 40 dB, suggesting good stability for the induced pulses.

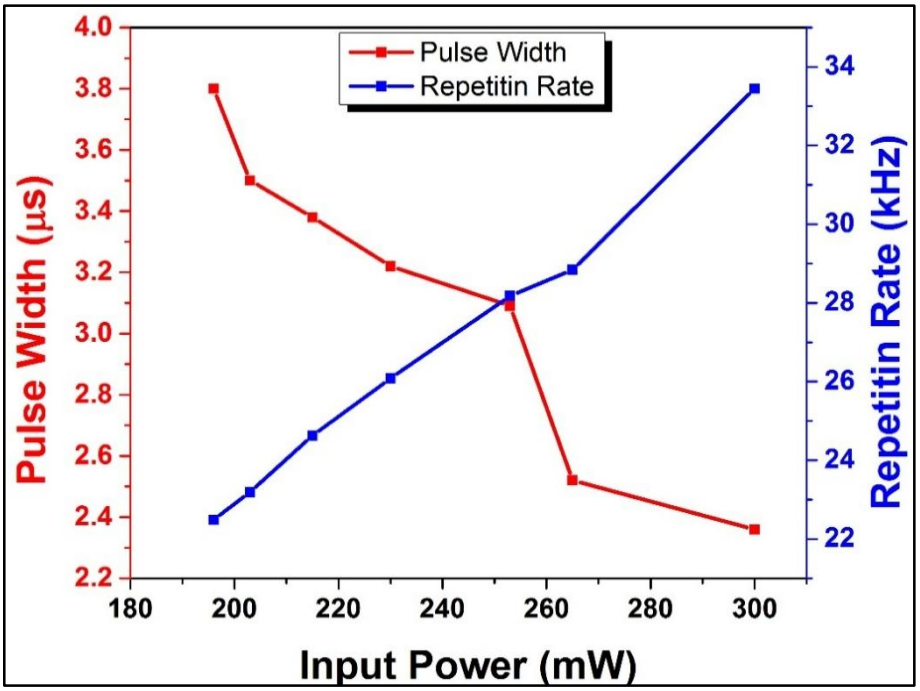

Figure (2.25): Pulse width and repetition rate with the pump power increment.

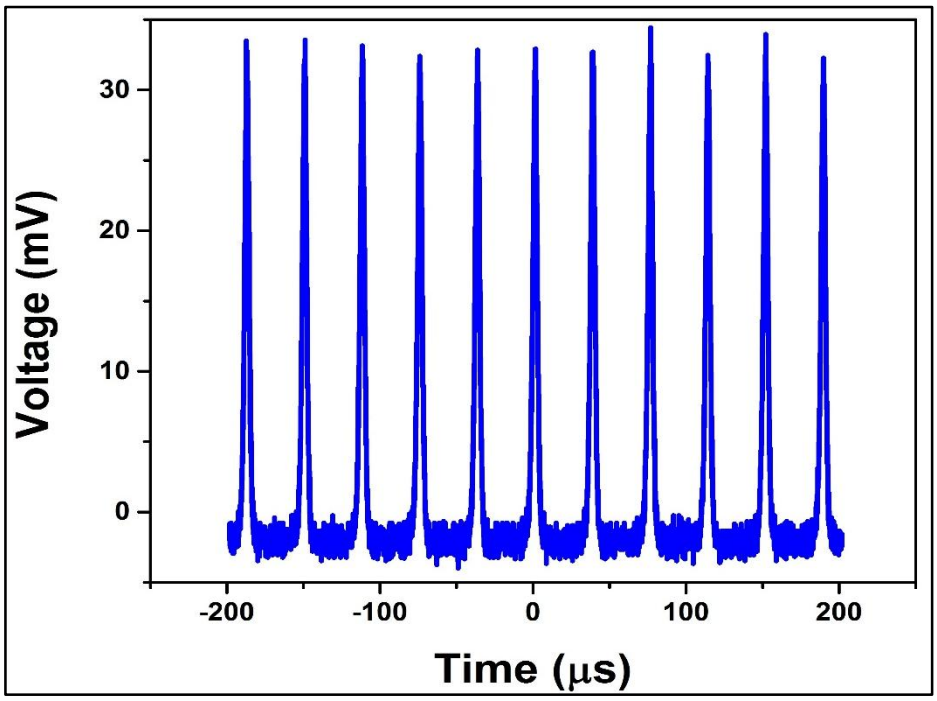

Figure (2.26): Pulse train at 300 mW pump power.

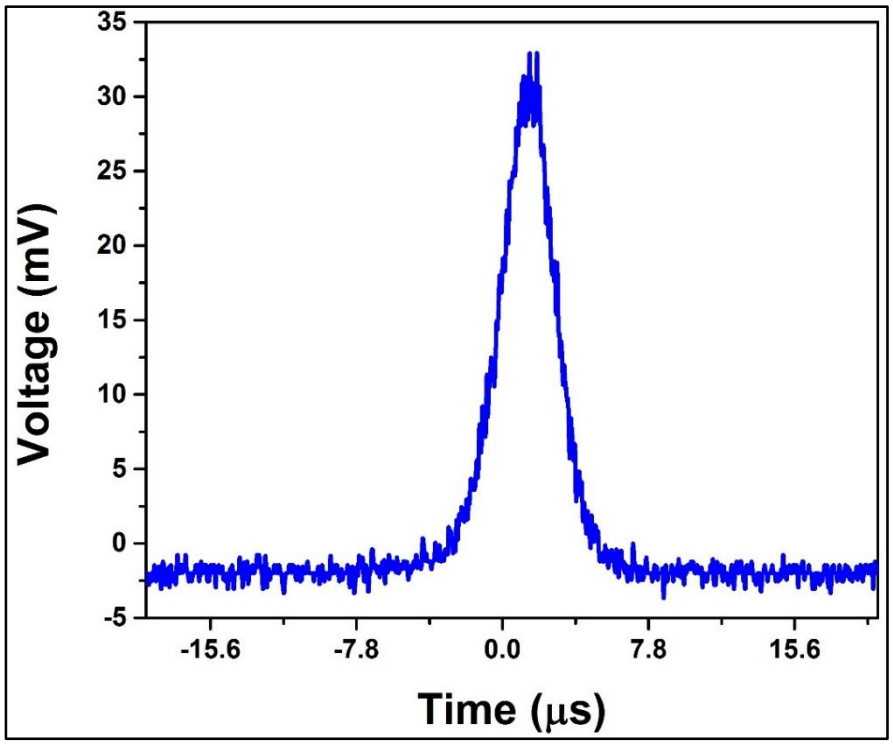

Figure (2.27): Single pulse at 300 mW pump power.

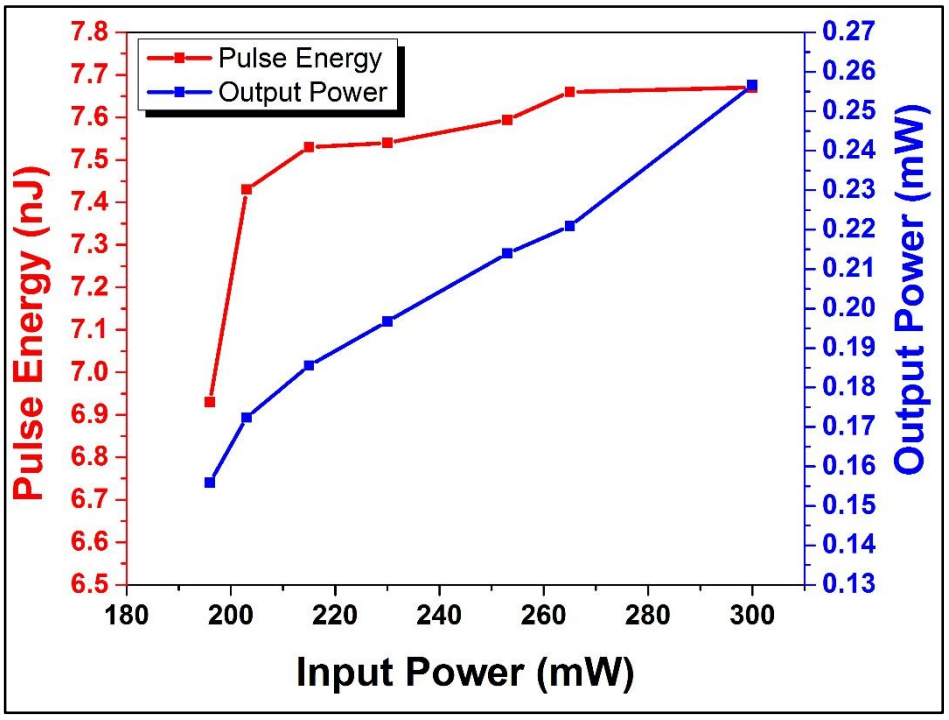

Figure (2.28): Pulse energy and average power and with the pump power increment.

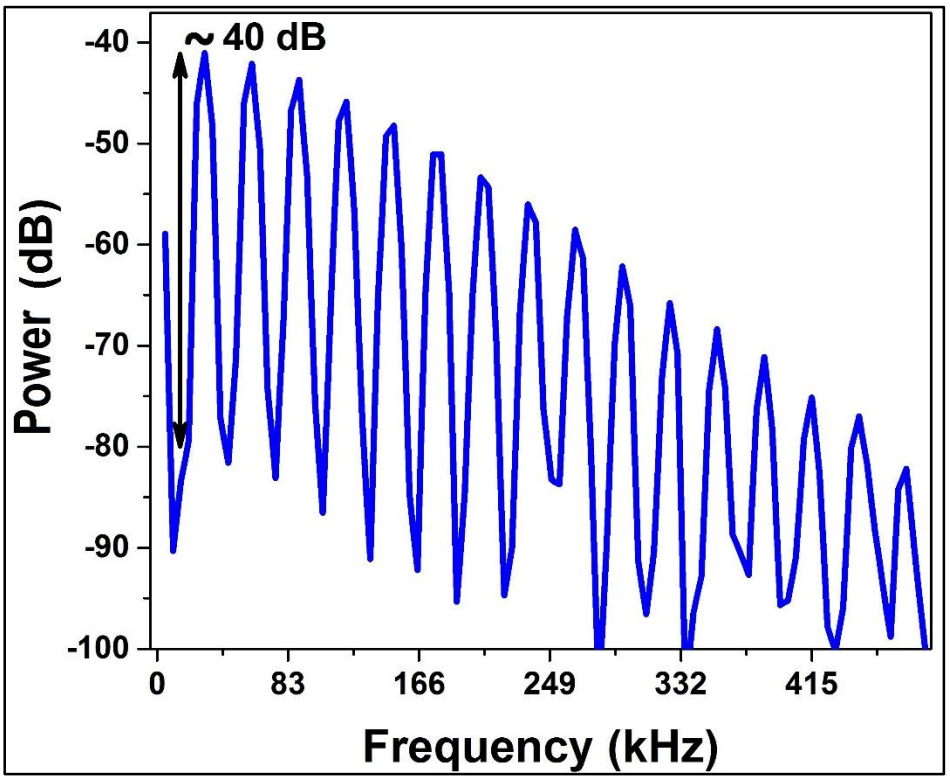

Figure (2.29): RF spectrum.

A brief summary of the main results related to the EDFL ring cavity is presented in Table (2-5). A new metal nanomaterials was successfully implemented in generating multiwavelength and Q-switched EDFL. The performance of laser was characterized using two basic setups with and without including the comb filter. In both setups a piece of Al/PVA thin film were sandwiched between two fiber ferrules to serve as SA.

Table (2-5): Summary of the research findings in Chapter 2.

	Gain Medium	**Operation State**	**Type of NL Material**	**Min. Pulse width (μs)**	**No. of λ**	**Center wavelength (nm)**
Without Filter	EDF	Q-Switching	Al/PVA	2.17	1	1567.6
With Filter	EDF	Q-Switching and Multiwavelength	Al/PVA	2.36	13	1563.18

Chapter Three

Multiwavelength and Q-switching Generation Based on Tungsten Oxide in EDFL and YDFL

CHAPTER THREE

Multiwavelength and Q-switching Generation Based on Tungsten Oxide in EDFL and YDFL

3.1 Introduction

In this chapter, highly nonlinear nanomaterial of tungsten oxide was used to produce a steady multiwavelength fiber laser in conjunction with pulse generation in EDFL and YDFL. Two separate procedures will be adopted to prepare WO_3 thin films. The first approach is to form a solid thin film by mixing with PVA polymer as a host matrix and the second approach is to form a liquid based SA by mixing with SDS as a surfactant. The nanomaterial was investigated by various techniques to determine its spectroscopic and morphological properties such as SEM, FTIR, XRD and saturable absorption measurement respectively. Sagnac loop filter was included to provide a fixed spacing between adjacent laser modes and consequently more enhanced stability at 1.5 μm band. On the other hand, dual and triple wavelength oscillations were achieved using tungsten oxide in ytterbium-doped fiber laser at 1μm band. Pulse parameters such as pules width, pulse energy, average power etc. was quantified and discussed as shown below. The structure of chapter three is presented in Fig. (3-1).

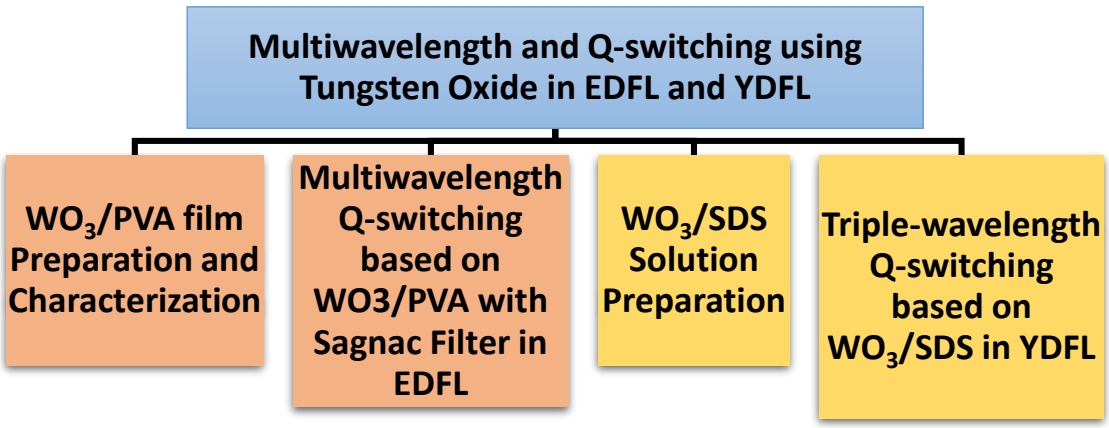

Figure (3.1): Structure of chapter three.

3.2 Multiwavelength Q-switching Generation based on WO_3/PVA with Sagnac Filter in EDFL

This section contains the details about film preparation, experimental setup, results, and discussion of the proposed multiwavelength EDFL based on WO_3/PVA thin film.

3.2.1 WO_3/PVA Film Preparation

In this part, the fabrication process of the WO_3-PVA thin film is demonstrated as follows: In the beginning, the polymer suspension was made by adding 1 g of PVA granules to 100 ml of deionized water, giving rise to a concentration of 10 mg/ml. Full decomposition was obtained by powerfully stirring the mixture for a period about 45 min at ~130°C until the solution was transparent and homogenous. Later, 0.005 g of WO_3 round NPs having a diameter of 50 nm and purity of 99% was mixed to 5 ml of polymer solution providing a mass to the volume ratio of 1 mg/ml. The composition was retained under a low stirring rate for 1 h. Next, the prepared compound was emptied into a plastic plate and let to dehydrate at the ambient room temperature for 7 days to create a uniformly distributed film without forming any voids or defects. Subsequently, the resultant WO_3/PVA film was removed from the dish and chopped into small parts to be employed to the EDFL system. The deposition of WO_3 film by drop-casting is a simple physical method without complex equipment needed.

3.2.2 WO_3 Nanoparticles and Film Characterization

The examination of the structure and shape of WO_3 NPs by scanning electron microscopy (SEM) is presented in Fig. (3-2), which obviously shows rounded nanopowder. Moreover, the nanostructures were analyzed by x-ray diffraction (XRD) to determine the crystallinity of WO_3, as presented in Fig. (3-3). The XRD diffraction peaks show pure WO_3 particles. The

detected peaks were compatible with findings recognized previously [103,104]. The FTIR spectrum is shown in Fig. (3-4). The wide absorption in the range between 500 to 1000 cm^{-1} are accredited to the stretching vibrations of W–O and O–W–O bonds, whilst hydroxyl bond OH and water vapor absorb nearby 1602 and 3446 cm^{-1} [105,106]. The prepared film has a thickness of about 26 μm being measured with a microscope supplied with a digital camera to measure the dimensions. The nonlinear features of the prepared WO_3 film were recognized by using the twin detector approach. The fitting was performed according to the two-level saturation model, as illustrated in Fig. (3-5). The processed WO_3 film owns a modulation depth of 20% and a saturation intensity of 100 MW/cm^2. The NL film manifests a higher modulation depth than some of the famously-known 2D materials [107].

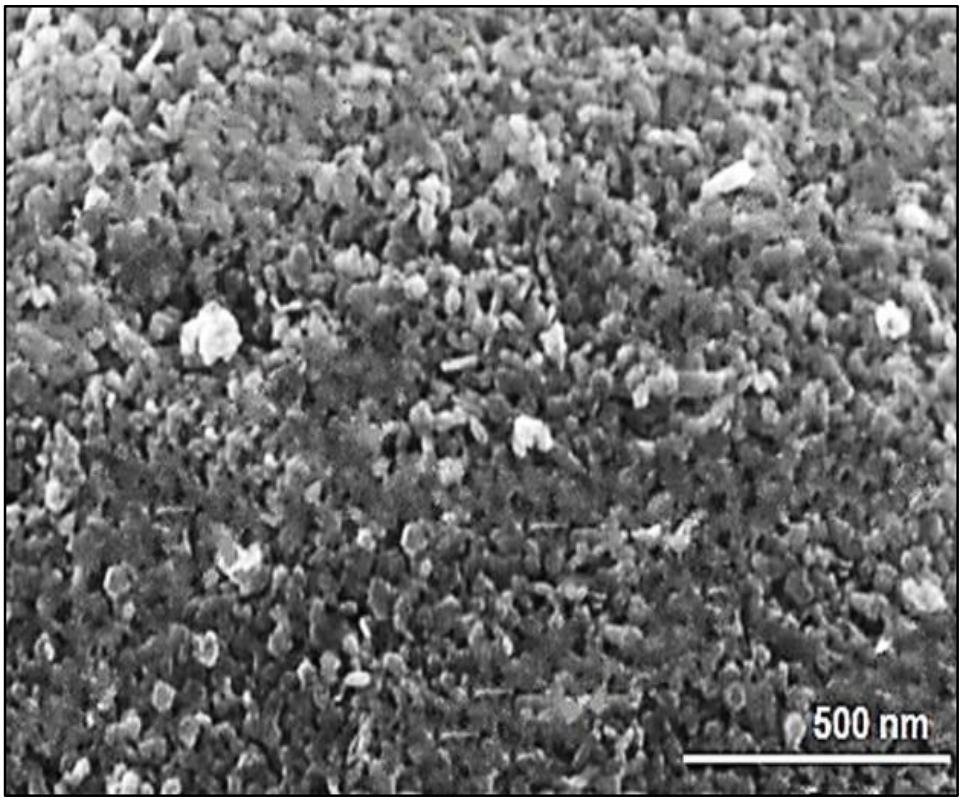

Figure (3.2): SEM of WO_3 NPs [108].

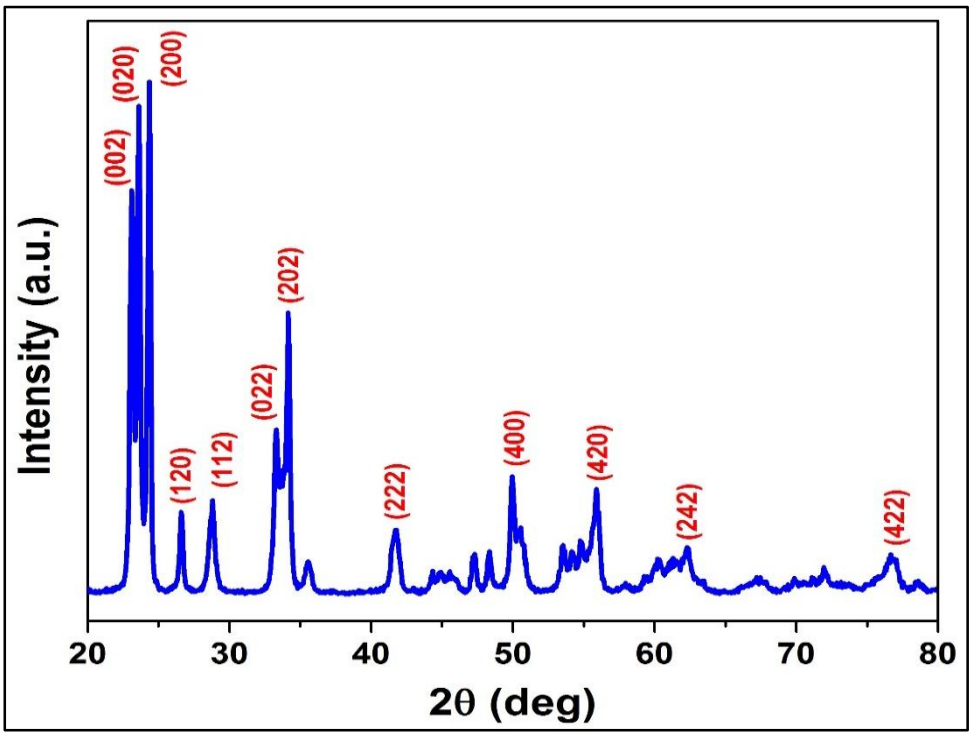

Figure (3.3): XRD of WO_3 NPs.

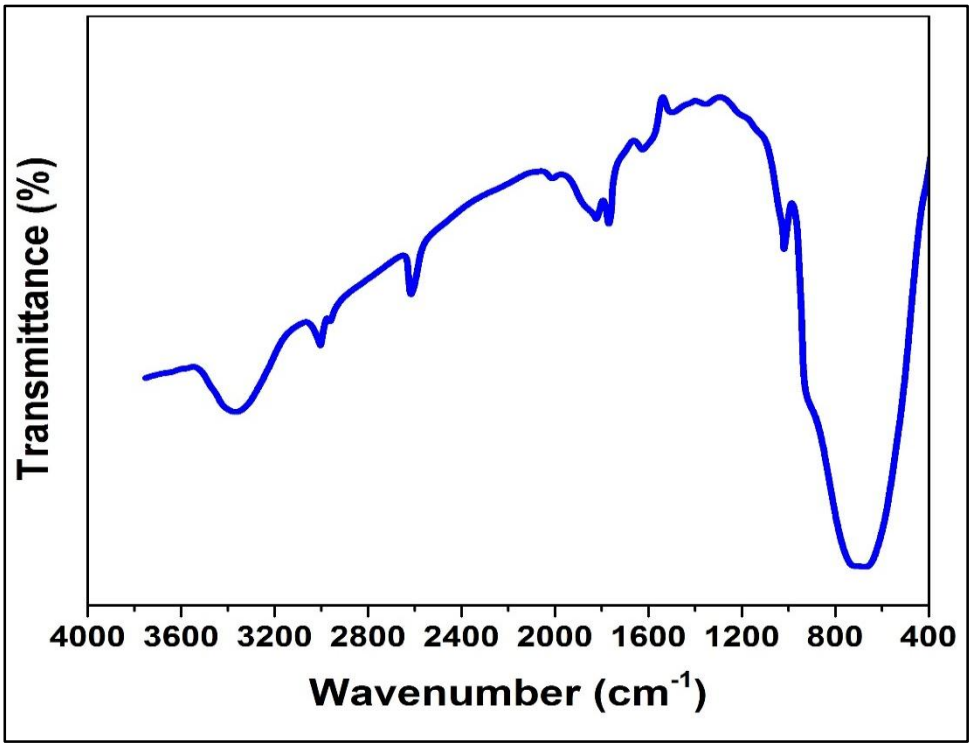

Figure (3.4): FTIR of WO_3 NPs.

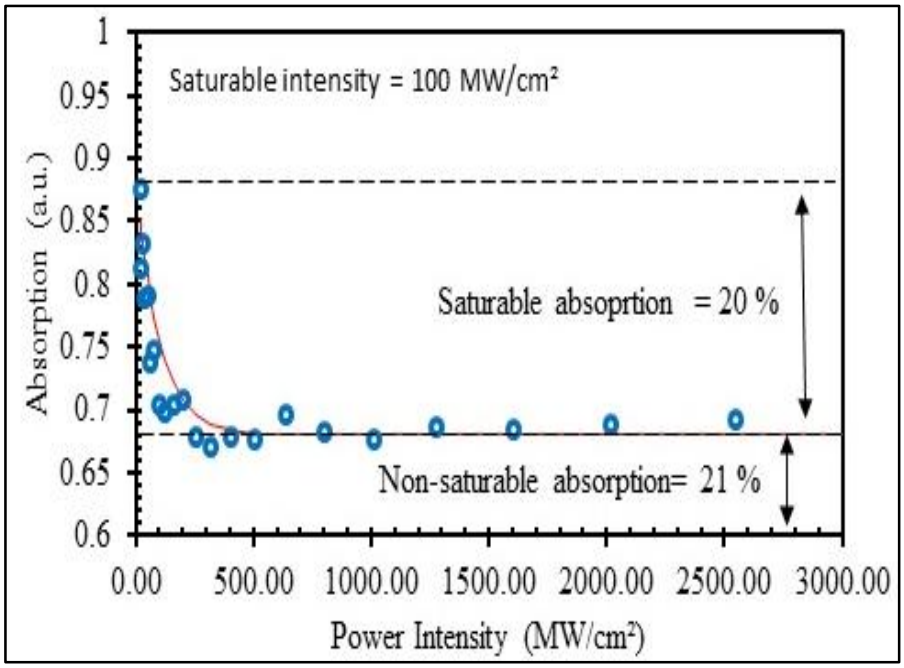

Figure (3.5): The nonlinear absorption of WO_3-PVA film.

3.2.3 Experimental Details

The experimental setup for multiwavelength EDFL based on WO_3 as shown in Fig. (3-6). It contains the standard components for ring cavity to initialize laser operation. Besides, the cavity includes a Sagnac loop filter for wavelength stabilizations which has been designed previously.

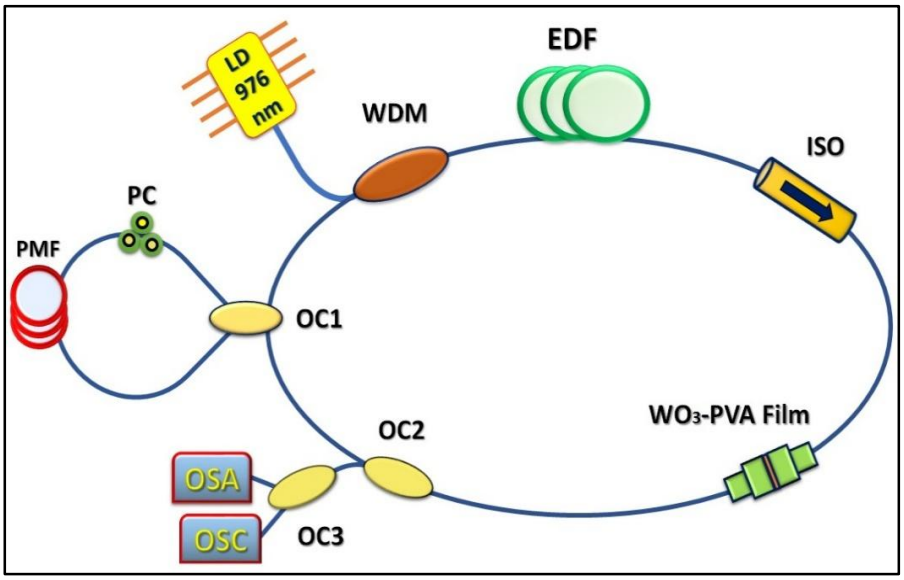

Figure (3.6): Setup of the multiwavelength EDFL based on WO_3.

3.2.4 Results and Discussion

Firstly, a Q-switching operation was self-started after incorporating the SA device at a threshold value of 118.5 mW of pump power. Fig. (3-7) reveals the scope trace of pulses when pumped at different powers. The single-pulse shape at 300 mW is represented in Fig. (3-8).

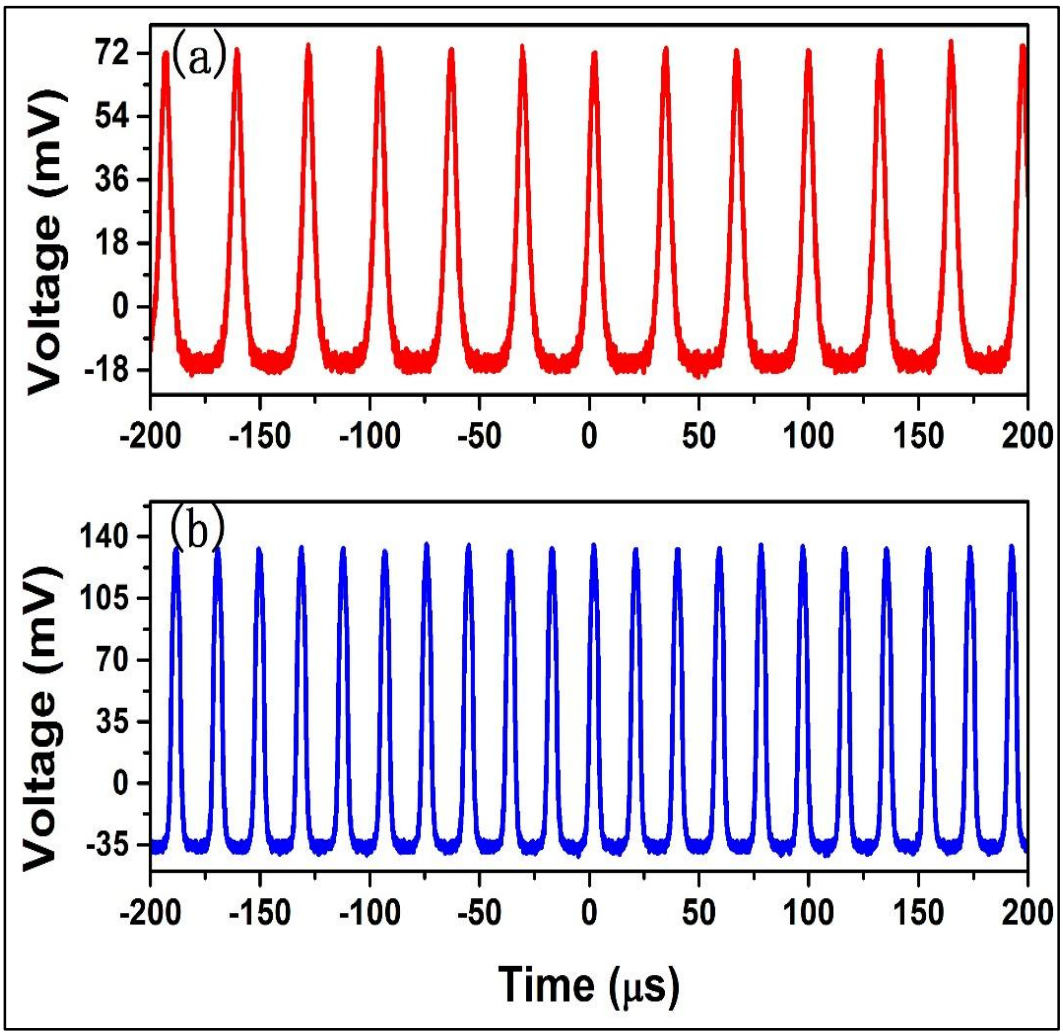

Figure (3.7): Trains of pulse at (a) 118.5 mW and (b) 300 mW pump power.

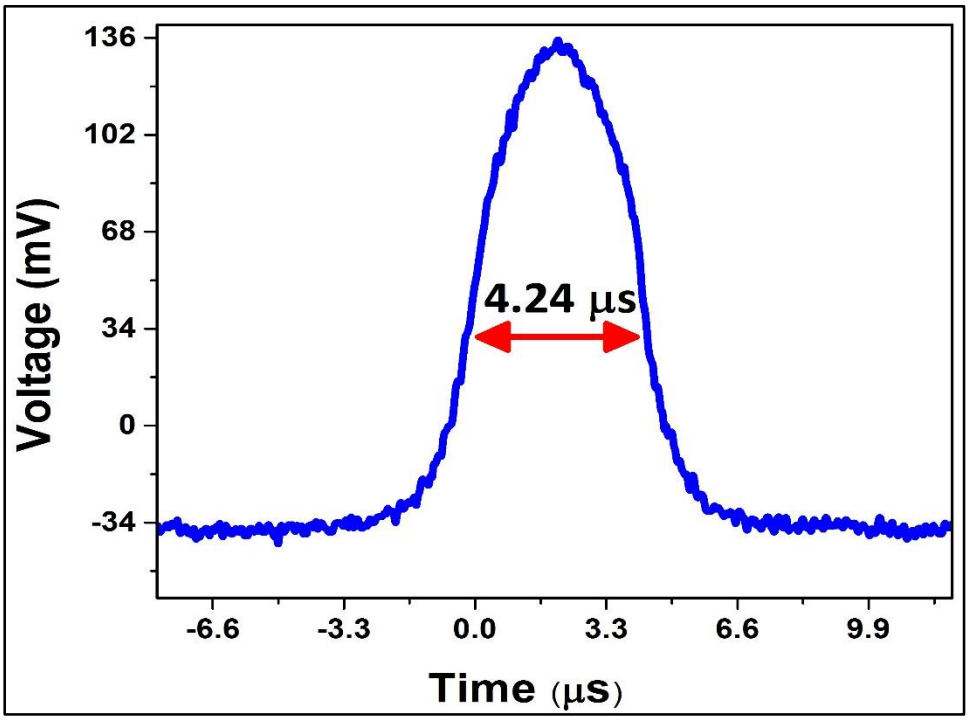

Figure (3.8): Q-switched pulse shape.

It is obviously noticed that pulse appearance follows the tendency of a standard Q-switched behavior. The transient response of the produced pulses has good stability with consistent and symmetrical pulse envelope. The least pulse width was 4.24 µs, and the highest repetition rate was 52.49 kHz as illustrated in Fig. (3-9). The comprehensive assessment of the pulse energy and average power when the pump level is adjusted is drawn in Fig. (3-10). The highest registered pulse energy was 21.9 nJ and the largest output power was 1.15 mW. The slope efficiency of Q-switched fiber laser was 0.63%. Fig. (3-11) shows the RF spectrum at 300 mW of pump level. A signal-to-noise ratio (SNR) of ~60 dB was acquired at the fundamental frequency of 52.49 kHz which point out a high level of the Q-switching stability.

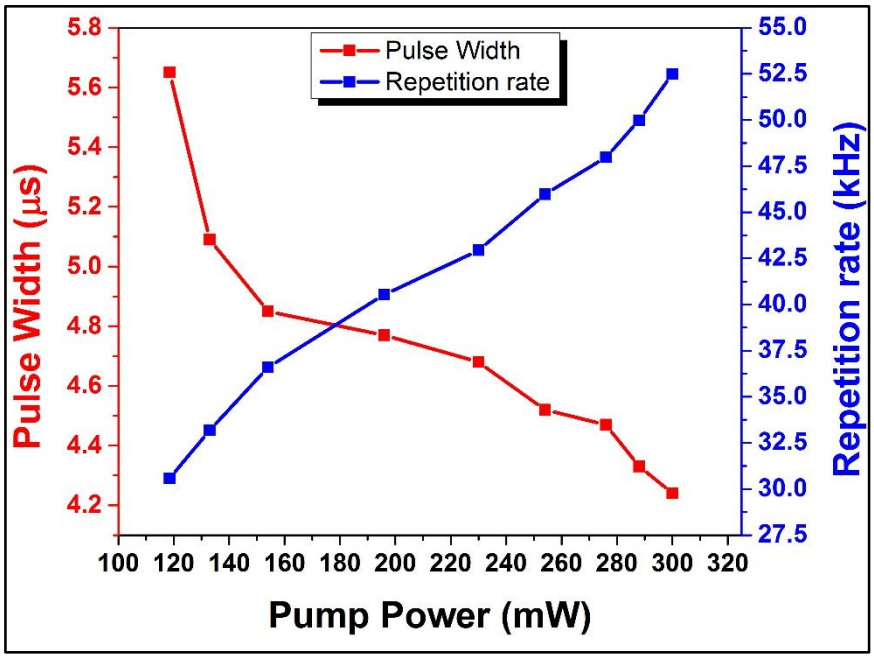

Figure (3.9): Pulse width and repetition rate relation with the increase of pump power.

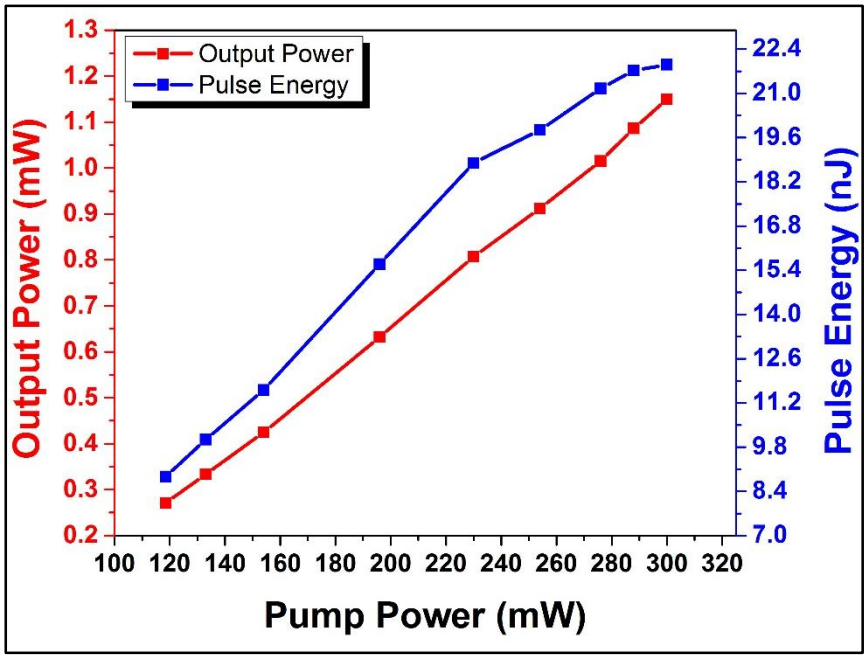

Figure (3.10): Pulse energy and output power relation with the increase of pump power.

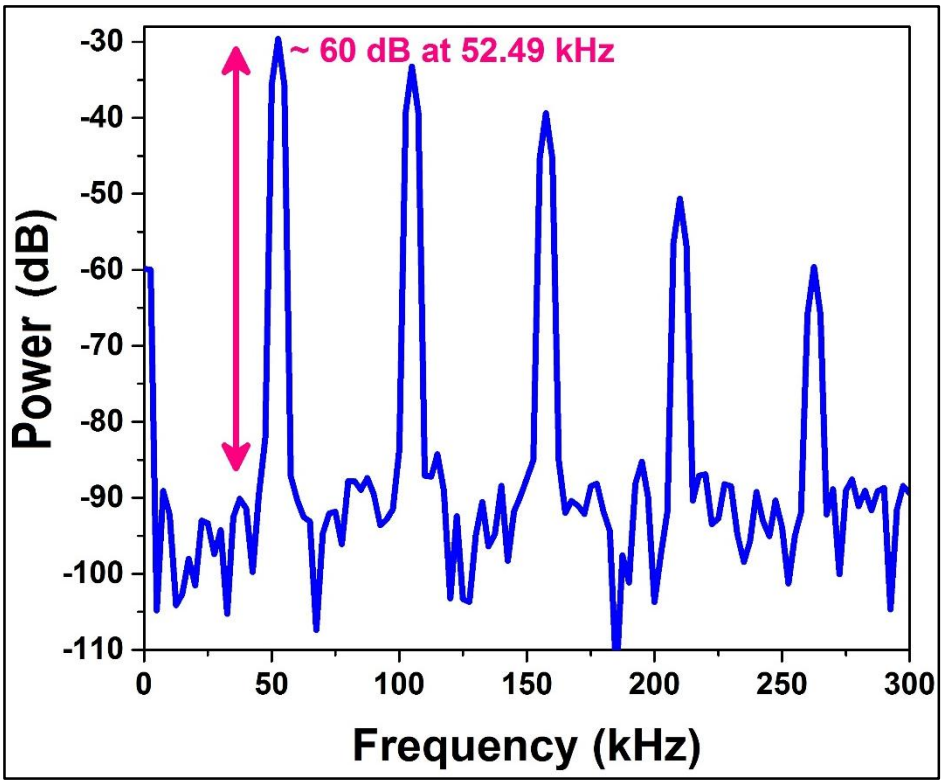

Figure (3.11): RF spectrum.

Meanwhile, fifteen peaks were reached in the multiwavelength regime, by regularly increasing the pump level from 66.5 to 300 mW assisted with the precise setting of the polarization controller. The spectra have a 0.48 nm channel spacing and signal to noise ratio of more than 40 dB within a bandwidth of about 7 nm located at 1563.95, as demonstrated in Fig. (3-12) and Fig. (3-13). The analysis of stability, which is very crucial for practical applications, was tested at room temperature. The laser spectra were measured for a half-hour at 300 mW, as presented in Fig. (3-14). The proposed multi-oscillation laser manifested sufficient stability since the fluctuations in power level remained within ~5 dB. Also, the drift in wavelength operation with time has shown good stability performance with little deviation from the centers of the main peaks.

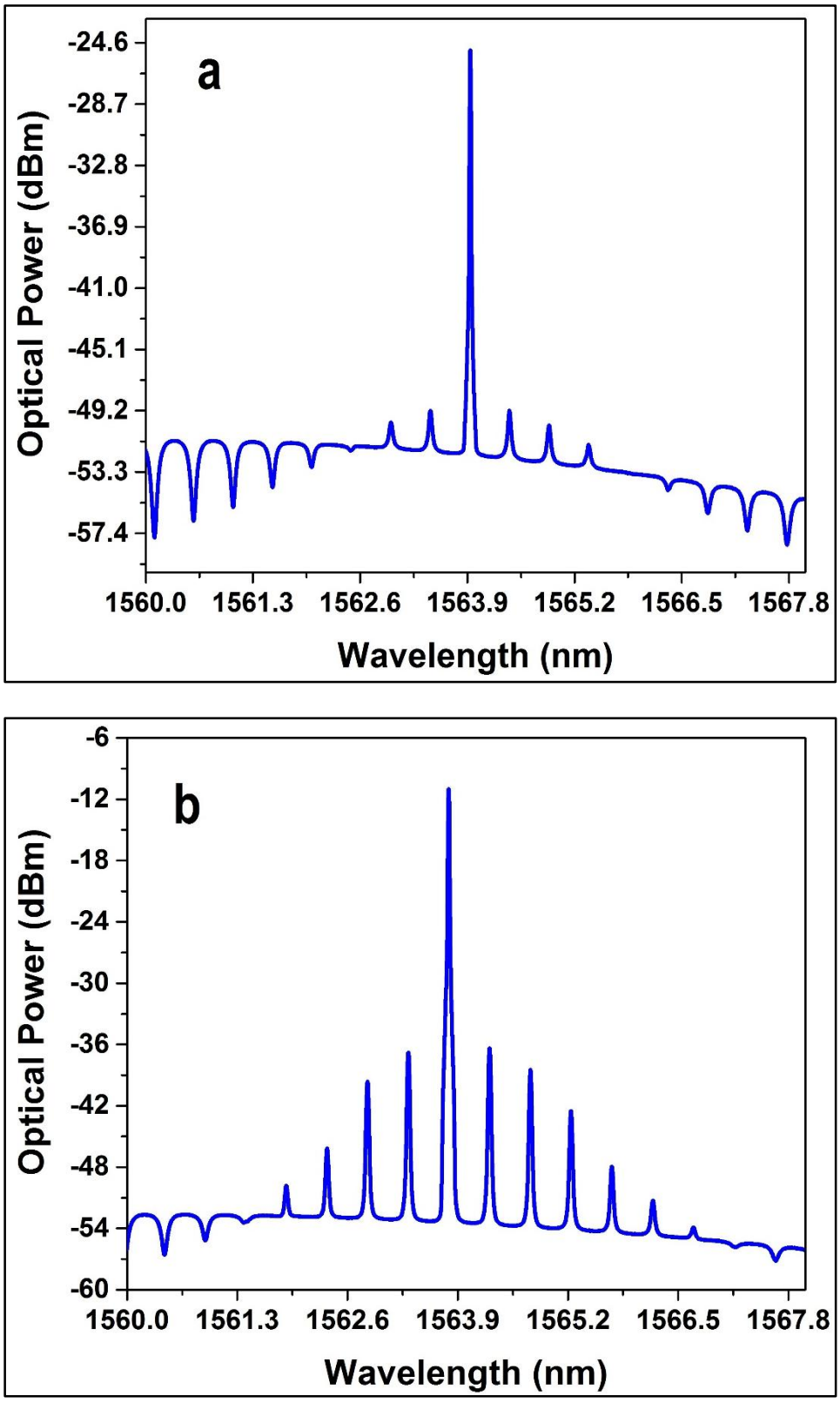

Figure (3.12): Multiwavelength spectra based on WO_3-PVA at various pump power: (a) 66.5 mW (b) 118.5 mW.

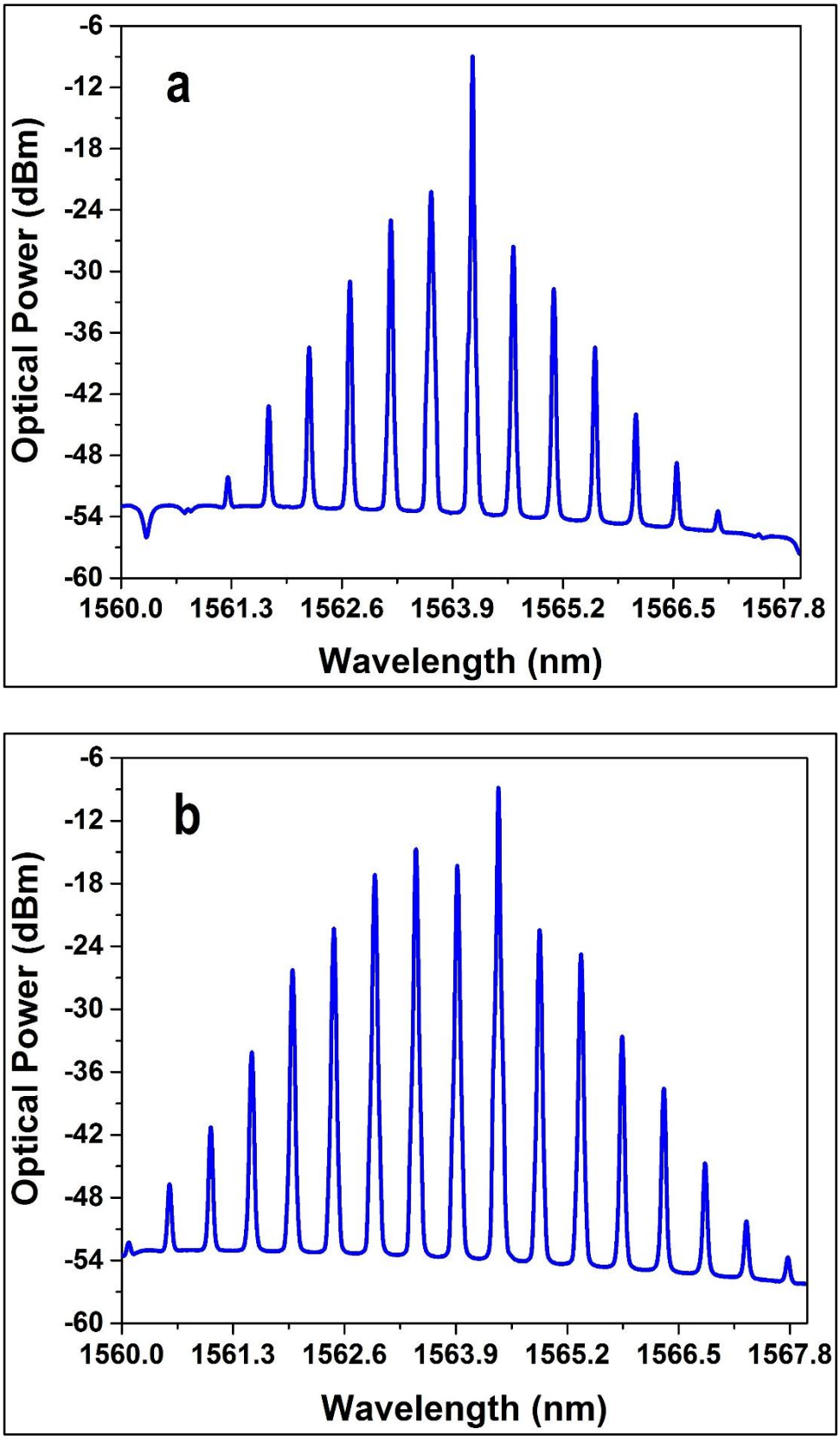

Figure (3.13): Multiwavelength spectra based on WO_3-PVA at various pump power: (a) 189 mW (b) 300 mW.

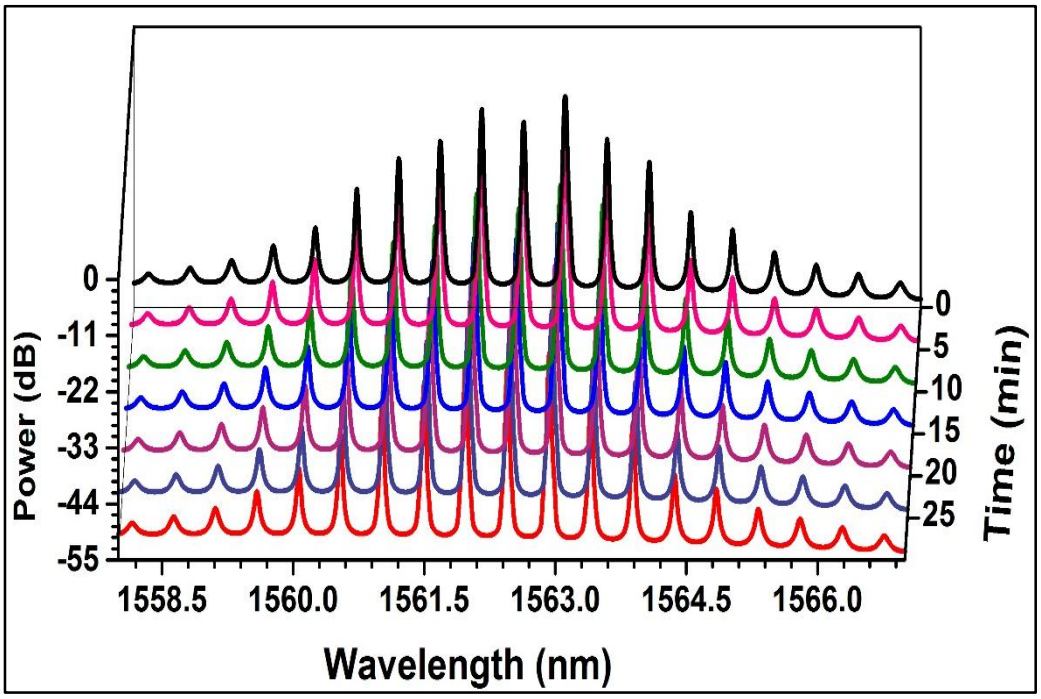

Figure (3.14): Multiwavelength stability spectra based on based on WO_3-PVA thin film.

The prepared WO_3/PVA thin film was interchanged with a length of ~2.3 km of SMF in the ring cavity to compare their nonlinear performance as shown in Fig. (3-15). By using SMF to induce the FWM effect, only five peaks were obtained, as presented in Fig. (3-16). It can be seen clearly the advantage of WO_3 NPs in the case of the multiwavelength performance. Profiting from WO_3 NPs high nonlinearity, the improved FWM effect represents a pivotal role in the reduction of mode competition at room temperature. Integrating WO_3 thin film into the cavity notably minimizes the length of the cavity in contrast with the methods utilizing SMF or expensive specialized fibers [31,32]. Furthermore, the reduced length decreases the necessary pump level. The number of transmitted wavelength can be enlarged substantially by the elevation of the injected power and reduction of the cavity and thin-film loss.

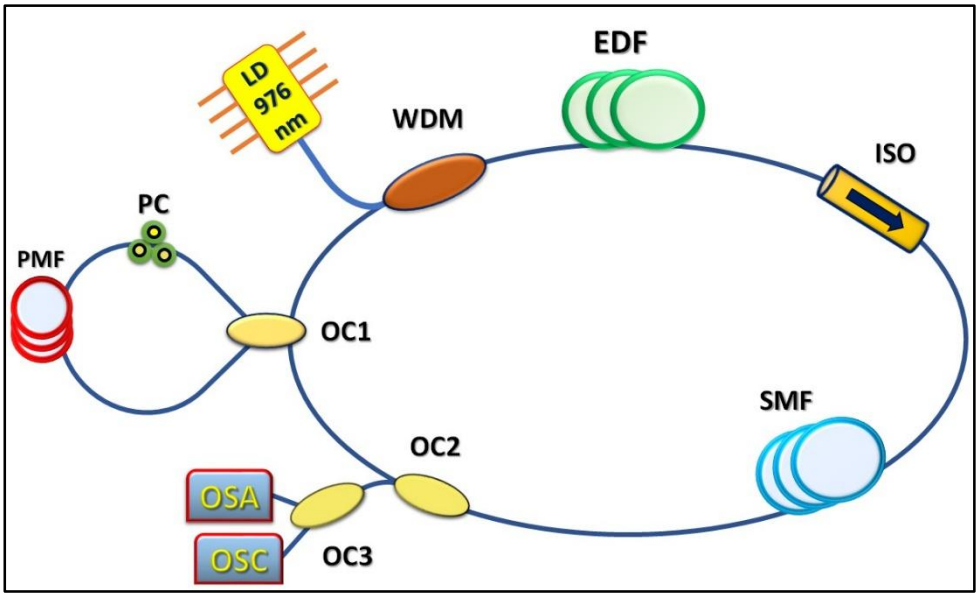

Figure (3.15): Setup of the multiwavelength EDFL based on SMF.

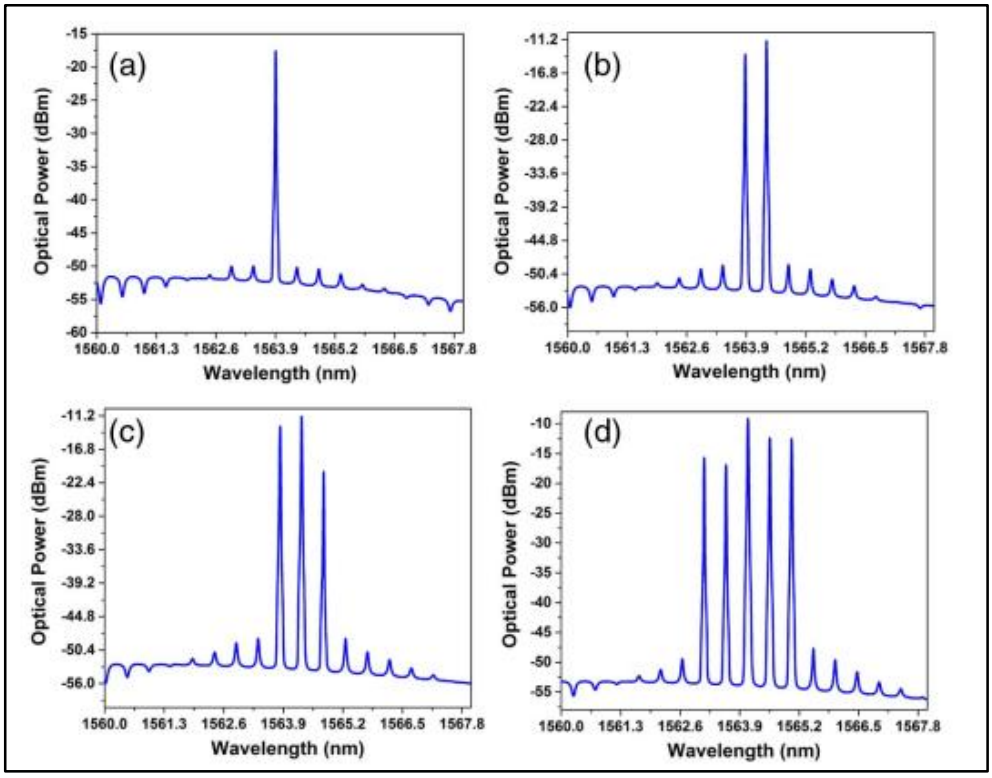

Figure (3.16): Multiwavelength spectra based on SMF at various pump power: (a) 88 mW (b) 126 mW (c) 160 mW and (d) 300 mW.

3.3 Triple-wavelength Q-switching Generation based on WO_3/SDS in YDFL

This part contains aspects of film formation, laboratory setup, results, and discussion of the proposed multiwavelength YDFL based on WO_3-SDS suspension.

3.3.1 WO_3/SDS Solution Preparation

In order to prepare WO_3 solution, firstly, pure sodium dodecyl sulfate (SDS) aqueous solution with a resulting concentration of 10 wt% was obtained in DI water. SDS as an anionic hydrophilic surfactant is used to reduce the attractive electrostatic forces and to de-aggregate nanoparticles.

Next, 5 mg of commercial WO_3 NPs with ultra-purity ~ 99 % and average particle size of ~ 50 nm were added to a 20 mL of SDS solution and continuously mixed at moderate speed for 20 min with the help of a magnetic mixer. Then, the suspension was processed by ultrasonic unit for ~ 16 min to obtain a homogenous dispersion of the nanomaterial. To dissipate excessive heat during sonication, the specimen container was immersed in a water bath. Because of the simplicity of the preparation, absence of expensive equipment and fewer production steps result in a straightforward and cost-effective method to fabricate the SA.

The quality of SA greatly depends on the crystal structure, surface morphology and film composition of WO_3. Finally, the resulting yellow solution was kept in plastic container.

3.3.2 Experimental Details

The schematic diagram of the multiwavelength Q-switched ytterbium-doped fiber laser (YDFL) is plotted in Fig. (3-17). A 976 nm butterfly packaged laser diode with an utmost power of 300 mW was used as a source to pump the gain medium via a 980/1060 nm wavelength-division

multiplexer (WDM). The gain medium consists of a segment of ~ 1.5 m Yb-doped fiber (YDF). The isolator (ISO) was inserted within the laser cavity to preserve unidirectional propagation of light in the fiber core and consequently limit the possibility of any backscattering, which can likely affect pulse stability.

A polarization controller (PC) with an adjustable fiber squeezer was inserted to manipulate the polarization orientation and consequently the cavity birefringence. A 10 dB output coupler (OC) was used to circulate 90% of the optical power back to the WDM to complete the ring cavity and pass 10% as a laser output for measurements. The prepared WO_3 SA was introduced by coating the fiber ferrule between the OC and the ISO. The output laser was investigated with an optical spectrum analyzer (Yokogawa AQ6370C, 600-1700 nm) with a resolution of 20 pm, while the pulse temporal behavior was observed by a digital phosphor oscilloscope (Tektronix DPO3052, 500 MHz bandwidth, 2 G samples/second) joined with 5GHz PIN photo-diode (Thorlabs DET08CFC) for the conversion of the optical signal into AC electrical signal and finally a fiber coupled power meter (EXFO FPM-300) was employed to record the average optical power.

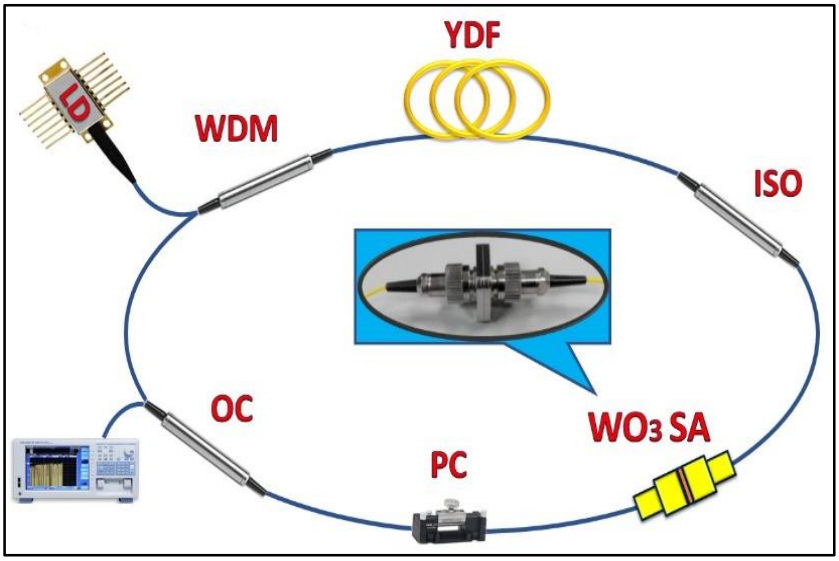

Figure (3.17): Setup of the triple-wavelength YDFL based on WO_3/SDS Suspension.

3.3.3 Results and Discussion

Two successive coatings were applied by dropping the WO_3 suspension onto fiber tip and followed by drying at room temperature. Since the modulation depth can be varied with the number of deposited layers on the fiber end. In contrast to the WO_3/PVA film, the concentration of dropped WO_3 NPs onto the fiber facet is slightly higher which consequently induces more absorption. The above-mentioned technique can significantly minimize the SA insertion loss and also reduce the pump threshold.

After SA insertion into the YDFL cavity, the lasing threshold for mono-wavelength operation was recorded at 170 mW centered at 1040.57 nm. The Q-switching pulses were obtained at a bleaching threshold of 179 mW and its operation was sustained up to the highest pump power of 275 mW with a minimum pulse width of 2.92 μs. Fig. (3-18) and Fig. (3-19) display the stable train of pulses at the highest repetition frequency and the enlarged image of the single pulse respectively. In the meantime, the repetition frequency was varied between 14.8-71.3 kHz as presented in Fig. (3-20). In addition, the measured average output power and the calculated peak power are given in Fig. (3-21) which indicate nearly linear relationship with pump power. Moreover, the maximum achieved pulse energy was 9.26 nJ which corresponds to a maximum peak power of 3.17 mW. The fundamental frequency of 71.3 kHz was affirmed by the RF spectrum obtained from Fourier transform. A peak to pedestal ratio of about 50 dB with frequency span of 500 kHz is clearly presented in Fig. (3-22) which indicates high quality pulses. Varying the pump radiation between maximum and minimum permissible values has no effect on the quality of the produced Q-switched pulses indicating that the SA remained intact.

By progressively adjusting the pump power to 275 mW as well as modifying the PC compression and rotational forces, dual and triple-wavelength operation were achieved. The dual-emission with wavelengths

of 1033.01nm and 1036.83 nm has appeared when the pump level has reached to 210 mW as shown in Fig. (3-23). As the pumping power was further increased to 244 mW, triple-emission output was attained. The three peaks were located at 1030.01 nm, 1032.122 nm and 1036.21 nm as obtained from OSA data shown in Fig. (3-24). However, more wavelengths were obtained with different tuning conditions of PC, but they suffered from instability issues which can be further stabilized by adding intracavity filter. During the experiment, the output emissions were observed for 5 consecutive sweeps to confirm the multiwavelength stability at the maximum power as presented in Fig. (3-25) and Fig. (3-26). It manifests no vital fluctuations neither in power nor in wavelength within the testing time, which suggests almost steady operation at room temperatures. In this experiment, it is noticeable that the multiwavelength generation was achieved in the absence of any filtering device inside the YDFL cavity. Moreover, the high-nonlinearity of WO_3-NPs coupled with the gain of the YDFL support the excitation of multiwavelength lasing [109].

The mechanism of multiwavelength oscillation is mainly restricted by the loss of the ring cavity, birefringence and the gain of the Yb^{+3} doped-fiber. The liquid form of WO3 based on SDS solution has lower insertion loss than PVA-based film. Stable dispersions are necessary for the fabrication of optically homogeneous composite SAs, as the surfactant molecules are expected to encapsulate and stabilize the dispersion, preventing any particle aggregation and sedimentation. Otherwise, aggregates are allowed to form, leading to scattering losses and unreliable device performance.

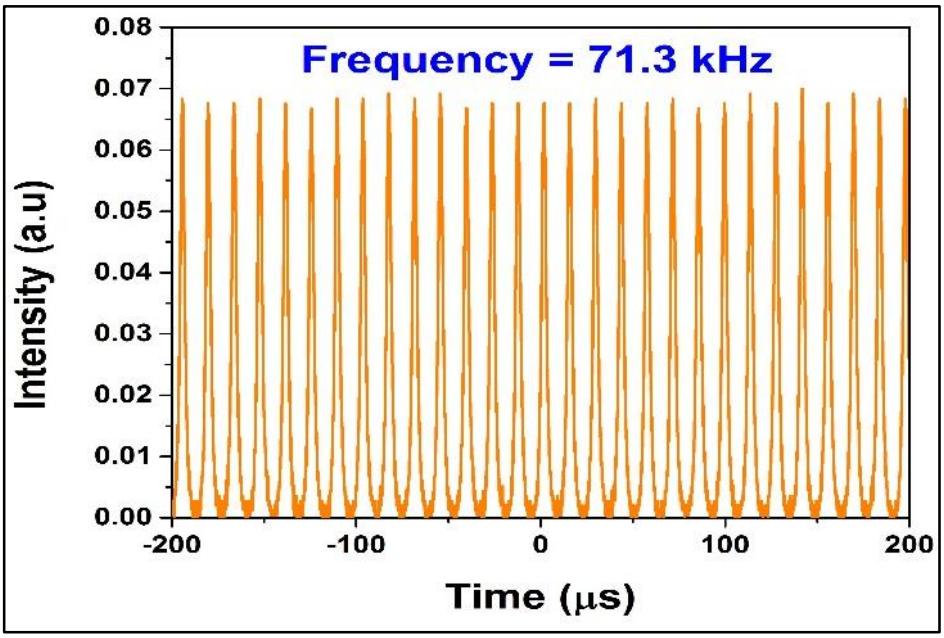

Figure (3.18): Pulse train of the Q-switched YDFL.

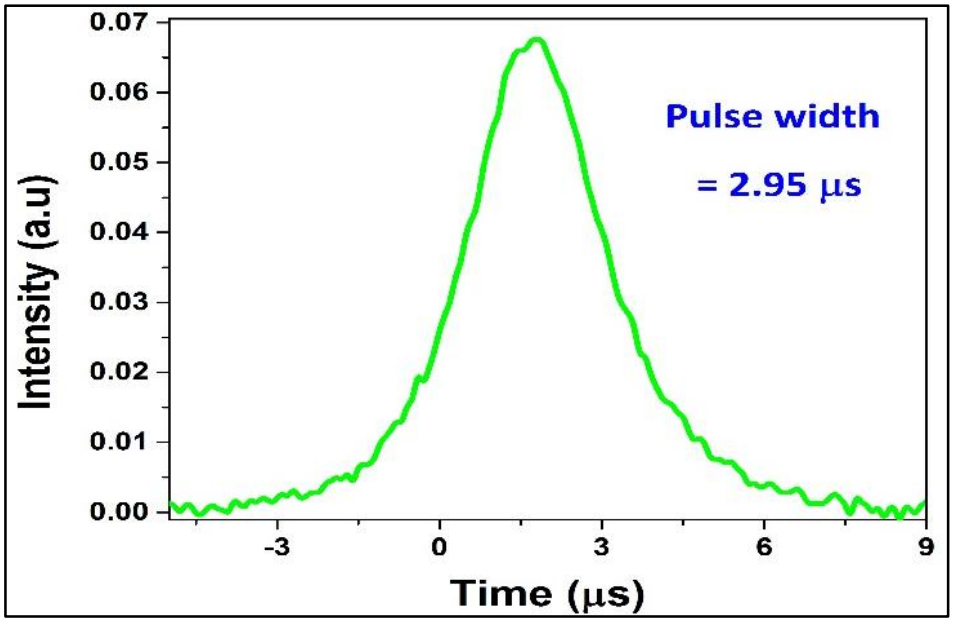

Figure (3.19): The form of single pulse.

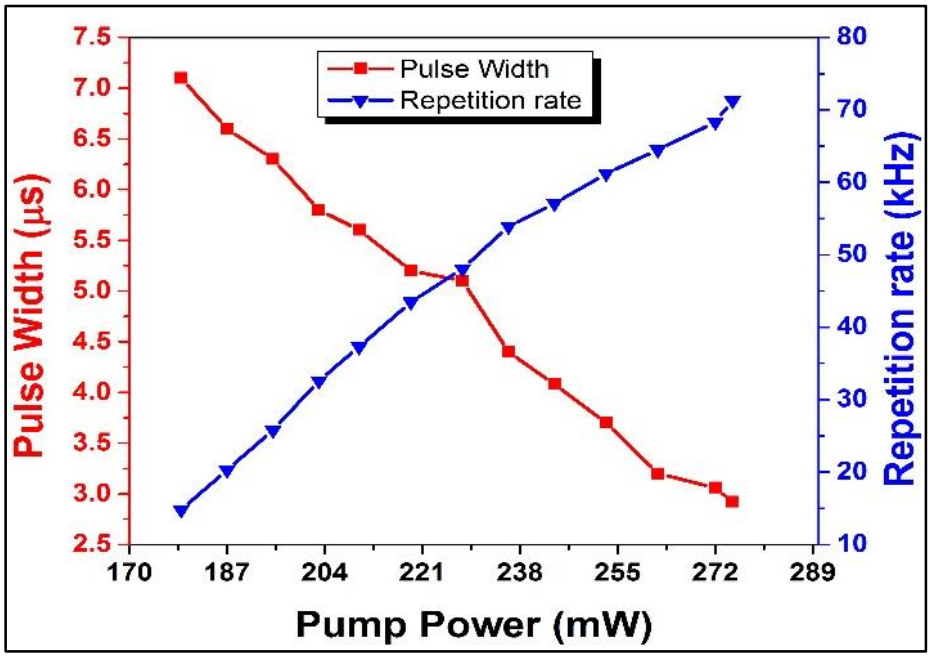

Figure (3.20): Response of pulse width and pulse repetition rate with pump power increment.

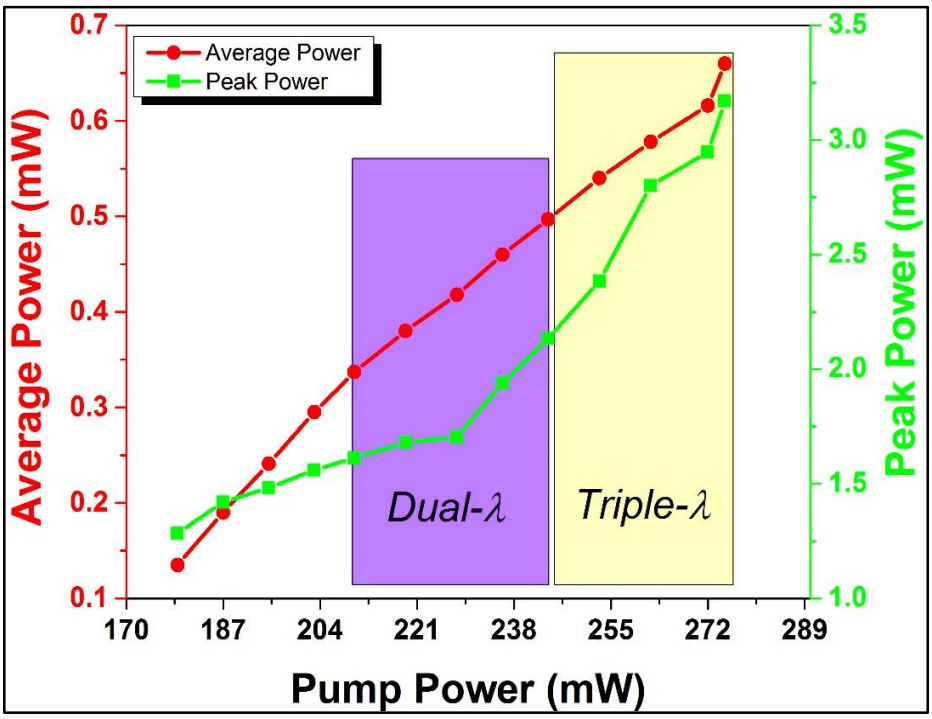

Figure (3.21): Response of peak power and average power with pump power increment.

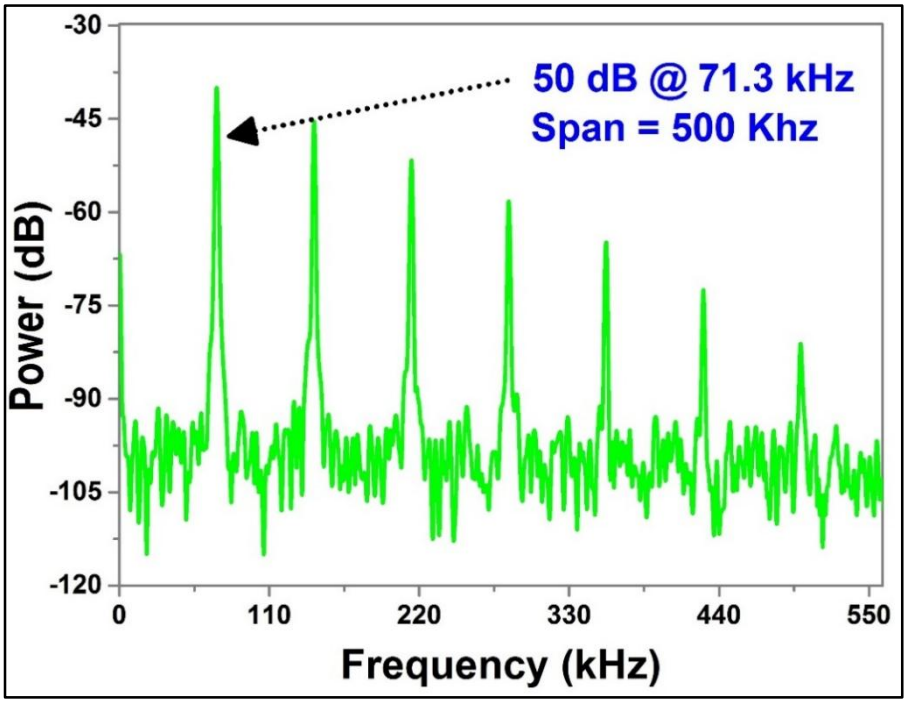

Figure (3.22): RF spectrum.

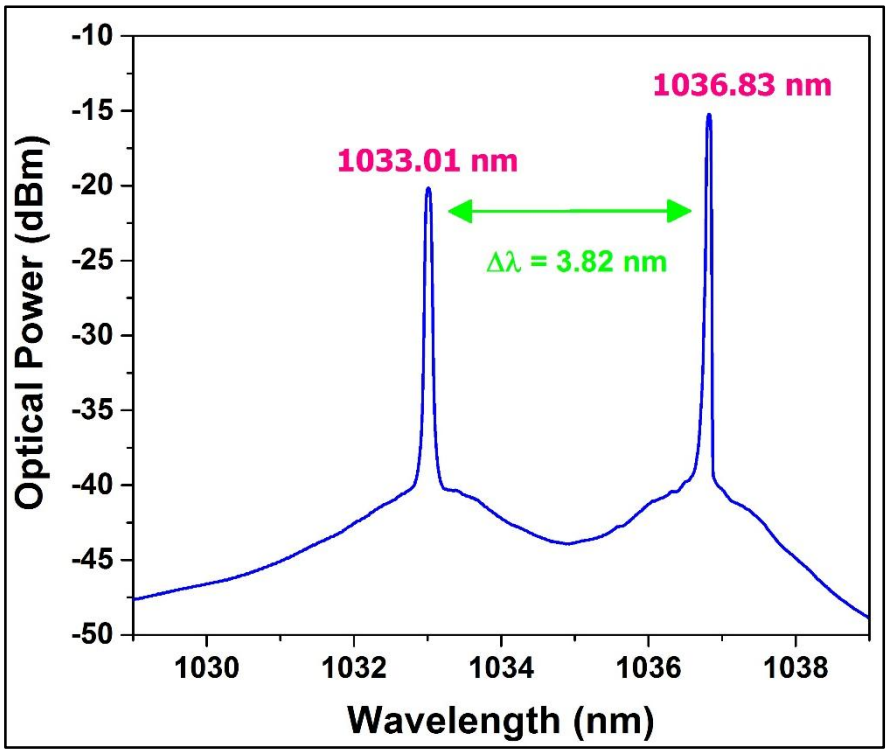

Figure (3.23): Dual-wavelength emission based on WO_3/SDS.

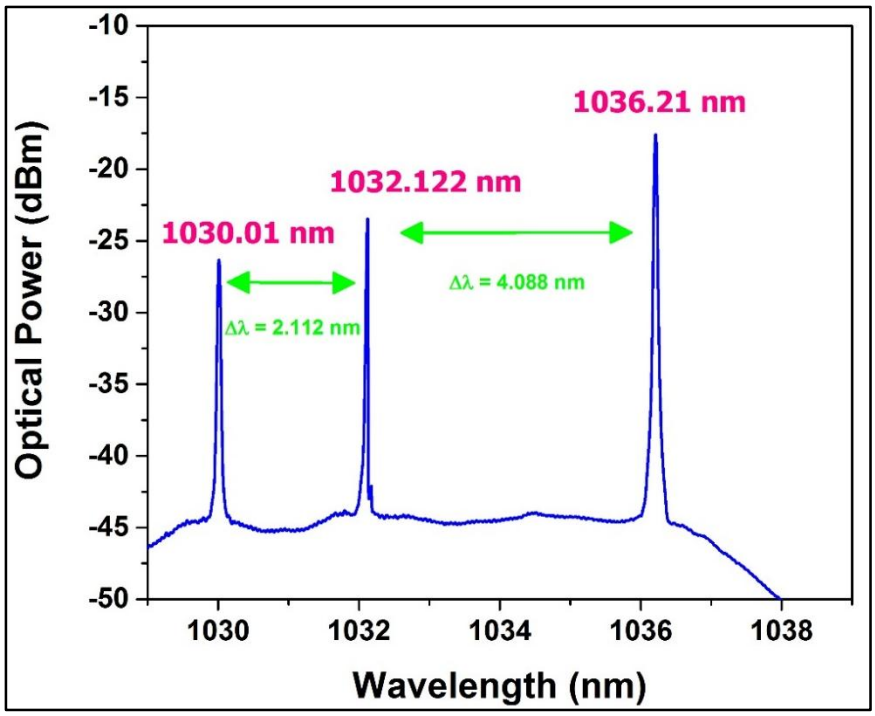

Figure (3.24): Triple-wavelength emission.

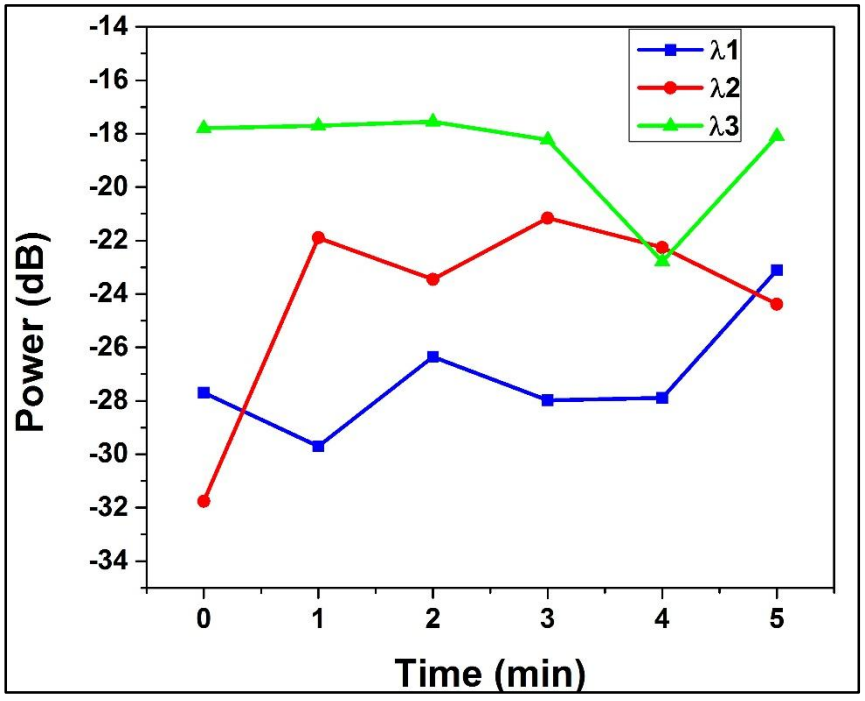

Figure (3.25): Power stability with time.

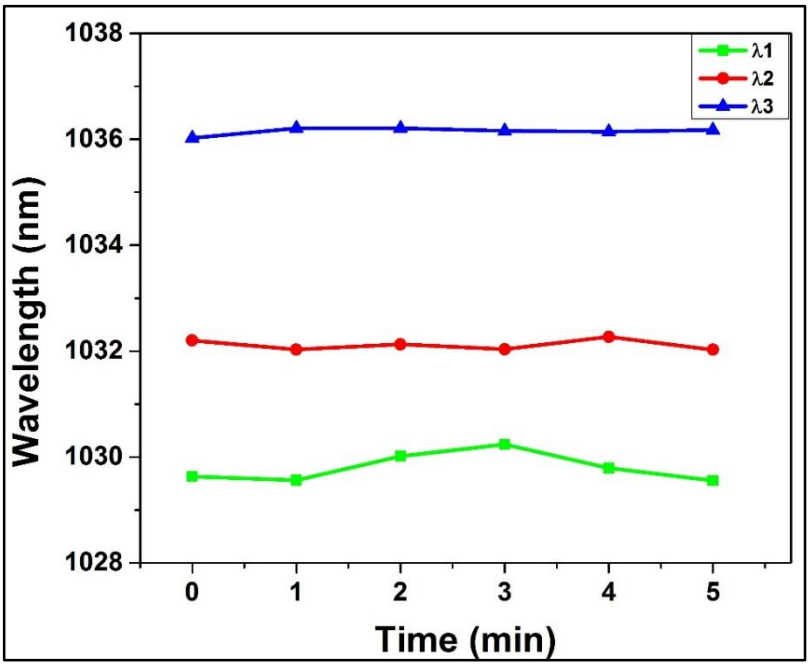

Figure (3.26): Wavelength stability with time.

Table (3-1) presents a concise summary of the major outcomes achieved in EDFL and YDFL using WO_3 NP that was prepared in two different methods. The strong 3rd nonlinearity of WO_3 NP is a key contribution to generate multiwavelength as well as Q-switching operation simultaneously.

Table (3-1): Summary of the obtained results in Chapter 3.

	Gain Medium	Operation State	Type of NL Material	Min. Pulse width (μs)	No. of λ	Center wavelength (nm)
With Filter	EDF	Q-Switching and Multiwavelength	WO_3/PVA	4.24	15	1563.95
Without Filter	YDF	Q-Switching and Multiwavelength	WO_3/SDS	2.92	3	1040.57

Chapter Four

Conclusions and Suggestions for

Future Work

CHAPTER FOUR

Conclusions and Suggestions for Future Work

4.1 Conclusions

This thesis presents the investigation of two nonlinear nanomaterials to realize multiwavelength and Q-switching operations namely aluminum and tungsten oxide. Nanomaterial-induced four-wave mixing is utilized to assist multi-frequency oscillation and to suppress mode competition and mode hopping in rare-earth-doped fiber lasers. Besides that, Q-switching operation has been observed concurrently. In this study, two types of fiber lasers have been employed; erbium-doped fiber laser at 1.5 μm band and ytterbium-doped fiber laser at 1 μm band. Additionally, Sagnac loop filter has been included to form a figure of 8-cavity which aided the stabilization of multiwavelength operation.

The following are highlights of the main conclusions of this thesis:

1. A new saturable absorber based on aluminum/PVA thin film has been successfully employed to achieve passive Q-switching operation in EDFL. The SA has the lowest saturation intensity ever reported.
2. WO_3-based SA has shown a large modulation depth compared with some of the well-known 2D materials like MoS_2, $MoSe_2$, WS_2, and WSe_2 of about 20%.
3. Sagnac loop filter based on highly birefringent fiber was designed and fabricated for EDFL. The loop filter was simple efficient and inexpensive. By carefully tuning the paddles of polarization controller the number of emitted lasing lines can be controlled.
4. The liquid form of WO_3 based on SDS solution has lower insertion loss than polymer-based film due to reduced scattering and absorption in such cases and therefore it can generate Q-switching at low

threshold power. Although, the concentration of nanoparticles cannot be controlled precisely in liquid suspension, this process provides a simple and effortless method to obtain a nonlinear layer.

5. It clearly seen that nanostructures can have effectively higher χ^3 than SMF which consequently assisted FWM generation to obtain more lasing lines. Also, the OSNR was higher with employment of thin film based-nanomaterial. This outcome is expected due to reduced losses in a few-micron film compared to several meters of SMF.
6. Sagnac loop filter based on highly birefringent fiber was designed and fabricated for YDFL using 5 m of panda fiber. However, high insertion losses of the filter have prevented the lasing operation and only ASE has been obtained.
7. Wavelength tunable laser operation has not been observed. Continuous tuning of lasing wavelengths is in principle not possible, the main effect of such operation would be a change in the fringe pattern by changing the panda fiber length.

4.2 Suggestions for Future Work

To improve the multiwavelength Q-switched laser performance and to develop more efficient nonlinear saturable absorber materials, we suggest the following future work:

1. Examination of Q-switching, mode-locking and multiwavelength operation in thulium and holmium doped fibers at 2 μm band.
2. Design and fabrication of inline microfiber based filter to achieve tunable multiwavelength operation in EDFL and YDFL.
3. Realization of flat-gain multiwavelength operation by using multiple cascaded filters in EDFL and YDFL.
4. Exploring innovative ways to obtain new high NL materials. Nanocomposites present an adaptable and specific approach to tailor the bandgap and non-linear properties of the materials. By adjusting the composition of metal, metal oxide or chalcogenide, binary and ternary composite can be attained with tunable characteristics.
5. Optimization of the cavity out-coupling is needed by changing the coupling ratio other than that of 90:10.
6. Higher pumping power must be considered to obtain efficient nonlinear phenomena. Pump power in the range of 1 W is sufficient for fiber-based NL applications.

References

[1] Y. Liu, P. Wang, L. Wang, H. Li, G. Shi, and T. He, “Stable multi-wavelength fiber laser with single-mode fiber in a Sagnac loop,” *Applied Optics*, vol. 55, no. 12, p. 3339, 2016.

[2] W. He, C. Shangguan, L. Zhu, M. Dong, and F. Luo, “Tunable and stable multi-wavelength erbium-doped fiber laser based on a double Sagnac comb filter with polarization-maintaining fibers,” *Optik*, vol. 137, pp. 254–261, 2017.

[3] J. C. and Z. T. and W. Z. and L. X. and H. Pan, “Research on tunable multiwavelength fiber lasers with two-section birefringence fibers and a nonlinear optical loop,” *Laser Physics*, vol. 28, no. 5, p. 55107, 2018.

[4] Z. Zhang, L. Zhang, and Z. Xu, “Tunable multiwavelength ytterbium-doped fiber laser based on nonlinear polarization rotation,” *Journal of Nonlinear Optical Physics & Materials*, vol. 21, no. 03, p. 1250041, 2012.

[5] A. W. Al-Alimi, N. A. Cholan, M. H. Yaacob, A. F. Abas, M. T. Alresheedi, and M. A. Mahdi, “Wide bandwidth and flat multiwavelength Brillouin-erbium fiber laser,” *Optics Express*, vol. 25, no. 16, pp. 19382–19390, 2017.

[6] C. H. Yeh, C. W. Chow, Y. F. Wu, F. Y. Shih, C. H. Wang, and S. Chi, “Multiwavelength erbium-doped fiber ring laser employing Fabry–Perot etalon inside cavity operating in room temperature,” *Optical Fiber Technology*, vol. 15, no. 4, pp. 344–347, 2009.

[7] A. Zakiah Malek, N. A. M. Ahmad Hambali, M. H. A. Wahid, and M. M. Shahimin, “Fiber bragg grating assisted cavity loss reduction in the generation of multiwavelength brillouin fiber laser,” *Optik*, vol. 157, pp. 684–692, 2018.

[8] M. Bianchetti, J. M. Sierra-Hernandez, R. I. Mata-Chavez, E. Gallegos-Arellano, J. M. Estudillo-Ayala, D. Jauregui-Vazquez, A. A.

Fernandez-Jaramillo, G. Salceda-Delgado, and R. Rojas-Laguna, “Switchable multi-wavelength laser based on a core-offset Mach-Zehnder interferometer with non-zero dispersion-shifted fiber,” *Optics & Laser Technology*, vol. 104, pp. 49–55, 2018.

[9] A. González-García, O. Pottiez, R. Grajales-Coutiño, B. Ibarra-Escamilla, and E. A. Kuzin, “Switchable and tuneable multi-wavelength Er-doped fibre ring laser using Sagnac filters,” *Laser Physics*, vol. 20, no. 3, pp. 720–725, 2010.

[10] Z. Luo, M. Zhou, J. Weng, G. Huang, H. Xu, C. Ye, and Z. Cai, “Graphene-based passively Q -switched dual-wavelength erbium-doped fiber laser,” *Optics Letters*, vol. 35, no. 21, pp. 3709–3711, 2010.

[11] D. Z. Mohammed and A. H. Al-Janabi, “Passively Q-switched erbium doped fiber laser based on double walled carbon nanotubes-polyvinyl alcohol saturable absorber,” *Laser Physics*, vol. 26, no. 11, p. 115108, 2016.

[12] S. K. M. Al-Hayali and A. H. Al-Janabi, “Dual-wavelength passively Q-switched ytterbium-doped fiber laser using Fe3O4-nanoparticle saturable absorber and intracavity polarization,” *Laser Physics*, vol. 195, no. 28, p. 035103, 2018.

[13] Z. Luo, Y. Huang, M. Zhong, Y. Li, J. Wu, B. Xu, H. Xu, Z. Cai, J. Peng, and J. Weng, “1-, 1.5-, and 2-μm fiber lasers Q-switched by a broadband few-layer MoS2 saturable absorber,” *Journal of Lightwave Technology*, vol. 32, no. 24, pp. 4077–4084, 2014.

[14] O. P. Varnavski, T. Goodson, M. B. Mohamed, and M. A. El-Sayed, “Femtosecond excitation dynamics in gold nanospheres and nanorods,” *Physical Review B - Condensed Matter and Materials Physics*, vol. 72, no. 23, pp. 1–9, 2005.

[15] Y. Zhang and Y. Wang, “Nonlinear optical properties of metal

nanoparticles: a review," *RSC Advances*, vol. 7, no. 71, pp. 45129–45144, 2017.

[16] Z. Kang, Q. Li, X. J. Gao, L. Zhang, Z. X. Jia, Y. Feng, G. S. Qin, and W. P. Qin, "Gold nanorod saturable absorber for passive mode-locking at 1 μm wavelength," *Laser Physics Letters*, vol. 11, no. 3. p. 035102, 2014.

[17] J. Wang, Z. Chen, Y. Wang, S. Liu, W. Liu, L. Li, R. Lv, and W. Ren, "Ferroferric-oxide nanoparticle based Q-switcher for a 1 μm region," *Optical Materials Express*, vol. 9, no. 2, p. 731, 2019.

[18] S. K. M. Al-Hayali, D. Z. Mohammed, W. A. Khaleel, and A. H. Al-Janabi, "Aluminum oxide nanoparticles as saturable absorber for C-band passively Q-switched fiber laser," *Applied Optics*, vol. 56, no. 16, pp. 4720–4726, 2017.

[19] F. Mitschke, Fiber Optics: Physics and Technology. Springer Berlin Heidelberg, 2010.

[20] M. Azadeh, Fiber optics engineering. Springer, 2009.

[21] A. Al-Azzawi, Fiber Optics: Principles and Practices. CRC Press, 2007.

[22] L. Dong and B. Samson, Fiber Lasers: Basics, Technology, and Applications. CRC Press, 2017.

[23] R. Paschotta, "Field guide to optical fiber technology," 2010.

[24] A. Ghatak and K. Thyagarajan, Introduction to Fiber Optics. Cambridge University Press, 1998.

[25] J. M. Senior, Optical Fiber Communications: Principles and Practice, 3rd ed. Pearson, 2009.

[26] R. Paschotta, Field Guide to Lasers. Society of Photo Optical, 2008.

[27] V. V. Ter-Mikirtychev, Fundamentals of fiber lasers and fiber amplifiers. Springer, 2014.

[28] S. W. Harun and H. Arof, Current Developments in Optical Fiber

Technology. IntechOpen, 2013.

[29] R. W. Boyd and D. Prato, Nonlinear Optics, 3rd ed. Elsevier Science, 2008.

[30] G. Agrawal, Nonlinear Fiber Optics, 5th ed. Elsevier Science, 2013.

[31] Z. Luo, M. Zhou, Z. Cai, C. Ye, J. Weng, G. Huang, and H. Xu, "Graphene-Assisted Multiwavelength Erbium-Doped Fiber Ring Laser," *IEEE Photonics Technology Letters*, vol. 23, no. 8, pp. 501–503, 2011.

[32] R. Paschotta, Field guide to laser pulse generation, vol. 14. SPIE press Bellingham, 2008.

[33] A. E. Siegman, Lasers. University Science Books, 1986.

[34] O. Svelto, Principles of Lasers. Springer US, 2010.

[35] R. Menzel, Photonics: linear and nonlinear interactions of laser light and matter, 2nd ed. Springer, 2007.

[36] S. Yamashita, "A Tutorial on Nonlinear Photonic Applications of Carbon Nanotube and Graphene," *Journal of Lightwave Technology*, vol. 30, no. 4, pp. 427–447, 2012.

[37] M. Zhang, E. J. R. Kelleher, S. V Popov, and J. R. Taylor, "Ultrafast fibre laser sources: Examples of recent developments," *Optical Fiber Technology*, vol. 20, no. 6, pp. 666–677, 2014.

[38] I. D. Jung, F. X. Kärtner, N. Matuschek, D. H. Sutter, F. Morier-Genoud, Z. Shi, V. Scheuer, M. Tilsch, T. Tschudi, and U. Keller, "Semiconductor saturable absorber mirrors supporting sub-10-fs pulses," *Applied Physics B: Lasers and Optics*, vol. 65, no. 2, pp. 137–150, 1997.

[39] J. Jeon, J. Lee, and J. H. Lee, "Numerical study on the minimum modulation depth of a saturable absorber for stable fiber laser mode locking," *Journal of the Optical Society of America B*, vol. 32, no. 1, pp. 31–37, 2015.

[40] J. Du, M. Zhang, Z. Guo, J. Chen, X. Zhu, G. Hu, P. Peng, Z. Zheng, and H. Zhang, "Phosphorene quantum dot saturable absorbers for ultrafast fiber lasers," *Scientific Reports*, vol. 7, no. 1, p. 42357, 2017.

[41] G. D. Houser and E. Garmire, "Balanced detection technique to measure small changes in transmission," *Applied Optics*, vol. 33, no. 6, pp. 1059–1062, 1994.

[42] V. Bianchi, T. Carey, L. Viti, L. Li, E. H. Linfield, A. G. Davies, A. Tredicucci, D. Yoon, P. G. Karagiannidis, L. Lombardi, F. Tomarchio, A. C. Ferrari, F. Torrisi, and M. S. Vitiello, "Terahertz saturable absorbers from liquid phase exfoliation of graphite," *Nature Communications*, vol. 8, no. 1, p. 15763, 2017.

[43] J. Hecht, Understanding lasers: an entry-level guide, 3rd ed. Wiley-IEEE Press, 2008.

[44] M. J. F. Digonnet, Rare-earth-doped fiber lasers and amplifiers, revised and expanded, 2nd ed. CRC press, 2001.

[45] W. Koechner and M. Bass, Solid-State Lasers: A Graduate Text. Springer New York, 2003.

[46] J. J. M. i Ponsoda, C. Ye, J. P. Koplow, M. J. Söderlund, J. J. Koponen, and S. K. Honkanen, "Analysis of temperature dependence of photodarkening in ytterbium-doped fibers," *Optical Engineering*, vol. 50, no. 11, pp. 1–10, 2011.

[47] T. Schneider, Nonlinear Optics in Telecommunications. Springer, 2004.

[48] A. Acharya, M. N. Ambia, M. A. Rob, A. S. M. Mohsin, and A. S. M. Shihavuddin, "A comparative analysis between the Step Index fiber and Polarization Maintaining fiber on the basis of their modal solutions," *International Conference on Electronics and Information Engineering, Proceedings*, vol. 2, pp.35-39, 2010.

[49] G. P. Agrawal, Fiber-Optic Communication Systems. Wiley, 2010.

[50] G. Agrawal, Applications of Nonlinear Fiber Optics, 1st ed. Academic Press, 2001.

[51] G. Das and J. W. Y. Lit, "Ring resonator for multiwavelength fiber laser using a Sagnac loop filter," *Optical Engineering*, vol. 42, no. 8, pp. 2257–2262, 2003.

[52] Z. Luo, M. Zhou, D. Wu, C. Ye, J. Weng, J. Dong, H. Xu, Z. Cai, and L. Chen, "Graphene-Induced Nonlinear Four-Wave-Mixing and Its Application to Multiwavelength Q-Switched Rare-Earth-Doped Fiber Lasers," *Journal of Lightwave Technology*, vol. 29, no. 18, pp. 2732–2739, 2011.

[53] N. J. C. Libatique and R. K. Jain, "A broadly tunable wavelength-selectable WDM source using a fiber Sagnac loop filter," *IEEE Photonics Technology Letters*, vol. 13, no. 12, pp. 1283–1285, 2001.

[54] H. Ahmad, N. E. Ruslan, M. A. Ismail, Z. A. Ali, S. A. Reduan, C. S. J. Lee, and S. W. Harun, "Silver nanoparticle-film based saturable absorber for passively Q-switched erbium-doped fiber laser (EDFL) in ring cavity configuration," *Laser Physics*, vol. 26, no. 9, p. 95103, 2016.

[55] A. R. Muhammad, M. T. Ahmad, R. Zakaria, H. R. A. Rahim, S. F. A. Z. Yusoff, K. S. Hamdan, H. H. M. Yusof, H. Arof, and S. W. Harun, "Q-Switching Pulse Operation in 1.5-μm Region Using Copper Nanoparticles as Saturable Absorber," *Chinese Physics Letters*, vol. 34, no. 3, pp. 2015–2018, 2017.

[56] M. T. A. and A. R. M. and R. Z. and H. R. A. R. and K. S. H. and H. H. M. Y. and H. A. and S. W. Harun, "Gold nanoparticle based saturable absorber for Q-switching in 1.5 μ m laser application," *Laser Physics*, vol. 27, no. 11, p. 115101, 2017.

[57] F. Naseri and D. Dorranian, "Effect of aluminum nanoparticles on the linear and nonlinear optical properties of PVA," *Optical and Quantum*

Electronics, vol. 49, no. 1. p. 4, 2017.

[58] R. Kuladeep, L. Jyothi, P. Prakash, S. M. Shekhar, M. D. Prasad, and D. N. Rao, "Investigation of optical limiting properties of aluminium nanoparticles prepared by pulsed laser ablation in different carrier media," *Journal of Applied Physics*, vol. 114, no. 24, p. 243101, 2013.

[59] K. Park, D. Lee, A. Rai, D. Mukherjee, and M. R. Zachariah, "Size-resolved kinetic measurements of aluminum nanoparticle oxidation with single particle mass spectrometry," *Journal of Physical Chemistry B*, vol. 109, no. 15, pp. 7290–7299, 2005.

[60] P. Zhang, W. Jin, and W. Liang, "Size-Dependent Optical Properties of Aluminum Nanoparticles: From Classical to Quantum Description," *Journal of Physical Chemistry C*, vol. 122, no. 19, pp. 10545–10551, 2018.

[61] D. O. Sigle, E. Perkins, J. J. Baumberg, and S. Mahajan, "Reproducible deep-UV SERRS on aluminum nanovoids," *Journal of Physical Chemistry Letters*, vol. 4, no. 9, pp. 1449–1452, 2013.

[62] K. Ray, M. H. Chowdhury, and J. R. Lakowicz, "Aluminum nanostructured films as substrates for enhanced fluorescence in the ultraviolet-blue spectral region," *Analytical Chemistry*, vol. 79, no. 17, pp. 6480–6487, 2007.

[63] Q. Hao, C. Wang, H. Huang, W. Li, D. Du, D. Han, T. Qiu, and P. K. Chu, "Aluminum plasmonic photocatalysis," *Scientific Reports*, vol. 5, pp. 1–7, 2015.

[64] J. J. Wang, F. Walters, X. Liu, P. Sciortino, and X. Deng, "High-performance, large area, deep ultraviolet to infrared polarizers based on 40 nm line/78 nm space nanowire grids," *Applied Physics Letters*, vol. 90, no. 6, p. 061104, 2007.

[65] B. Wu, X. Liu, T. Z. Oo, G. Xing, N. Mathews, and T. C. Sum, "Resonant Aluminum Nanodisk Array for Enhanced Tunable

Broadband Light Trapping in Ultrathin Bulk Heterojunction Organic Photovoltaic Devices," *Plasmonics*, vol. 7, no. 4, pp. 677–684, 2012.

[66] I. Lachebi, A. Fedala, T. Djenizian, T. Hadjersi, and M. Kechouane, "Morphological and optical properties of aluminum nanoparticles deposited by thermal evaporation on heated substrates," *Surface and Coatings Technology*, vol. 343, pp. 160–165, 2018.

[67] F. Wang, C. Di Valentin, and G. Pacchioni, "Semiconductor-to-metal transition in WO3-x: Nature of the oxygen vacancy," *Physical Review B*, vol. 84, no. 7, p. 73103, 2011.

[68] A. Staerz, S. Somacescu, M. Epifani, T. Russ, U. Weimar, and N. Barsan, "WO3 Based Gas Sensors," *Proceedings*, vol. 2, no. 13. p. 826, 2018.

[69] X. P. Wang, B. Q. Yang, H. X. Zhang, and P. X. Feng, "Tungsten Oxide Nanorods Array and Nanobundle Prepared by Using Chemical Vapor Deposition Technique," *Nanoscale Research Letters*, vol. 2, no. 8, p. 405, 2007.

[70] D. Susanti, N. Stefanus Haryo, H. Nisfu, E. P. Nugroho, H. Purwaningsih, G. E. Kusuma, and S.-J. Shih, "Comparison of the morphology and structure of WO3 nanomaterials synthesized by a sol-gel method followed by calcination or hydrothermal treatment," *Frontiers of Chemical Science and Engineering*, vol. 6, no. 4, pp. 371–380, 2012.

[71] D. Huang, C. Zheng, L. Huang, X. Wu, and L. Chen, "Linear and nonlinear optical properties of ultrafine WO3 nanorods," *Optik*, vol. 156, pp. 994–998, 2018.

[72] D. Huang, C. Zheng, W. Li, W. Chen, L. Huang, L. Chen, and X. Wu, "Shape dependence of nonlinear optical activities of tungsten oxide nanostructures," *Proceedings of SPIE*, vol.11046, p.23, 2019.

[73] E. L. Falcão-Filho, C. B. de Araújo, C. A. C. Bosco, L. H. Acioli, G.

Poirier, Y. Messaddeq, G. Boudebs, and M. Poulain, “Nonlinear optical properties of tungstate fluorophosphate glasses,” *Journal of Applied Physics*, vol. 96, no. 5, pp. 2525–2529, 2004.

[74] O. Muller and P. Gibot, “Optical limiting properties of templated Cr2O3 and WO3 nanoparticles,” *Optical Materials*, vol. 95, p. 109220, 2019.

[75] S. Chen, Y. Xiao, W. Xie, Y. Wang, Z. Hu, W. Zhang, and H. Zhao, “Facile strategy for synthesizing non-stoichiometric monoclinic structured tungsten trioxide (WO3−x) with plasma resonance absorption and enhanced photocatalytic activity,” *Nanomaterials*, vol. 8, no. 7, p. 553, 2018.

[76] S. Tripathi, G. K. Mehrotra, and P. K. Dutta, “Physicochemical and bioactivity of cross-linked chitosan–PVA film for food packaging applications,” *International Journal of Biological Macromolecules*, vol. 45, no. 4, pp. 372–376, 2009.

[77] S. Mahendia, A. Kumar Tomar, P. K. Goyal, and S. Kumar, “Tuning of refractive index of poly(vinyl alcohol): Effect of embedding Cu and Ag nanoparticles,” *Journal of Applied Physics*, vol. 113, no. 7, p. 73103, 2013.

[78] B. Qiao, Y. Liang, T.-J. Wang, and Y. Jiang, “Surface modification to produce hydrophobic nano-silica particles using sodium dodecyl sulfate as a modifier,” *Applied Surface Science*, vol. 364, pp. 103–109, 2016.

[79] J. H. Werth, M. Linsenbühler, S. M. Dammer, Z. Farkas, H. Hinrichsen, K.-E. Wirth, and D. E. Wolf, “Agglomeration of charged nanopowders in suspensions,” *Powder Technology*, vol. 133, no. 1–3, pp. 106–112, 2003.

[80] P. Wang, D. Weng, K. Li, Y. Liu, X. Yu, and X. Zhou, “Multi-wavelength Erbium-doped fiber laser based on four-wave-mixing

effect in single mode fiber and high nonlinear fiber," *Optics Express*, vol. 21, no. 10, pp. 12570–12578, 2013.

[81] L. Ma, Z. Kang, Y. Qi, and S. Jian, "Tunable dual-wavelength fiber laser based on an MMI filter in a cascaded Sagnac loop interferometer," *Laser Physics*, vol. 24, no. 4, p. 45102, 2014.

[82] T. Huang, X. Li, P. P. Shum, Q. J. Wang, X. Shao, L. Wang, H. Li, Z. Wu, and X. Dong, "All-fiber multiwavelength thulium-doped laser assisted by four-wave mixing in highly germania-doped fiber," *Optics Express*, vol. 23, no. 1, pp. 340–348, 2015.

[83] F. A. A. Rashid, S. R. Azzuhri, M. A. M. Salim, R. A. Shaharuddin, M. A. Ismail, M. F. Ismail, M. Z. A. Razak, and H. Ahmad, "Using a black phosphorus saturable absorber to generate dual wavelengths in a Q-switched ytterbium-doped fiber laser," *Laser Physics Letters*, vol. 13, no. 8, p. 85102, 2016.

[84] H. Ahmad, N. A. Hassan, S. N. Aidit, and Z. C. Tiu, "Generation of tunable multi-wavelength EDFL by using graphene thin film as nonlinear medium and stabilizer," *Optics and Laser Technology*, vol. 81, no. 4. pp. 67–69, 2016.

[85] J. Liu, Y. Chen, Y. Li, H. Zhang, S. Zheng, and S. Xu, "Switchable dual-wavelength Q-switched fiber laser using multilayer black phosphorus as a saturable absorber," *Photonics Research*, vol. 6, no. 3, pp. 198–203, 2018.

[86] S. Li, Y. Yi, Y. Yin, Y. Jiang, H. Zhao, Y. Du, Y. Chen, E. Lewis, G. Farrell, S. W. Harun, and P. Wang, "A Microfiber Knot Incorporating a Tungsten Disulfide Saturable Absorber Based Multi-Wavelength Mode-Locked Erbium-Doped Fiber Laser," *Journal of Lightwave Technology*, vol. 36, no. 23, pp. 5633–5639, 2018.

[87] S. Li, Y. Yin, E. Lewis, G. Garrell, and P. Wang, "A twelve-wavelength Thulium-doped fibre laser based on a microfibre coil

resonator incorporating black phosphorus," *Optics Communications*, vol. 437, pp. 342–345, 2019.

[88] M. A. M. Salim, S. R. Azzuhri, M. I. M. Abdul Khudus, M. Z. A. Razak, N. S. Nasir, and I. S. Amiri, "Generation of dual-wavelength ytterbium-doped fibre laser using a highly nonlinear fibre," *Laser Physics*, vol. 28, no. 11, p. 115107, 2018.

[89] A. H. H. Al-Masoodi, M. H. M. Ahmed, H. Arof, and S. W. Harun, "Multi-Wavelength Q-Switched Ytterbium-Doped Fiber Laser with Multi-Walled Carbon Nanotubes," *Fiber and Integrated Optics*, vol. 37, no. 2. pp. 92–102, 2018.

[90] S. K. M. Al-Hayali and A. H. Al-Janabi, "Triple-wavelength passively Q-switched ytterbium-doped fibre laser using zinc oxide nanoparticles film as a saturable absorber," *Journal of Modern Optics*, vol. 65, no. 13, pp. 1559–1564, 2018.

[91] Q. Hu, M. Li, P. Li, Z. Liu, Z. Cong, and X. Chen, "Dual-Wavelength Passively Mode-Locked Yb-Doped Fiber Laser Based on a SnSe2-PVA Saturable Absorber," *IEEE Photonics Journal*, vol. 11, no. 4, pp. 1–13, 2019.

[92] S. Li, Y. Yin, G. Ran, Q. Ouyang, Y. Chen, M. Tokurakawa, E. Lewis, S. W. Harun, and P. Wang, "Dual-wavelength mode-locked erbium-doped fiber laser based on tin disulfide thin film as saturable absorber," *Journal of Applied Physics*, vol. 125, no. 24, p. 243104, 2019.

[93] C. Mahendiran, R. Ganesan, and A. Gedanken, "Sonoelectrochemical synthesis of metallic aluminum nanoparticles," *European Journal of Inorganic Chemistry*, vol. 2009, no. 14, pp. 2050–2053, 2009.

[94] Y. J. L. and C. L. and H. M. Lee, "Synthesis of oxide-free aluminum nanoparticles for application to conductive film," *Nanotechnology*, vol. 29, no. 5, p. 55602, 2018.

[95] S. R. Ghanta and K. Muralidharan, "Chemical synthesis of aluminum

nanoparticles," *Journal of Nanoparticle Research*, vol. 15, no. 6, p. 1715, 2013.

[96] W. Y. and N. X. and H. Zhang, "Nonlinear absorption properties of indium selenide and its application for demonstrating pulsed Er-doped fiber laser," *Laser Physics Letters*, vol. 15, no. 10, p. 105101, 2018.

[97] M. F. A. Rahman, M. Z. Zhalilah, A. A. Latiff, A. H. A. Rosol, M. Q. Lokman, A. R. Bushroa, K. Dimyati, and S. W. Harun, "Pure antimony film as saturable absorber for Q-switched erbium-doped fiber laser," *Journal of Modern Optics*, vol. 65, no. 7, pp. 811–817, 2018.

[98] J. Guo, H. Zhang, C. Zhang, Z. Li, Y. Sheng, C. Li, X. Bao, B. Man, Y. Jiao, and S. Jiang, "Indium tin oxide nanocrystals as saturable absorbers for passively Q-switched erbium-doped fiber laser," *Optical Materials Express*, vol. 7, no. 10, pp. 3494–3502, 2017.

[99] R. I. Woodward, R. C. T. Howe, T. H. Runcorn, G. Hu, F. Torrisi, E. J. R. Kelleher, and T. Hasan, "Wideband saturable absorption in few-layer molybdenum diselenide (MoSe2) for Q-switching Yb-, Er- and Tm-doped fiber lasers," *Optics Express*, vol. 23, no. 15, pp. 20051–20061, 2015.

[100] N. A. Siddiq, W. Y. Chong, Y. K. Yap, Y. H. Pramono, and H. Ahmad, "Tin(IV) oxide nanoparticles as a saturable absorber for a Q-switched erbium-doped fiber laser," *Laser Physics*, vol. 28, no. 12, p. 125104, 2018.

[101] "Manual Fiber Polarization Controllers." [Online]. Available: https://www.thorlabs.com/newgrouppage9.cfm?objectgroup_id=343.

[102] A. H. H. Al-Masoodi, I. A. M. Alani, M. H. M. Ahmed, A. H. H. Al-Masoodi, A. A. Alani, P. Wang, and S. W. Harun, "Cobalt oxide nanocubes thin film as saturable absorber for generating Q-switched fiber lasers at 1 and 1.5 μm in ring cavity configuration," *Optical Fiber Technology*, vol. 45, no. June, pp. 128–136, 2018.

[103] W. H. Hu, G. Q. Han, B. Dong, and C. G. Liu, “Facile synthesis of highly dispersed WO3·H2O and WO3 nanoplates for electrocatalytic hydrogen evolution,” *Journal of Nanomaterials*, vol. 2015, p. 6, 2015.

[104] H. H. Afify, S. A. Hassan, M. Obaida, I. Moussa, and A. Abouelsayed, “Preparation, characterization, and optical spectroscopic studies of nanocrystalline tungsten oxide WO3,” *Optics & Laser Technology*, vol. 111, pp. 604–611, 2019.

[105] F. Liu, X. Chen, Q. Xia, L. Tian, and X. Chen, “Ultrathin tungsten oxide nanowires: oleylamine assisted nonhydrolytic growth, oxygen vacancies and good photocatalytic properties,” *RSC Advances*, vol. 5, no. 94, pp. 77423–77428, 2015.

[106] T. M. Perfecto, C. A. Zito, and D. P. Volanti, “Room-temperature volatile organic compounds sensing based on WO3·0.33H2O, hexagonal-WO3, and their reduced graphene oxide composites,” *RSC Advances*, vol. 6, no. 107, pp. 105171–105179, 2016.

[107] B. Chen, X. Zhang, K. Wu, H. Wang, J. Wang, and J. Chen, “Q-switched fiber laser based on transition metal dichalcogenides MoS2, MoSe2, WS2, and WSe2,” *Optics Express*, vol. 23, no. 20, pp. 26723–26737, 2015.

[108] “Yellow WO3 Tungsten Trioxide Nanoparticles.” [Online]. Available: https://www.hwnanomaterial.com/yellow-wo3-tungsten-trioxide-nanoparticles_p51.html.

[109] S. Li, Y. Yin, E. Lewis, G. Farrell, M. Tokurukawa, A. H. A. Rosol, S. W. Harun, and P. Wang, “Multiwavelength Q-switched pulse operation with gold nanoparticles as saturable absorber,” *Optical Engineering*, vol. 58, no. 6, pp. 1–7, 2019.

LIST OF PUBLICATIONS

- **First-Author Publications**

1. **Ali A. Salman** and A. H. Al-Janabi, "Aluminum nanoparticles saturable absorber as a passive Q-switcher for erbium-doped fiber laser ring cavity configuration," Laser Physics, Vol. 29, No. 4, p. 045102, 2019, Published.
2. **Ali A. Salman** and A.H. Al-Janabi, " Multiwavelength Q-switched erbium-doped fibre laser-based aluminum nanoparticles saturable absorber and Sagnac loop filter," Laser Physics., Vol. 29, No. 6, p. 065103, 2019, Published.
3. **Ali A. Salman** and A. H. Al-Janabi, " Q-switching near-infrared multiwavelength generation by intracavity tungsten-oxide-induced four-wave mixing in an erbium-doped fiber laser," Applied Optics, Vol. 58, No. 16, p.4332, 2019, Published.
4. **Ali A. Salman** and A. H. Al-Janabi, " Triple-Wavelength Q-switched Ytterbium-doped Fiber Laser Based on Tungsten Oxide as Saturable Absorber," 2020, Microwave and Optical Technology Letter, Accepted.

- **Co-Author Publications**

1. Ansam M. Salman, **Ali A. Salman**, and Abdulhadi Al-Janabi, " Stable L-band multiwavelength erbium-doped fiber laser based on four-wave mixing using nickel nanofluid," Applied Optics, Vol. 58, No. 22, p. 6136, 2019, Published.
2. Hiba Hassana, **Ali A. Salman**, Mohammed A. Munshida, Abdulhadi Al-Janabi, " Passive Q-switching using Lead Sulfide suspension as a saturable absorber in 1.5μm region," Optical Fiber Technology, Vol. 52, No. p. 101969, 2019, Published.

PAPER (1)

IOP Publishing | Astro Ltd
Laser Physics
Laser Phys. **29** (2019) 045102 (7pp)
https://doi.org/10.1088/1555-6611/ab02f8

Aluminum nanoparticles saturable absorber as a passive Q-switcher for erbium-doped fiber laser ring cavity configuration

Ali A Salman[1] **and A Hadi Al-Janabi**

Institute of Laser for Postgraduate Studies, University of Baghdad, Baghdad, Iraq

E-mail: ali.ab.salman@gmail.com and hadi.janabi@ilps.uobaghdad.edu.iq

Received 8 September 2018, revised 20 December 2018
Accepted for publication 10 January 2019
Published 7 March 2019

Abstract

We report on the generation of a passively *Q*-switched erbium-doped fiber laser (EDFL) at 1567.6 nm, using aluminum nanoparticles (AlNPs) as a saturable absorber (SA). The synthesized film was fabricated by implanting AlNPs into polyvinyl alcohol as a host matrix. The SA thin film has a modulation depth of 7% and saturable intensity of 0.0015 MW cm^{-2}. A small piece of composite film was inserted between two fiber ferrules to initiate *Q*-switching in the EDFL. Upon reaching a pump threshold of 156 mW, a stable *Q*-switching was achieved. As the pump power is steadily tuned from 156–300 mW, the repetition rate changes from 34.13–48.8 kHz, while the corresponding pulse duration varies from 3.4–2.17 μs. To the best of the authors' knowledge, this the first demonstration of passive *Q*-switching employing an AlNP-based saturable absorber.

Keywords: aluminum nanoparticles (AlNPs), passive *Q*-switched laser, Er-doped fiber laser (EDFL), saturable absorber (SA)

(Some figures may appear in colour only in the online journal)

1. Introduction

Saturable absorbers (SAs) as passive elements have contributed significantly to the field of short and ultrashort optical pulse generation. They have been widely used to produce passively *Q*-switched fiber lasers, which have undergone extensive investigation owing to their widespread applications in the fields of optical communication, sensing, spectroscopy, and material processing [1–4]. Compared to active *Q*-switching techniques, passive methods are more favorable due to their inherent features of compactness, easy fabrication, and cost-effective design [5, 6]. Up to date, various SA materials have been demonstrated to achieve passive *Q*-switching such as graphene and carbon nanotubes [7, 8]. In addition to carbon-based materials, transition metal oxides like zinc oxide, iron oxide, aluminum oxide (Al_2O_3) and copper oxide have gained much interest in photonic applications due to their good nonlinear optical response and ultrafast switching in the mid-infrared (IR) region [9–12]. Metal nanoparticles are also drawing more attention for their high third-order susceptibility, the excitation of surface plasmon resonance and rapid response time [13, 14]. Many research groups have reported the utilization of metal NPs as an SA. For example, silver nanoparticles as passive *Q*-switcher in an erbium-doped fiber laser (EDFL) have been reported by Guo *et al* and Ahmad *et al* in 2016 [15, 16]. Moreover, Ahmad *et al* have verified passive *Q*-switching in EDFL induced by gold nanoparticles [17]. Recently, a copper (CuNP) based SA for a *Q*-switching operation in a C-band has been demonstrated by Muhammad *et al* [18]. However, insufficient attention was paid to aluminum nanoparticles (AlNPs) in the field of ultrafast optics. Recently, a single-beam *Z*-scan technique was employed to analyze the optical nonlinear effects of AlNPs embedded in polyvinyl alcohol (PVA) film [19]. The synthesized

[1] Author to whom any correspondence should be addressed.

PAPER (2)

IOP Publishing | Astro Ltd
Laser Physics
Laser Phys. **29** (2019) 065103 (8pp)
https://doi.org/10.1088/1555-6611/ab13b5

Multiwavelength *Q*-switched erbium-doped fibre laser-based aluminum nanoparticles saturable absorber and sagnac loop filter

Ali A Salman[1] **and A Hadi Al-Janabi**

Institute of Laser for Postgraduate Studies, University of Baghdad, Baghdad, Iraq

E-mail: ali.ab.salman@gmail.com

Received 5 November 2018
Accepted for publication 18 March 2019
Published 25 April 2019

Abstract

In this paper, we experimentally demonstrate a stable multiwavelength *Q*-switched erbium-doped fiber laser generation based on aluminum nanoparticles (AlNPs) as the saturable absorber (SA), with the aid of a Sagnac loop filter for the first time, to the best of author's knowledge. The fabricated AlNPs-SA has a modulation depth, a non-saturable loss and saturable intensity of 7%, 10% and 0.0015 MW cm^{-2}, respectively. By carefully adjusting the polarization controller and progressively increasing the pump power, up to 11 lasing lines in the *Q*-switching regime are obtained with a channel spacing and an optical signal-to-noise ratio of 0.48 nm and 30 dB, respectively. Meanwhile, the *Q*-switched performance has a minimum pulse width of 2.36 μs and a maximum pulse repetition rate of 33.45 kHz by varying the pump power to 300 mW. The proposed laser may become valuable for numerous applications such as dense wavelength division multiplexing technology.

Keywords: multiwavelength fibre laser, *Q*-switching, saturable absorber (SA), sagnac loop filter, aluminum nanoparticles (AlNPs)

(Some figures may appear in colour only in the online journal)

1. Introduction

Generation of multiwavelength from one laser source represents a challenge and a need. The diversity of laser active mediums, the intended application and the laser output are the major parameters that drive scientific motivation. A fiber laser, with its unique features, seems a promising candidate for this job. In the past decade, considerable research efforts have been devoted to the development of multiwavelength erbium-doped fiber lasers (MEDFLs) because of their attractive features and potential applications in numerous fields, including optical communication, sensing, testing and spectroscopy [1–4]. However, due to the inherent homogenous broadening of the EDFL, it is difficult to achieve stable multiwavelength at room temperature [5]. A variety of approaches have been proposed to mitigate the gain competition between the lasing lines, such as four-wave mixing (FWM), nonlinear polarization rotation and stimulated Brillouin scattering [6–8]. In the ring cavity configuration, a comb filter can be inserted to achieve multiwavelength lasing. Several filtering techniques have been suggested and demonstrated, such as the Fabry–Perot filter, fiber Bragg grating and Mach–Zehnder interferometer [9–11]. Besides that, the Sagnac loop filter has a particular interest because of its several unique characteristics, for instance, simple configuration, low insertion loss, robust to temperature changes, polarization independent, large signal-to-noise ratio (SNR), real-time tuning of lasing lines using a polarization controller and less expensive compared to other techniques requiring circulators and nonlinear fibers [12]. Another merit of a Sagnac filter is that the wavelength spacing between adjacent channels can be tuned wide or narrow, depending only on the length of the birefringent fiber in the loop filter [13]. On the other hand, passive *Q*-switched fiber lasers have been extensively investigated in recent years owing to their favorable properties, such as compactness, easy fabrication and low cost [14]. Many saturable absorbers

[1] Author to whom any correspondence should be addressed.

PAPER (3)

4332 Vol. 58, No. 16 / 1 June 2019 / Applied Optics Research Article

applied optics

Q-switching near-infrared multiwavelength generation by intracavity tungsten-oxide-induced four-wave mixing in an erbium-doped fiber laser

ALI A. SALMAN* AND A. HADI AL-JANABI

Institute of Laser for Postgraduate Studies, University of Baghdad, Baghdad, Iraq
**Corresponding author: ali.ab.salman@gmail.com*

Received 1 April 2019; revised 5 May 2019; accepted 6 May 2019; posted 6 May 2019 (Doc. ID 363867); published 24 May 2019

We report on the generation of a stable multiwavelength *Q*-switched erbium-doped fiber laser based on tungsten oxide nanoparticles (WO_3 NPs) combined with an intracavity comb filter for the first time, to the best of our knowledge. The prepared WO_3-PVA thin film has a modulation depth and saturable intensity of 20% and 100 MW/cm^2, respectively. A spectrum of up to 15 peaks with a channel spacing of 0.48 nm has been obtained. In the *Q*-switching regime, a minimum pulse width of 4.24 μs and a maximum repetition rate of 52.49 kHz were achieved at a maximum pump power of 300 mW. The dual effect of WO_3 NPs in saturable absorption and high optical nonlinearity has induced pulsed and four-wave mixing effects. Therefore, the intrinsic advantages of WO_3 nanomaterial provide a promising source for the realization of a stable multiwavelength fiber laser. © 2019 Optical Society of America

https://doi.org/10.1364/AO.58.004332

1. INTRODUCTION

Near-infrared (NIR) multiwavelength fiber, especially 1.55 μm wavelength fiber lasers, have rapidly evolved in recent years [1–4]. They have been extensively studied for their numerous advantages, such as eye-safe wavelength and minimum attenuation for transmission through fused silica fibers, which make them a desirable choice for many photonic applications such as light detection and ranging (LIDAR) and dense wavelength-division multiplexing (DWDM) [5–8]. Different methodologies have been adopted to stabilize the multiwavelength generation in erbium-doped fiber lasers (EDFLs) at ambient temperature including the Mach–Zehnder interferometer, Lyot filter, four-wave mixing (FWM), nonlinear polarization rotation (NPR), and Sagnac loop filter [9–13]. Moreover, many researchers have demonstrated a stable multiwavelength generation based on the FWM technique using highly efficient nonlinear 2D material such as graphene, black phosphorus, and tungsten disulfide [14–16]. Applying a few layers of these materials into the EDFL cavity can act simultaneously as a multioscillation stabilizer and a saturable absorber (SA). Such behaviors are generally associated with the real and imaginary parts of the strong third-order nonlinearity in these materials [17]. Recent studies have found that transition metal oxides (TMO) possess a considerable high third-order nonlinearity, fast recovery time, and low saturable intensity, which makes them a promising SA [18–21]. Tungsten oxide as a metal oxide emerges as a potential candidate for nonlinear photonic applications. The WO_3 has received less attention and remained unexploited material for both pulsed and multiple wavelength generation. Recently, a *z*-scan procedure was performed on tungsten oxide (WO_3) nanorods showing a promising nonlinear optical response [22]. Furthermore, A previous study showed that the third-order susceptibility, the nonlinear absorption coefficient, and the nonlinear refractive index in tungstate fluorophosphate glasses have been improved by increasing WO_3 doping due to hyperpolarization of tungsten–oxygen bond [23]. Also, it showed that the nonlinear temporal characteristics were in the femtosecond range in tungsten-based glasses. The tungsten trioxide also exhibits n-type semiconducting features with a bandgap of ~2.5 eV in addition to good mechanical and thermal properties, which is beneficial for the SA material to obtain high pulse energy and to dissipate the accumulated heat as well as to have a large damage threshold [22,24]. In this article, a simple and low-cost multiwavelength *Q*-switched EDFL generation in the infrared regime based on WO_3 nanoparticles (NPs) in conjunction with a Sagnac loop filter is successfully demonstrated for the first time to the best of the authors' knowledge. A few-micron thickness of polyvinyl alcohol (PVA) – WO_3 thin film was directly attached onto the fiber facet to form the SA nonlinear device in an all-fiber laser system. This configuration has the ability to produce up to 15 peaks centered at 1563.95 with a constant spectral spacing of 0.48 nm by fine tuning the pump power and the orientation of the polarization state with a wavelength. Meanwhile, the

1559-128X/19/164332-05 Journal © 2019 Optical Society of America

PAPER (4)

6136 Vol. 58, No. 22 / 1 August 2019 / Applied Optics Research Article

applied optics

Stable L-band multiwavelength erbium-doped fiber laser based on four-wave mixing using nickel nanofluid

ANSAM M. SALMAN,* ALI A. SALMAN, AND ABDULHADI AL-JANABI

Institute of Laser for Postgraduate Studies, University of Baghdad, Baghdad, Iraq
**Corresponding author: ansamm.salman@eng.nahrainuniv.edu.iq*

Received 24 May 2019; revised 3 July 2019; accepted 3 July 2019; posted 5 July 2019 (Doc. ID 368394); published 31 July 2019

A simple continuous-wave multiwavelength erbium-doped fiber laser based on four-wave mixing has been successfully demonstrated utilizing nickel nanofluid (Ni-NF) for the first time, to the best of our knowledge. By fine adjustment of the laser diode pump power up to 196 mW and without any intracavity filtering, stable dual-, triple-, and quadruple-lasing lines in the L-band have been observed at 1595.6 nm, 1596.8 nm, 1598 nm, and 1599.2 nm, respectively, with a signal-to-noise ratio ~43 dB. The induced L-band wavelengths showed high stability with wavelength shifts <0.07 nm and power fluctuation of <3 dB by monitoring the output spectra for a duration of 30 min at room temperature. Taking into account the superiority of Ni-NF in terms of compactness, low cost, and easy fabrication, this design can be practically used in a variety of nonlinear photonic applications.

https://doi.org/10.1364/AO.58.006136

1. INTRODUCTION

Recently, the L-band spectrum (1565–1625) nm has attracted a lot of interest in optical telecommunications due to the low attenuation loss of silica fibers in this region and high transmission capacity [1–3]. Multiwavelength fiber lasers are of significant importance because of their wide applications in many fields including wavelength division multiplexing [4], sensing systems [5], microwave optics [6], testing, signal processing, and spectroscopy [7–9]. The multiwavelength laser based erbium-doped fiber (EDF) offers various advantages such as a low polarization dependent gain, narrow linewidth, flat gain spectrum, high conversion efficiency, and low lasing threshold [10]. However, EDF experiences a strong homogeneous broadening gain at room temperature, which leads to severe mode competition and consequently affects the laser stability [10,11]. To date, different approaches have been proposed and demonstrated to generate stable multiwavelength fiber lasers, such as liquid nitrogen cooling [12], fiber Bragg gratings [13], polarization maintaining fiber (PMF)-based Sagnac filters [14–16], Lyot filters [17,18], Mach–Zehnder (M–Z) interferometers [19,20], hybrid gain media [21], and high nonlinear material [22–25]. Recently, nonlinear effects in optical fibers such as the stimulated scattering effect [26,27] and four-wave mixing (FWM) [28–30] have also been adopted to generate multiwavelength lasers. FWM is a potential technique to suppress the homogeneous broadening in rare-earth-doped fibers by distributing the energy among different modes, which leads to stable multiwavelength generation with equal channel spacing between them [31–33]. Generally, FWM in optical fiber refers to optical nonlinear phenomena occurring when two photons are annihilated and two new photons are created at different frequencies where energy and phase matching are conserved. Phase matching is a key parameter that determines the FWM conversion efficiency. To generate high conversion efficiency, the phase matching condition must be satisfied:

$$k = \Delta k_l + \Delta k_{nl} \approx 0, \tag{1}$$

where Δk_l is the linear phase mismatch related to the dispersion condition, and $\Delta k_{nl} = 2\gamma P$ is the nonlinear phase mismatch, which is related to self-phase modulation and cross-phase modulation [34,35]. In an optical fiber, there is the possibility of degenerate FWM when two photons with the same frequency ($w_1 = w_2$) are absorbed and two new photons ($w_3 = 2w_1 - w_2$ and $w_4 = 2w_2 - w_1$) are created [34,36]. Different approaches to achieve FWM by using several meters of high nonlinear fiber [11,37], photonic crystal fiber [32], dispersion shifted fiber [37], and single-mode fiber [11] have been investigated. Recently, innovative nonlinear materials such as graphene [15,38], black phosphor [39], and tungsten disulfide [40], which have high performance and low cost, have gained much attention as promising nonlinear gain media to generate multiwavelength-based FWM. More recently, transition metals have attracted much interest due to their distinguished optical properties such as large third-order nonlinearity, broadband plasmon resonance

1559-128X/19/226136-08 Journal © 2019 Optical Society of America

PAPER (5)

Optical Fiber Technology 52 (2019) 101969

Contents lists available at ScienceDirect

Optical Fiber Technology

journal homepage: www.elsevier.com/locate/yofte

Passive Q-switching using Lead Sulfide suspension as a saturable absorber in 1.5 μm region

Hiba Hassan[a,b,*], Ali A. Salman[b], Mohammed A. Munshid[a], Abdulhadi Al-Janabi[b]

[a] Department of Laser and Optoelectronics Engineering, University of Technology, Baghdad, Iraq
[b] Institute of Laser for Postgraduate Studies, University of Baghdad, Baghdad, Iraq

ARTICLE INFO

Keywords:
Passive Q-switching
Fiber laser
PbS
Saturable absorber
Nonlinear material

ABSTRACT

We report on Lead Sulfide (PbS) dispersed in sodium dodecyl sulfate (SDS) used as a saturable absorber (SA) in erbium-doped fiber laser (EDFL) ring cavity configuration. It has been fabricated in a suspension form by simple method for flexible usage with high stability. Then, the prepared SA was integrated in the EDFL cavity producing passively Q-switched pulses at wavelength of 1566.3 nm with 3 dB bandwidth of 4.23 nm. Stable short pulses of 8.55–3.43 μs were generated as the corresponding pump power increased from 73 to 300 mW while the repetition rate tuned from 14.86 to 38.71 kHz accordingly. The maximum pulse energy obtained by the present setup was 10.6 nJ at maximum input pump power. The high signal-to-noise ratio (SNR) of proposed PbS-SDS based SA of ~63 dB represents a considerable stable Q-switched EDFL and proves a high prospect to be used in practical photonic applications.

1. Introduction

Q-switching is outshining technique for generating short pulses with high peak power and/or high pulse energy at temperate pump power. Since the first demonstration of Q-switched laser [1] a huge number of research papers have appeared. All the progress in this field had focused on using active and passive Q-switching techniques mostly in solid-state lasers. When high power diode lasers became available, a real revolution has occurred in the field of fiber lasers. Those diodes became suitable to pump fiber lasers. Nowadays, the scientific endeavors are focused on Q-switched fiber laser due to their cost-effective, simple arranging and size compactness [2,3]. The high-intensity Q-switched fiber lasers have found potential application in different fields including medicine, optical fiber sensing, range finder and free space communication [4–7]. Both the active and passive techniques were used to achieve Q-switching in fibers. The active type can be realized by inserting externally powered modulator such as electro-optics and/or acousto-optics to produce high cavity loss [8,9]. While the passive one is obtained via modulating the intra-cavity loss by controlling the optical pulse itself through the nonlinear element saturable absorber (SA). Due to simple preparation, cheap, high mechanical stability and no necessitate to external feedback, SA becomes a quite attractive method [10]. Different types of materials have been adopted with the pioneering work on semiconductor saturable absorber mirrors (SESAMs) [11] and later graphene has a unique feature of linear energy band structure leading to a broad band operation range [12–14] and carbon nanotubes [15–17]. Furthermore, the rapid development in the field of materials has led to new SA nanomaterials like topological insulators (Bi_2S_3 [18], Bi_2Te_3 [19,20], and Sb_2Te_3 [21]). Two-dimensional heterostructures such as graphene-Bi_2Te_3 has been investigated for Q-switching and mode-locking operation in Er doped fiber laser [22]. Another new type of 2D material as SA is MXene $Ti_3C_2T_x$ (T = F, O, or OH) which got a great attention due to its high nonlinear optical properties to generate ultrashort pulses [23]. Black phosphorus flakes were used as saturable absorber mirror at the 1046 nm wavelength solid state laser [24]. Bismuthene has a direct energy bandgap at 1550 nm was also used as an SA for generating femtosecond pulses [25]. Transition metal oxides (ZnO [26], TiO_2 [27]and CuO [28], Fe_3O_4 [29]), transition metal dichalcogenides (MoS_2 [30], WS_2 [31] and ReS_2 [32]) and Metal chalcogenide semiconductors (CdSe QDs [33] and InSe [34]) were became also a potential candidate as SA's. Metal chalcogenide semiconductor materials attract significant attention due to their very good optical, thermal and mechanical properties. Their formula is MX consisting of transition metal atom M and chalcogen atom (sulfur (S), selenium (Se), tellurium (Te)). Amongst these Metal chalcogenide semiconductor materials is Lead Sulfide (PbS) which is a IV-VI semiconductor group. It is one of the oldest semiconductor materials that found great attention in recent years due to its smallest direct band gap

* Corresponding author.
E-mail address: 140049@uotechnology.edu.iq (H. Hassan).

https://doi.org/10.1016/j.yofte.2019.101969
Received 12 May 2019; Received in revised form 14 June 2019; Accepted 26 June 2019

APPENDIX (A)

PM Fiber Specifications

THORLABS

Polarization-Maintaining Fiber: Panda Style

PM1550-XP

Description

Thorlabs' polarization-maintaining fibers, designed for use from 1440 to 1625 nm, are optimized for data and telecom applications where ultra-low attenuation over long distances and resistance to radiation-induced damage are critical.

Specifications

Geometrical & Mechanical	
Core Diameter	8.5 µm
Cladding Diameter	125 ± 2 µm
Coating Diameter	245 ± 15 µm
Core-Clad Offset	≤0.5 µm
Coating Concentricity	≤5 µm
Coating Material	UV Cured, Dual Acrylate
Operating Temperature	-40 to 85 °C
Proof Test Level	≥ 200 kpsi (1.4 GN/m²)

Optical	
Numerical Aperture	0.125
Attenuation	<1.0 dB/km @ 1550 nm
Operating Wavelength	1440 - 1625 nm
Second Mode Cut-off	1380 ± 60 nm
Mode Field Diameter (1/e² fit - near field)	10.1 ± 0.4 µm @ 1550 nm
Beat Length	≤5.0 mm @ 1550 nm
Normalized Cross Talk	≤-40 dB @ 4 m @ 1550 nm

US, Canada, & South America: +1-973-300-3000 | France: +33 (0) 970 444 844 | Europe: +49 (0) 8131-5956-0 | UK & Ireland: +44 (0)1353-654440
Brazil: +55-16-3413 7062 | Scandinavia: +46-31-733-30-00 | Japan & Asia: +81-3-5979-8889 | China: +86 (0)21-60561122
www.thorlabs.com

June 10, 2017
TTN019885-S01, Rev C

APPENDIX (B)

3dB Coupler Specifications

THORLABS

Wideband Fiber Optic Coupler 1550 nm, 50:50 Ratio

TW1550R5F2

Description

Thorlabs' TW1550R5F2 single mode wideband fiber coupler is designed to operate from 1450 to 1650 nm with ≤0.15 dB of excess loss.

Specifications

TW1550R5F2	
Coupling Ratio[a]	50:50
Coupling Ratio Tolerance	±5.0%
Center Wavelength	1550 nm
Minimum Bandwidth	±100 nm
Insertion Loss[a]	≤3.6 dB/≤3.6 dB
Excess Loss[a]	≤0.15 dB
Uniformity[a]	≤0.5 dB
Polarization-Dependent Loss (PDL)[a]	≤0.15 dB
Optical Return Loss (ORL) / Directivity[a]	≥60 dB
Max Power Level[b]	1 W (With Connectors or Bare Fiber) 5 W (Spliced)
Fiber Type[c]	SMF-28e+
Fiber Cut-Off Wavelength	≤1260 nm
Port Configuration	2x2
Fiber Lead Length and Tolerance	1 m +0.075 m/-0.0 m
Connectors	2.0 mm Narrow Key FC/PC
Package Size	Ø0.12" x 2.76" (Ø3.2 mm x 70 mm)
Jacket	Ø900 µm Hytrel® Loose Tube
Pigtail Tensile Load	10 N
Operating Temperature Range	-40 to 85 °C
Storage Temperature Range	-40 to 85 °C

a. All values are specified at room temperature over the bandwidth without connectors and measured through the white input port as indicated below; similar performance (≤0.05 dB difference) is achieved when the blue port is used as the input.
b. Specifies the total maximum power allowed through the component. Coupler performance and reliability under high-power conditions must be determined within the user's setup. See Usage Tips for safety and handling information.
c. Other fiber types may be available upon request. Please contact techsupport@thorlabs.com with inquiries.

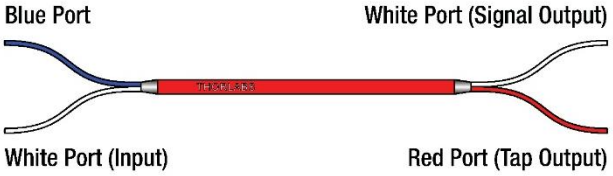

Specifications Subject to Change without Notice

May 25, 2017
TTN035887-S01, Rev B

APPENDIX (C)

PC Specifications

Item #	FPC560	FPC561	FPC562
Paddle Material	Black Delrin		
Number of Paddles	3		
Loop Diameter	2.2" (56 mm)		
Paddle Rotation	±117.5°		
Foot Print (L x W)	12.5" x 1.0" (317.5 mm x 25.4 mm)		
Fiber	None	SMF-28-J9	
Operating Wavelength Range[a]	N/A	1260 - 1625 nm	
Design Wavelength[b]	N/A	1310 nm	
Mode Field Diameter	N/A	9.2 ± 0.4 µm @ 1310 nm 10.4 ± 0.5 µm @ 1550 nm	
Cladding Diameter	N/A	125 ± 0.7 µm	
Coating Diameter	N/A	242 ± 5 µm	
Tubing Diameter	N/A	Ø900 µm Tight Buffer	
Numerical Aperture	N/A	0.14	
Loop Configuration[c]	N/A	3-6-3	
Connectors	N/A	FC/PC	FC/PC
Bend Loss	N/A	≤0.1 dB	

a. Retardance varies as a function of wavelength. Refer to Chapter 2 for more information.
b. Devices with preloaded fiber are optimized for this wavelength.
c. For polarization controllers with fiber preinstalled.

الخلاصة

الغاية الرئيسية لهذا الاطروحة هوتوليد اطوال موجية متعددة في الليزر الليفي المشوب بالإربيوم و الليزر الليفي المشوب باليتربيوم بواسطة المواد النانوية ذات خواص بصرية غير خطية عالية.

استخدم في هذه الدراسة نوعين من المواد النانوية غير الخطية ، وهما معدن (الألومنيوم) و أكسيد فلز (أكسيد التنغستن). حيث تم تحضير اغشية رقيقة مشوبة من Al وWO_3عن طريق وضع هذه الحبيبات النانوية في وسط مضيف وهو بولي فينيل الكحول PVA.كذلك تم تحضيرWO_3 بطريقة اخرى بخلطه مع مادة SDS لتقليل الشد السطحي ومنع تكتل الحبيبات النانوية. تم عمليا توليد ليزر الليف المشوب بالاربيوم EDFL نبضي ذو عامل نوعية Q-switching بواسطة جسيمات الالمنيوم المشوبة في غشاء رقيق من البوليمر حيث كان عمق التعديل MD للغشاء ٧ %. تم توليد نبضات مستقرة ذات تكرار نبضي يتراوح بين ٣٤،١٣ كيلوهرتز و ٤٨،٨ كيلو هرتز مع زيادة قدرة الضخ من حد العتبة إلى٣٠٠ ملي واط. وكان الحد الأدنى لمدة النبضة ٢،١٧مايكرو ثانية.

من ناحية اخرى استعملت حبيبات الالمنيوم النانوية لانتاج حزمة من ١٣ طول موجي في ليزر الليف المشوب بالاربيوم EDFL حيث كان تباعد بين الاطوال الموجية ٠,٤٨ نانومتر بمساعدة مرشح سانياك Sagnac المكون من ليف الضوئي من نوع panda PMF يحافظ على استقطاب الضوء الداخل لليف البصري. كذلك تم الحصول بصورة متزامنة على نبضات ليزرية وكان اقصر مدة للنبضة عند اعلى قدرة ضخ هي ٢,٣٦ مايكروثانية.

بالاضافة لذلك عند استعمال غشاء رقيق مشوب بحبيبات WO_3 في ليزر الليف المشوب بالاربيوم EDFL تولد طيف من ١٥ طول موجي من خلال إجراء التعديلات المناسبة لقدرة الضخ ومتحكم الاستقطاب حيث كان عمق التعديل MD للغشاء ٢٠ %. في هذه التجربة العملية تحققت سلسلة نبضات مستقرة كان الحد الادنى لها ٤,٢٤ مايكرو ثانية.

بالنسبة لليزر الليفي المشوب باليتربيوم YDFL، كانت الجسيمات النانوية WO_3 المخلوطة مع محلول معلق من SDS قد وضعت على طرف الليف عن طريق الترسيب المباشر. تم تحقيق نبضات ذات عامل نوعية Q-switching عند حد عتبة تبلغ ١٧٩ ملي وات ولديها حد أدنى لعرض النبضة يبلغ ٢,٩٢ مايكروثانية وقدرة قصوى للنبض تبلغ ٣,١٧ ملي وات. من خلال زيادة طاقة الضخ والتغيير المناسب لوحدة التحكم في الاستقطاب تم الحصول على ليزر ثنائي وثلاثي الطول الموجي عند قدرة المضخة البالغة ٢١٠ ملي وات و ٢٧٥ ملي وات على التوالي. أن هذه الانواع من الليزرات المتعددة الاطوال الموجية ذات فائدة كبيرة في منظومات الاتصالات البصرية الحديثة حيث توفر نطاق واسع من الموجات لنقل البيانات الرقمية.

وزارة التعليم العالي والبحث العلمي

جامعة بغداد

معهد الليزر للدراسات العليا

ليزر الليف المشوب المتعدد الطول الموجي ذي مفتاح عامل النوعية المعتمد على الجسيمات النانوية كممتص مشبع

أطروحة مقدمة الى

معهد الليزر للدراسات العليا /جامعة بغداد /لاستكمال متطلبات نيل شهادة دكتوراه فلسفة في الليزر/ الهندسة الالكترونية والاتصالات

من قبل

علي عبد الله سلمان

بكالوريوس هندسة الليزر والالكترونيات بصرية - ٢٠٠٨
ماجستير هندسة الليزر والالكترونيات بصرية - ٢٠١٢

بإشراف

الاستاذ الدكتور عبد الهادي مطشر الجنابي

١٤٤١ هـ **٢٠١٩ م**